5080-573
E[illegible]c & Hybrid Vehicle System
[illegible]arch & Development Project

DOE/CS-54209-22
Distribution Category UC-96

Advanced Vehicle Systems Assessment

Volume II: Subsystems Assessment

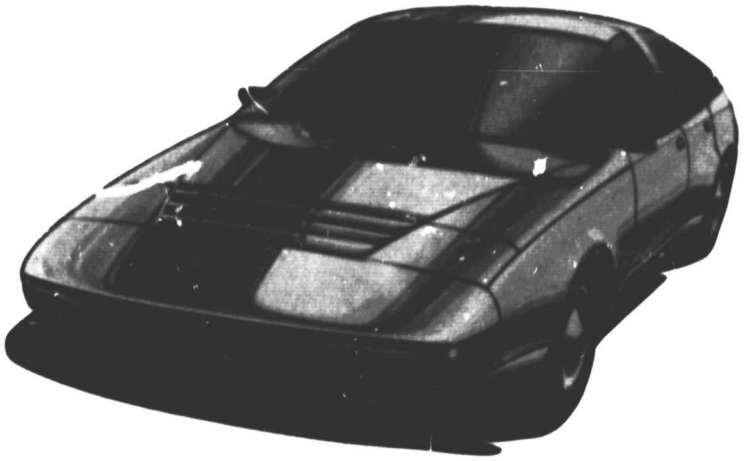

March 1985

Prepared for
U.S. Department of Energy
Through an Agreement with
National Aeronautics and Space Administration
by
Jet Propulsion Laboratory
California Institute of Technology
Pasadena, California

JPL Publication 84-79

TECHNICAL REPORT STANDARD TITLE PAGE

1. Report No. 84-79	2. Government Accession No.	3. Recipient's Catalog No.
4. Title and Subtitle Advanced Vehicle Systems Assessment, Vol. II: Subsystems Assessment		5. Report Date March 1985 6. Performing Organization Code
7. Author(s) K. Hardy		8. Performing Organization Report No.
9. Performing Organization Name and Address JET PROPULSION LABORATORY California Institute of Technology 4800 Oak Grove Drive Pasadena, California 91109		10. Work Unit No. 11. Contract or Grant No. NAS7-918 13. Type of Report and Period Covered JPL Publication
12. Sponsoring Agency Name and Address NATIONAL AERONAUTICS AND SPACE ADMINISTRATION Washington, D.C. 20546		14. Sponsoring Agency Code

15. Supplementary Notes Sponsored by the U.S. Department of Energy through Interagency Agreement DE-AI01-78CS54209 with NASA; also identified as DOE/CS-54209-22, Vol. II, and as JPL Project No. 5030-573 (KTOP or Customer Code 778-36-05-01).

16. Abstract

Volume II (Subsystems Assessment) is part of a five-volume report entitled Advanced Vehicle Systems Assessment. Other volumes are the Executive Summary (Vol. I), Systems Assessment (Vol. III), Supporting Analyses (Vol. IV), and Appendices (Vol. V). Volume II presents the projected performance capabilities and cost characteristics of applicable subsystems, considering an additional decade of development. Subsystems of interest include energy storage and conversion devices as well as the necessary powertrain components and vehicle subsystems. Volume II also includes updated battery information based on the assessment of an independent battery review board (with the aid of subcontractor reports on advanced battery characteristics).

17. Key Words (Selected by Author(s))	18. Distribution Statement
air-breathing engines combustion and ignition ground transportation equipment	Unclassified-Unlimited

19. Security Classif. (of this report)	20. Security Classif. (of this page)	21. No. of Pages	22. Price
Unclassified	Unclassified	164	

5030-573
Electric & Hybrid Vehicle System
Research & Development Project

DOE/CS-54209-22
Distribution Category UC-96

Advanced Vehicle Systems Assessment

Volume II: Subsystems Assessment

March 1985

Prepared for
U.S. Department of Energy
Through an Agreement with
National Aeronautics and Space Administration
by
Jet Propulsion Laboratory
California Institute of Technology
Pasadena, California

JPL Publication 84-79

Prepared by the Jet Propulsion Laboratory, California Institute of Technology, for the U.S. Department of Energy through an agreement with the National Aeronautics and Space Administration.

JPL NASA Task RE-152, Amendment 170, DOE Interagency Agreement No. DE-AI01-78CS54209.

ABSTRACT

The Electric and Hybrid Vehicle Division of the U.S. Department of Energy established the Advanced Vehicle Task at the Jet Propulsion Laboratory to assess the potential of nonpetroleum passenger vehicles to compete with conventional vehicles of the 1990s. The objective of the task was to provide the technical foundation and make recommendations in support of nonpetroleum electric and hybrid vehicles from a systems perspective.

Volume II (Subsystems Assessment) is part of a five-volume report entitled Advanced Vehicle Systems Assessment. Other volumes are the Executive Summary (Vol. I), Systems Assessment (Vol. III), Supporting Analyses (Vol. IV), and Appendices (Vol. V). Volume II presents the projected performance capabilities and cost characteristics of applicable subsystems, considering an additional decade of development. Subsystems of interest include energy storage and conversion devices as well as the necessary powertrain components and vehicle subsystems. Volume II also includes updated battery information based on the assessment of an independent battery review board (with the aid of subcontractor reports on advanced battery characteristics).

ACKNOWLEDGMENTS

Appreciation is expressed to the contributors to the subsystems assessment, whose areas of responsibility are shown below:

Subsystems Assessment	Jet Propulsion Laboratory	Consultants
Batteries		Barry A. Askew Joseph A. Consiglio Philip C. Symons William J. Walsh
Power Peaking		Vernon P. Roan
Heat Engines	Horst W. Schneider	
Fuel Cells	Aiji A. Uchiyama	Vernon P. Roan
Propulsion	Wally E. Rippel	
Base Vehicle	Gerhard J. Klose Max A. Gyamfi	A. Marshall Zaun

Appreciation is extended to the Electric and Hybrid Vehicle Project management for guidance and support throughout this task:

Task Manager	Keith S. Hardy
Task Area Manager	John M. Langendoen
Project Managers	James L. Long Jack F. Park

Dr. Robert S. Kirk of the U.S. Department of Energy, the sponsor of this activity, is also acknowledged for his insight in providing the opportunity to perform this assessment.

JPL is indebted to the many individuals and organizations who contributed data essential to this assessment.

CONTENTS

SECTION I

SUMMARY

A. INTRODUCTION

The Electric and Hybrid Vehicle (EHV) Division of the U.S. Department of Energy (DOE) established the Advanced Vehicle (AV) Development Project to assess the potential of nonpetroleum passenger vehicles that fully compete with conventional petroleum-fueled heat-engine vehicles in the 1990s. The Jet Propulsion Laboratory (JPL), in its role as the EHV Systems R&D Project Office, was given the AV Assessment Task to provide the technical foundation and make recommendations for research in support of the most promising nonpetroleum electric or hybrid vehicles from a systems perspective. Therefore, the objectives of the assessment are to characterize and prioritize the various subsystem technologies and system concepts through the use of vehicle simulation, based on projections of the subsystem capabilities in the next 10 years (Figure 1-1).

This summary describes the overall methodology of the task as well as the primary results of the subsystems assessment activity. The detailed assessments of energy storage and conversion subsystems, powertrain components, and the vehicle subsystem (chassis, etc.) follow in Sections II through V.

B. ASSESSMENT METHODOLOGY

The assessment of advanced subsystem technologies is but one of the primary areas of analysis of the AV Assessment (as shown in Figure 1-2).

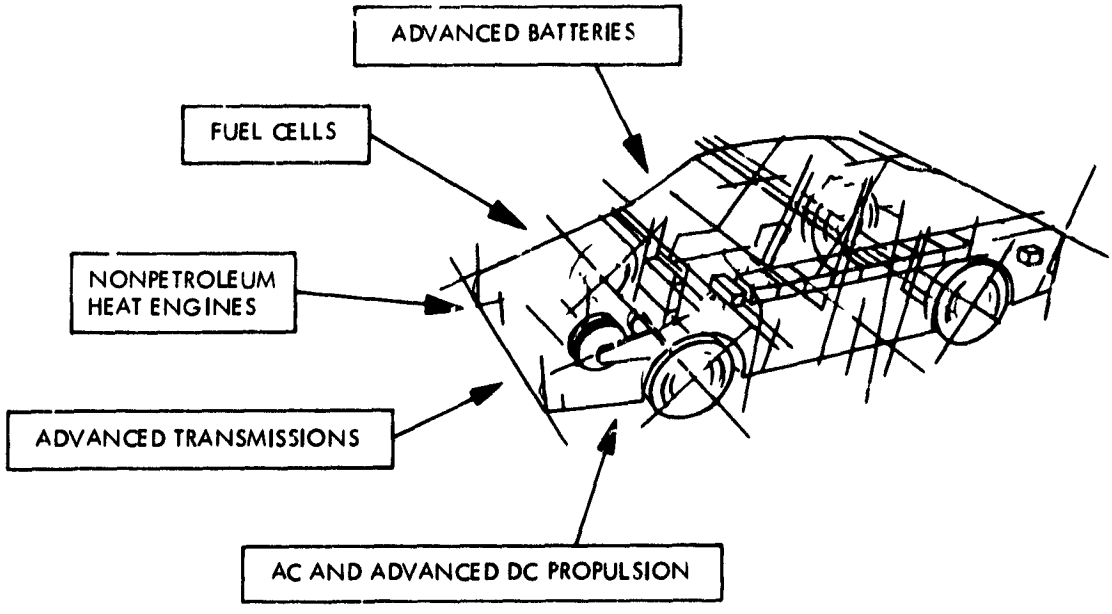

Figure 1-1. Advanced Vehicle Subsystem Options

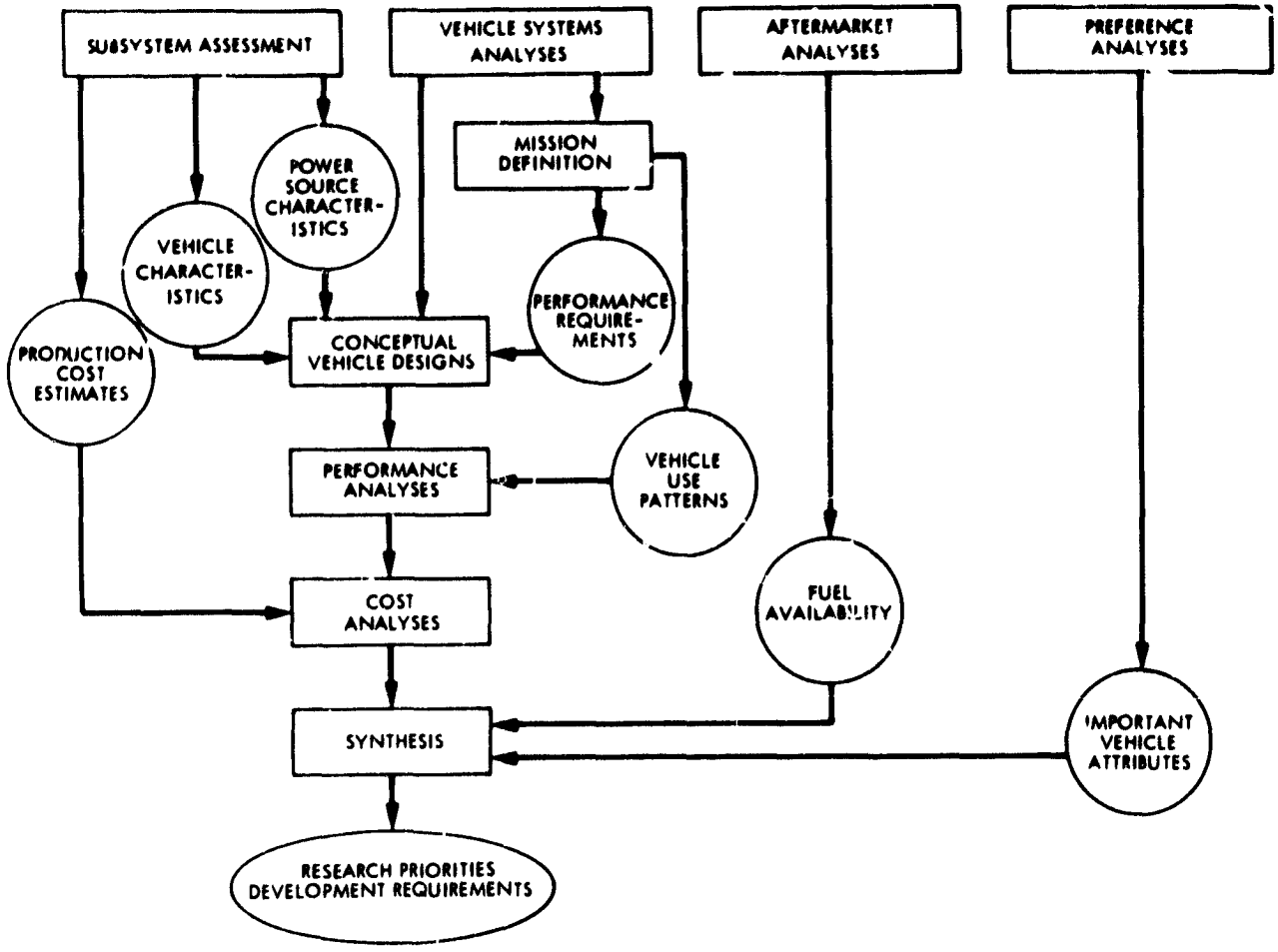

Figure 1-2. Advanced Vehicle Assessment Methodology

However, this evaluation is the basis of the vehicle analyses and cost evaluations that are reported in Volume III of this report. As such, this assessment includes all aspects of the subsystems required for modeling and simulation; that is, vehicle subsystem characteristics, power-source characteristics, and production-cost estimates.

The approach to assessing the various subsystems was based on extrapolation from present designs and concepts. This approach involved the evaluation of present status, an assessment of the necessary technological developments, and a judgment of the likelihood of successful development. One example of this approach is the battery assessment. Several developers were solicited to provide their assessment of the capabilities of their batteries, given specific design targets in terms of power and energy. An independent review board was assembled to judge the potential of the batteries, using the subcontractor reports and their experience as inputs. Their projections are contained in this report. However, the reports of the subcontractors (as submitted) are contained in the Appendices (Volume V). The other subsystems were evaluated in a less formal manner by members of the JPL technical staff or by consultants.

C. SUMMARY OF SUBSYSTEM CHARACTERISTICS

1. Energy-Storage Subsystems

a. Batteries. The technologies of interest to the AV Assessment Task include the aqueous-mobile batteries (formerly known as near-term), flow batteries, high-temperature, and metal-air batteries. These technologies are in various states of development, ranging from electrode/cell experimentation to developmental battery packs. The primary effort of this task, therefore, has been to assess the mature (long-term) characteristics based on extrapolation from current designs. Projections of performance within the next decade (1990s) have been based on assessing the current status, identifying fundamental technical and data deficiencies and, with the aid of the developers and the cognizant national laboratories, estimating the probabilities of overcoming these deficiencies in the time range considered (given adequate developmental funding).

Projected battery discharge curves and peak-power characteristics, in conjunction with a refined fractional utilization battery model, are used in the JPL EHV simulation program, ELVEC, for performance prediction. The details of the battery characterizations are beyond the scope of this summary; however, constant-discharge and peak-power capabilities, consistent with the detailed models, are shown in Table 1-1. (The range of values represents projections for different battery designs.) The detailed assessments, which follow in Section II of this report, include performance characteristics, energy efficiency, unique operational characteristics, cost, cycle life, aftermarket support, and safety concerns.

b. Power-Peaking Devices. Mechanical peaking devices were investigated as a means to make up for power deficiencies of some of the AV candidates, reduce life-cycle costs, and improve energy efficiency. The prospects included flywheels, compressed air, hydraulic accumulators, elastomers, linear elastic materials, and liquid springs. A comparison of the energy characteristics is shown in Table 1-2.

Characterizing the total systems under consideration is difficult because of the lack of vehicle-size component information. However, costs and performance characteristics of continuously variable transmissions (CVTs) to support the flywheel system are expected to be comparable to automatic transmissions. The ancillary components for the compressed-air and hydraulic accumulator systems (i.e., motors, compressors, pumps, and heat exchangers) are expected to be bulkier and more expensive than the flywheel/CVT system. Therefore, the flywheel system is considered the most promising, even though it is probably the most commonly overrated system on a theoretical basis. Development of the ETV-2 vehicle system at the Garrett Corporation and vehicle testing at JPL have demonstrated that a smaller, more efficient flywheel system would be a better trade-off; therefore, a composite flywheel of 0.25 to 0.5 kWh, with a mechanical CVT, is considered the most desirable choice when mechanical power-peaking devices are justified. However, the most promising AV subsystem candidates are expected to have sufficient power capabilities, and the added complexity of a flywheel system might not be necessary.

Table 1-1. Projected Battery Characteristics

Battery type	Specific energy, Wh/kg at 20W/kg	30-s Specific power, W/kg at 10% SoC	Annual efficiency, %	Life cycles, 80%	OEM cost[a]		
					a	b	c
Pb/Acid	38 to 45	80 to 100	75	750	43	9	400
Bipolar	50	275	85	750	80	0	0
Ni/Fe	48 to 56	75 to 110	58	1500	100	12	800
Ni/Zn	60	155	70	600	130		
Zn/Br_2	40 to 67	52 to 94	46	750	20	10	700
Zn/Cl_2	42 to 89	80 to 115	48	1500	10	45	1150
Fe/Air	52 to 109	102 to 146	50	500	8	25	700
Li/FeS	72 to 102	90 to 107	60	750	70	10	750
Na/S	73 to 121	129 to 220	66	750	25	45	1000
Al/Air	158	157	18	NA[b]	0	42	0

[a]All cost estimates are Original Equipment Manufacturer (OEM) costs in 1982 dollars. Battery costs represent the lower bound of the AV Battery Review Board estimates, OEM Cost = a x kWh + b x kW + c.

[b]Not applicable.

2. Energy-Conversion Subsystems

a. Fuel Cells/Methanol. The purpose of the fuel-cell investigations was to assess various cell types and fuel alternatives that are applicable to AV systems. This task is made difficult by the lack of vehicle-size fuel cells in operation, thereby establishing the need to authenticate their potential, to identify technical data deficiencies, and to establish developmental priorities. Although several types of cells and fuels were originally considered, the decision was made to focus on three fuel-cell study contracts issued by the Los Alamos National Laboratory (LANL), which specifically targeted the vehicle application with methanol fuel. Phosphoric acid fuel cell (PAFC) designs were prepared by the United Technologies Corporation (UTC) and the Energy Research Corporation (ERC). ERC also reported on an advanced acid design, trifluoromethane sulfonic acid (TFMSA). The General Electric Company (GE) designed a system based on their solid polymer electrolyte (SPE) technology.

All of the systems are based on the use of methanol and air as reactants to get the hydrogen and oxygen necessary for the cell stack. LANL specified

Table 1-2. Characteristics of Mechanical Peaking Devices

Peaking device	Specific energy,[a] Wh/kg	Energy density,[a] Wh/l
Composite flywheel	20 to 40	20 to 40
Hydraulic accumulator	3 to 5	1 to 5
Compressed air[b]	20 to 40	5 to 15
Others[c]	NA	NA

[a]The values include only the energy-storage subsystem (i.e., transmissions, turbines, pumps, etc., are not included because they are sized for power).

[b]Based on using heated air from a heat engine; includes only storage tanks. The specific energy would drop to about 5 Wh/kg with ancillary components.

[c]Elastomers, liquid springs, and linear solids are projected to be less than 2.2 Wh/kg and were, therefore, eliminated from further consideration.

20-kW systems (60-kW peak). Comparisons of the results of the design studies are shown in Table 1-3.

Design studies, although not verified with hardware, indicate that the proposed fuel-cell designs are compatible with the LANL requirements in terms of weight, volume, and power demands. However, substantial developments (i.e., technical breakthroughs) are required to produce systems that exhibit the performance shown. The studies also indicate data deficiencies or uncertainties with respect to start-up, sustained peak power, transients, fuel-purity requirements, and cool-down rates. The projected costs of the systems are extremely high, relative to currently available heat engines.

b. Heat Engines/Nonpetroleum Fuels. The heat-engine assessment was undertaken to assess major nonpetroleum fuel effects on characteristics of engines representative of production engines of the 1990s, to identify unique requirements for engines in hybrid vehicle applications, and to compare alternatives. The approach was to assess the effects of nonpetroleum fuels (including methanol, ethanol, natural gas, and ammonia) on existing maps of developmental and production engines. The engine maps were chosen to represent baseline generic production engines (i.e., scaleable for engine size) in the time period of interest.

Table 1-3. Preliminary Fuel-Cell Design Characteristics[a]

Design characteristics	GE SPE[b]	UTC PAFC[c]	ERC PAFC[d]	ERC TFMSA[e]
Specific power, W/kg				
Continuous	131	80	88	93
Peak	431	240	269	329
Power density, W/l				
Continuous	59[f]	59[g]	59[g]	46[h]
Peak	194[f]	176[g]	179[g]	162[h]
Projected energy efficiency,[i] %	51	56	60	40 to 45
Cold start-up time, min	1 to 3	5 to 7	10 to 12	3

[a] 96-Vdc, 20-kW continuous system designs.

[b] Solid polymer electrolyte (General Electric).

[c] Phosphoric acid fuel cell (United Technologies Corporation).

[d] Phosphoric acid fuel cell (Energy Research Corporation).

[e] Trifluoromethane sulfonic acid (Energy Research Corporation).

[f] Component volume of 0.12 m^3 with 34% packing factor.

[g] Component volume of 0.23 m^3 with 60% packing factor.

[h] Component volume of 0.26 m^3 with 60% packing factor.

[i] At continuous rating.

The choices were made to take advantage of unique attributes for advanced vehicles (i.e., high-compression for the anti-knock properties of the alternate fuels, rotaries, and turbocharged engines for packaging compression-ignition for idle fuel economy). The Stirling and Brayton engines are advanced technology candidates but are not considered baseline production engines in the early 1990s.

The engine map conversion considered major fuel effects only and assumed constant mechanical efficiency with gasoline and alternate fuels. The spark-ignition engines chosen are controlled by throttling the air intake rather than the fuel flow as in the case of direct-injection, stratified-charge engines; further adjustments are required to approach the technology of the 1990s. For example, a 35% improvement in spark-ignition engine fuel economy and 20% improvement in compression-ignition engine fuel economy are expected over the present technologies. The projections for alternate-fueled

engines (Table 1-4), illustrate the differences between the nonpetroleum fuels, gasoline, and diesel.

The problems with heat engines in hybrid operation are magnified by the nonpetroleum fuels. Specifically, the alcohol-fueled (methanol and ethanol) engines are expected to have trouble starting, experience excessive wear (without new lubricants), and have potential emission problems. The primary disadvantage of methane is related to the storage problems.[1] Ammonia is the least desirable of the nonpetroleum fuels considered because the engines could experience up to 30% reduced engine speed and power output unless a specific engine is designed for this fuel. Storage and toxicity of ammonia are also significant problems.

Further research is required with respect to on/off hybrid operation in general, with a focus on excessive wear problems and transient emissions. Compression-ignition engines require investigation of alternate fuel/injection system compatibility, pilot fuels, and fuel improvements (additives).

3. Powertrain Components

The purpose of this assessment is to characterize critical powertrain components potentially available for use in the 1990s period. Specifically, the brush-type, dc-drive systems versus the dc brushless drives and inverter/ac-induction drives (and related ancillary components) now under development were reviewed as well as advanced transmissions. Important considerations are that (1) the motor/controller/transmission is a system, (2) optimality requires simultaneous design, and (3) the motor produces the electrical constraints. Another factor is that processor (i.e., controller) technology is in a state of rapid flux relative to motor technology.

Table 1-4. Projected Heat-Engine/Nonpetroleum Fuel Characteristics

Characteristics	Methanol	Ethanol	Methane	Ammonia
Thermal efficiency relative to gasoline	1.22	1.18	1.15	1.22
Specific fuel consumption relative to gasoline	1.81	1.38	0.77	1.92
Thermal efficiency relative to diesel	1.0	1.0	1.0	1.0
Specific fuel consumption relative to diesel	2.14	1.60	0.86	2.31

[1] Methane and ammonia are gaseous at standard temperature and pressure (STP).

The likely preferred system is a modulating-inverter, ac-induction drive. This choice is based primarily on the momentum of the already intensive industrial development. Hence, AV system development should be on a spin-off basis focusing on specific systems designs, inverter algorithms, topologies, and packaging. Tables 1-5 and 1-6 summarize the most probable system characteristics in the period of interest.

4. Vehicle Subsystems

This effort considered the "non-propulsion" vehicle characteristics, which affect the overall system performance even though they are not the central concern of the AV study. The factors include vehicle mass (and reduction thereof), aerodynamic drag, rolling resistance, and accessory loads. Baseline characteristics for conventional vehicles of the 1990s were established, and the more exotic alternatives were investigated (i.e., all-aluminum or advanced composite body and chassis). The characteristics in Table 1-7 summarize the baseline internal-combustion engine (ICE) characteristics (from which the AVs are derived) to be used in the system investigations. These values are not the most optimistic assumptions but represent an attempt to use realistic fleet characteristics.

Table 1-5. Comparison of Powertrain Components

Component	Specific power, W/kg[a]		
	DC brush	DC brushless	AC induction
Motor	150 to 225	330 to 1000	455 to 525
Controls	350 to 525	500 to 1250	2000 to 3000
Gearing	400 to 1000	400 to 1000	400 to 1000

[a]Continuous rating (one-half peak ratings assumed).

Table 1-6. Comparison of Overall Powertrain System Characteristics

Characteristics	System		
	DC brush	DC brushless	AC induction
Specific power, W/kg[a]	85 to 135	130 to 360	190 to 310
Efficiency, %	78 to 89	77 to 87	77 to 87

Table 1-7. Advanced Vehicle Baseline Internal-Combustion Engine Characteristics

Characteristics	Van	2-P[a]	4-P	5-P
Curb weight, kg	1080	500	670	895
Frontal area, m^2	2.50	1.70	1.85	2.00
Effective drag coefficient				
With radiator	0.47	0.32	0.32	0.32
Without radiator	0.45	0.30	0.30	0.30
Rolling resistance coefficient	0.011	0.01	0.01	0.01

[a]Denotes passenger capacity (two-, four-, five-passenger).

SECTION II

ENERGY-STORAGE SUBSYSTEMS

A. BATTERIES

The technologies of interest to this assessment include the aqueous-mobile, electrolyte-flow, high-temperature, and metal-air batteries. These technologies are in various states of development, ranging from electrode/cell experimentation to in-vehicle, developmental battery packs. Therefore, the primary effort of this task has been to assess the potential of these batteries within the next 10 years, based on extrapolation from present designs and concepts. The projections of this report (for complete battery packs) have been based on assessing the current status, identifying fundamental barriers to maturity, and estimating the possibility of overcoming these deficiencies in the next decade (1990s).

The approach to assessing the batteries was to use an independent team from outside JPL (referred to in this report as the AV Battery Review Board or "Board")[2] to project performance and cost characteristics, based on their best judgment and reports prepared by several battery developers, which describe specific designs for AV applications (design targets specified by JPL). Projections varied within the Board (especially regarding cost), and the range of estimates is presented in this section. The developers' projections varied from the Board as well, and their reports are included in total in Volume V (Appendices) for reference. The vehicle systems analyses and recommendations of Volume III (as well as the Executive Summary, Vol. I) are based on the projections of the Board, but the Sensitivity Analyses section of Volume III includes vehicle designs and comparative analyses based on the developers' projections.

The Board was asked to project the specific power and energy characteristics in addition to the Original Equipment Manufacturer (OEM) cost estimates, cycle life, relative maintenance, relative safety, efficiency, and salvage value. The projections were to be made for batteries designed for four different power-to-energy (P/E) ratios[3] defined by JPL (e.g., 1.0, 2.1, 2.4, and 3.3), which are specific to the AV applications under consideration. The battery section is a synopsis of their assessment; however, the reader should be aware of the speculative nature of this effort (concerning both the Board and the battery developers). Therefore, the battery projections are followed by a discussion of selling-price estimates, prepared by a member of the Board, which illustrate the differences between the projections of the various parties involved and the factors to consider in evaluating the feasibility of the projections.

---

[2]See Battery Consultants in Acknowledgment for list of members.

[3]P/E = 30-s specific power at 10% state of charge divided by the specific energy yielded if discharged at 20 W/kg.

1. Lead/Acid Batteries

a. Introduction. The lead/acid couple is among the oldest of all electrochemical couples, with a history dating back to 1859. It has been in practical use for more than a century and has been the most widely used of any battery system. Experience with electric vehicles (EVs) on the road has been almost totally with lead/acid batteries. Interest in continued development of this battery for EVs has not been extensive because of the low theoretical specific energy, but it represents the most viable system for limited-range missions within the near future. The electrode reactions, cell reaction, and cell potential are as follows:

$$\text{Negative:} \quad SO_4^{--} + Pb = PbSO_4 + 2e^-$$

$$\text{Positive:} \quad 2e^- + SO_4^{--} + 4H^+ + PbO_2 = PbSO_4 + 2H_2O$$

$$\text{Cell:} \quad 4H^+ + 2SO_4^{--} + PbO_2 + Pb = 2PbSO_4 + 2H_2O \ ,\ldots, \ E^o = 2.041 \text{ V}$$

The electrochemistry of the system is unique in that the same discharge product is formed at both electrodes.

There is some evidence to indicate that the optimum operating temperature of lead/acid batteries is above room temperature for maximum cycle life. This claim is controversial; however, elevated temperature definitely improves both power and energy characteristics. A thermal management system will undoubtedly be needed for optimum, overall performance.

An additional characteristic of the lead/acid system is the strong relationship between specific energy and rate of discharge. In addition, the peak-power capability strongly depends on the depth of discharge, a significant disadvantage in current designs of EV batteries.

The lead/acid couple has been used in a wide variety of applications; consequently, there are many variations in the designs. This assessment is concerned only with EV batteries, but it is worth noting that some of the design features of other batteries may eventually be incorporated into EV designs.

Alternatives to the conventional flat-plate and tubular designs have been under development for some years. These include the use of a "pulsed" electrolyte (to avoid acid stratification), lead-plastic composite grids (to reduce weight), and more recently the use of "flow through" electrolyte, which is projected to improve performance substantially during the latter part of discharge.

Deep-cycle batteries ordinarily use lead/antimony alloy grids because antimony is believed to play a necessary role in extending life cycle in batteries subjected to repeated deep discharges. However, recent results obtained in the testing of sealed deep-cycle photovoltaic batteries with non-antimonial positive grids, developed by Eagle Picher Industries (EPI), have shown that at low discharge rates, cycle lives of 1000 deep cycles can be obtained. This finding is likely to have implications in the development

of sealed lead/acid batteries for EV applications. The sealed cell or battery concept minimizes acid stratification without the complications of electrolyte circulation and should lead to greatly improved safety and reduced maintenance requirements as well as to allow more flexibility in packaging (e.g., horizontal electrodes).

b. Performance Projections. The Board projections for the performance of an improved conventional battery and for a completely redesigned battery are shown in Tables 2-1 and 2-2.

Table 2-1. Specific Energy (in Wh/kg) as a Function of Power-to-Energy Ratio and Power Density

Projections	P/E ratio	Power density, W/kg		
		20	60	100
A	1.0	45	31	NA
B	2.1	43	31	18
C	2.4	41	31	20
D	3.3	38	31	22
E	3.3	50	46	41

Table 2-2. Specific Power (in W/kg) as a Function of Power-to-Energy Ratio and State of Charge

Projections	P/E ratio	State of charge, %		
		50	30	10
A	1.0	120	105	80
B	2.1	135	115	90
C	2.4	135	115	90
D	3.3	145	125	100
E	3.3	400	325	200

The projections labeled A, B, C, and D in Tables 2-1 and 2-2 represent batteries based on improvements to the Globe Union ISOA (pulsed electrolyte) technology. Projection E shows the performance values the Board believes may be achievable with a sealed bipolar battery. Table 2-3 shows projections for the volume and mass density of batteries based on these technologies.

c. Original Equipment Manufacturer Cost. At this time, it is not possible to estimate the cost of the sealed technology with certainty due to the lack of public information concerning specific designs. At any rate, the OEM cost has been estimated at $80/kWh for the purposes of this study. On the other hand, the ISOA technology is well defined, and the cost projections of Table 2-4 include some consideration of scale and auxiliary requirements.

The values marked "A" in Table 2-4 represent the projected costs made collectively by the Board. The values marked "B" result from a more detailed analysis by one Board member (see Section II-A-10) for the conventional battery. The analogous value for the bipolar battery represents an arbitrary range of estimates for this emerging technology.

d. Other Characteristics. Table 2-5 shows the projected values of the other parameters that influence life-cycle costs and acceptance of the two technologies considered.

Table 2-3. Battery Volume and Mass Density (in liters/kg per liter)

Technology	Battery size, kWh/kW			
	50/50	12/25	25/60	15/50
Improved ISOA	505/2.2	127/2.2	277/2.2	179/2.2
Sealed bipolar	454/2.2	121/2.2	253/2.2	162/2.2

Table 2-4. Initial Battery Cost (OEM Cost in 1982 Dollars)

Technology	Battery size, kWh/kW							
	50/50		12/25		25/60		15/50	
	A	B	A	B	A	B	A	B
Improved ISOA	2800	3250	1300	1750	2000	2400	1580	2000
Sealed bipolar	4000	6000	960	1440	2000	3000	1200	1800

Table 2-5. Other Lead/Acid Battery Characteristics

Technology	Cycle life[a]	Relative maintenance,[b] 1 to 5	Efficiency,[c] %	Salvage, $/kWh	Relative safety,[d] 1 to 10
Improved ISOA	750	2	75	1.66	10
Sealed bipolar	750	1	75	1.66	10

[a]Equivalent full discharges.

[b]Expressed as figure of merit (1 = minimum maintenance).

[c]Based on average 29 mi per 24-h travel.

[d]Expressed as figure of merit (Baseline ICE vehicle-6), sealed technology assumed.

e. Development Assumptions. The projections made by the Board for improved ISOA-type, lead/acid batteries represent a substantial improvement in both performance (energy and power) and cycle life over what has been demonstrated under realistic conditions to date. The following key developments will be required to achieve the projected values:

(1) Improved active material utilization, especially at high rates of discharge.

(2) Significant reduction in grid weight (e.g., through the use of composite grids).

(3) Improved specific power toward the end of discharge.

(4) Reduction in battery volume, achieved through specific energy improvements.

(5) Cost reductions arising from improved performance and adoption of SLI-type[4] manufacturing processes.

(6) Cycle-life improvements with regard to capacity, maintenance, and power capability; reduced shedding and positive grid corrosion.

[4]Starting, lighting, and ignition (i.e., automotive-type battery).

(7) The successful demonstration of reliable pumps, central point-watering and thermal management systems.

Each of these improvements will be needed to achieve the projected performance, life, and cost values; however, in many cases the improvement in one parameter (e.g., specific energy) can lead to a reduction in another (e.g., life).

Projections for the sealed bipolar battery are far more uncertain than those discussed above. A number of key developments will be needed to demonstrate a practical bipolar system for EV application:

(1) High-conductivity, corrosion-resistant bipolar membrane.

(2) Development of reliable intra-cell sealing.

(3) Improved active material use.

(4) Demonstration of adequate cycle life in bipolar configuration.

(5) Demonstration of effective heat dissipation, especially during charge.

Although the projections for the bipolar system are most attractive for a lead/acid technology, the system is still at an early stage of development and is unlikely to be demonstrated as a full-size battery for some considerable time (but could be developed in the period of interest).

The lead/acid battery has many inherent characteristics that are especially well suited to EV applications:

(1) Low cost.

(2) High energy efficiency.

(3) High specific gravity (minimizing volume).

(4) High power density.

(5) Ease of thermal management.

In its present state of development the system is unlikely to find extensive application in general-purpose vehicles. Nevertheless, the Board expressed the opinion that through new technical approaches (e.g., the sealed bipolar design) the major constraints of the system as presently demonstrated are likely to be overcome, given adequate support for the technology.

2. Nickel/Iron Batteries

a. Introduction. The use of the nickel/iron (iron/nickel oxide) couple dates back to Edison near the turn of the century. The physical

design of the Edison cells, with the nickel oxide mixed with flaked nickel for a conductor and placed in perforated steel tubes, resulted in batteries with extremely long lives. These batteries were also very rugged, both mechanically and electrically, as they could be discharged to the point of cell reversal without damage. It was recognized that the theoretical energy density for this couple is about 33% higher than for lead/acid, and it seemed to be an attractive possibility to power electric vehicles. Research and development on EV-type nickel/iron batteries has been carried out in Japan and several countries in Europe. In the United States, Eagle Picher Industries is the only active developer of the technology for EV applications.

The electrode reactions, cell reaction, and cell potential include the following:

$$\text{Negative:} \quad 2OH^- + Fe = Fe(OH)_2 + 2e^-$$

$$\text{Positive:} \quad 2e^- + 2NiOOH + 2H_2O = 2Ni(OH)_2 + 2OH^-$$

$$\text{Cell:} \quad Fe + 2NiOOH + 2H_2O = Fe(OH)_2 + 2Ni(OH)_2 \text{ ,...., } E^o = 1.35 \text{ V}$$

EPI is pursuing a high-performance approach, which uses sintered nickel positive electrodes and negative electrodes developed by the Swedish National Development Company. Cost reduction is being addressed by the use of fewer, thicker electrodes. EPI has developed techniques for making nickel electrodes up to 3-mm thick, using the continuous wet-slurry method. Previously, electrodes made by this method were limited to thicknesses of 1 mm or less. The Swedish iron electrode uses a sintered iron plaque. It is a high-performance electrode that overcomes the poor low-temperature performance previously characteristic of the nickel/iron battery.

The most important advantages of the EPI approach are the long cycle life, tolerance to cell reversal, and a favorable power-to-energy ratio. Disadvantages of this couple include the low gassing overvoltages at the iron electrode, resulting in a high self-discharge rate and substantial hydrogen generation, especially close to full charge and at elevated temperatures.

EPI nickel/iron batteries are now in an advanced stage of development; full-size battery packs have been operated successfully in a number of in-vehicle field tests.

b. Performance Projections. Tables 2-6 and 2-7 show the projections of Ragone characteristics and specific peak power made by the Board.

The values are based on EPI technology with the assumption that marginal improvements will be made in cell performance and that batteries will be designed and built to the specific P/E ratio requirements.

The projections for battery volume for each of the four applications are shown in Table 2-8.

Table 2-6. Specific Energy (in Wh/kg) as a Function of Power-to-Energy Ratio and Power Density

P/E ratio	Power density, W/kg		
	20	60	100
1.0	56	44	NA
2.1	54	48	36
2.4	52	46	36
3.3	48	44	38

Table 2-7. Specific Power (in W/kg) as a Function of Power-to-Energy Ratio and State of Charge

P/E ratio	State of charge, %		
	50	30	10
1.0	120	105	75
2.1	141	120	90
2.4	141	120	90
3.3	160	140	110

Table 2-8. Battery Volume and Mass Density (in liters/kg per liter)

	Battery size, kWh/kW			
	50/50	12/25	25/60	15/50
Volume, liters	496/1.8	123/1.8	267/1.8	174/1.8

c. Original Equipment Manufacturer Cost. The Board's projections for OEM cost are given in Table 2-9.

The values marked "A" in Table 2-9 represent the projected costs made collectively by the Board. The values marked "B" result from a more detailed analysis by one Board member (see Section II-A-10).

d. Other Characteristics. Table 2-10 shows the projected values of the other parameters that influence life-cycle costs and acceptance of the nickel/iron technology.

Table 2-9. Initial Battery Cost (OEM Cost in 1982 Dollars)

	Battery size, kWh/kW							
	50/50		12/25		25/60		15/50	
	A	B	A	B	A	B	A	B
Battery cost	6400	5800	2300	2000	4020	3600	2900	2900

Table 2-10. Other Nickel/Iron Battery Characteristics

Characteristics	Value
Cycle life[a]	1500
Relative maintenance,[b] 1 to 5	2.5
Efficiency,[c] %	58
Salvage, $/kWh	6.56
Relative safety,[d] 1 to 10	7

[a]Equivalent full discharges.

[b]Expressed as figure of merit (1 = minimum maintenance).

[c]Based on average 29 mi per 24-h travel.

[d]Expressed as figure of merit (baseline ICE vehicle-6).

a. Development Assumptions. Presently available nickel/iron EV batteries do not show all the characteristics given in the previous section. In making their projections, the Board assumes improvements will be made in the following key areas:

(1) Use of thicker electrodes (i.e., greater fraction of active material weight) to improve specific energy and reduce cost.

(2) Some improvement in peak specific power despite use of thicker electrodes.

(3) Development of a reliable and safe water and gas management system for batteries.

(4) Reduction of amount of overcharge while maintaining high specific energy to increase the efficiency and reduce watering.

(5) Implementation of proposed cost reductions in large-scale battery manufacturing.

It will be necessary to achieve these key developments while still maintaining the excellent cycle life demonstrated to date.

With the exception of improved ISOA batteries (lead/acid), EPI nickel/iron batteries are in the most advanced stage of development of those considered in this review. Compared with lead/acid batteries, the system offers a somewhat higher specific energy (especially under actual driving conditions), slightly better peak-power capabilities, and a much longer cycle life under actual-use conditions. On the other hand, nickel/iron batteries with sintered plates will always be substantially more costly than lead/acid batteries. Indeed, the achievement of the first-cost projections and of the other factors affecting life-cycle cost should be a first priority in nickel/iron battery development.

3. Nickel/Zinc Batteries

a. Introduction. The nickel/zinc battery was not addressed by the AV Battery Review Board due to the lack of a battery subcontractor report and general acceptance of the currently available performance data (of the General Motors Delco Remy battery) as typical of the performance of a production battery of the future. This section was adapted from a previous JPL internal report, updated to be consistent with the latest performance information. Only one P/E ratio design was considered, that of the present system.

Early in the electric vehicle program it was recognized that the nickel/zinc couple has several characteristics that make it an attractive candidate for powering electric vehicles. Although the nickel/zinc cell has not been used previously, there had been a considerable history of cells with nickel/oxide electrodes (e.g., nickel/cadmium and nickel/iron) and cells with zinc electrodes (e.g., silver/zinc, mercury/zinc, and the so-called "carbon/zinc," or zinc/manganese dioxide). But these cells with zinc electrodes were

almost always primary (i.e., non-rechargeable) cells. Some silver-zinc cells had been made which were rechargeable, but the cycle life of these cells under deep-discharge conditions was quite limited.

The reason for taking the nickel-oxide electrode from the nickel/cadmium and nickel/iron experience, and zinc electrodes from the cells named above with zinc electrodes, was that cadmium, silver, and mercury were too expensive for EV application, manganese dioxide is almost non-rechargeable, and the theoretical energy density of nickel/zinc is attractive (superior to that of nickel/iron). The most obvious problem was to develop a zinc electrode that could withstand the required number of deep-discharge cycles. The problem has not been adequately solved, and lifetimes approaching that of nickel/iron cannot be foreseen at this time.

A variety of manufacturers have attacked the development of the nickel/zinc technology, including DOE-sponsored programs at Gould, the Energy Research Corporation, and Exide. Other efforts include a program at Yardney that was formerly sponsored by DOE and privately funded programs at the Delco Remy Division of General Motors Corporation, Eagle Picher, and the Electrochimica Corporation.

The electrode reactions and cell reaction are given below:

Negative: $Zn + 2OH^- \quad ZnO + H_2 + 2e^-$

Positive: $NiOOH + H_2O + e^- \quad Ni(OH)_2 + OH^-$

Cell: $2NiOOH + H_2O + Zn \quad 2Ni(OH)_2 + ZnO, \; E^o = 1.75 \; V$

There are several problems with zinc electrodes, and most are related to one fundamental characteristic: the high solubility of ZnO in strong alkaline solution with the formation of zincate ion, $HZnO_2$. This solubility results in dendrites, shape change, zinc migration, and capacity loss.

There is an additional zinc electrode problem, passivation, which is not caused by the solubility of ZnO. The most common attempts to eliminate dendrites have been separators that are more resistant to penetration. Separators have also been made that have a high degree of ion selectivity, in which the ratio of mobility of hydroxyl ion to zincate ion is maximized.

The development of the nickel/zinc battery has been proceeding outside the DOE program at the Delco Remy Division of General Motors Corporation since 1977. By any measure except specific energy, their present battery is superior to any of the other Ni/Zn candidates tested previously at JPL or Argonne National Laboratory (ANL).

The GM battery is unusual in several respects. First, the cell is flooded with electrolyte, yet the cell is "sealed." This unusual characteristic is achieved by careful charge control. In terms of performance, proper attention has been paid to the power-to-energy relationship, and the result is a favorable ratio of about 2.6. The cycle life of the battery is remarkable when compared to the best results of the Ni/Zn batteries tested by ANL (200 cycles at 80% depth of discharge to 75% of initial capacity), having achieved 300 cycles to 100% depth of discharge

(60% of initial capacity at the end of life). The goal of their program is 600 cycles under similar circumstances.

b. Performance Projections. The GM Delco-Remy battery is the most advanced of its type to date. The capabilities of high power and energy relative to current lead/acid technology, as well as the "stiff" energy characteristic (low sensitivity of energy capacity to discharge rate), make the battery attractive for EV applications.

The discharge characteristics and 30-s peak-power capabilities for nickel/zinc batteries are shown in Tables 2-11 and 2-12, respectively.

Table 2-13 shows the projections for volume of the various batteries.

c. Original Equipment Manufacturer Cost. Production cost is not one of the advantages of nickel/zinc batteries, with the selling price to the consumer estimated by GM to be about $200/kWh. Using the convention of a 50% markup over OEM cost implies about $130/kWh OEM. This would imply the costs of Table 2-14.

The values marked "A" in Table 2-14 represent the costs based on $130/kWh, while the "B" value represents an arbitrary uncertainty of 10%.

d. Other Characteristics. Table 2-15 shows the projected values of other parameters that influence life-cycle costs and acceptance of the nickel/zinc technology.

Table 2-11. Specific Energy (in Wh/kg) as a Function of Power-to-Energy Ratio and Power Density

	Power density, W/kg		
P/E ratio	20	60	100
2.6	60	58	53

Table 2-12. Specific Power (in W/kg) as a Function of Power-to-Energy Ratio and State of Charge

	State of charge, %		
P/E ratio	50	30	10
2.6	204	185	155

Table 2-13. Battery Volume and Mass Density (in liters/kg per liter)

	Battery size, kWh/kW			
	50/50	12/25	25/60	15/50
Volume, liters	500/1.7	120/1.7	250/1.7	190/1.7

Table 2-14. Initial Battery Cost (OEM Cost in 1982 Dollars)

	Battery size, kWh/kW							
	50/50		12/25		25/60		15/50	
	A	B	A	B	A	B	A	B
Battery cost	6500	7150	1560	1720	3250	3575	1950	2145

Table 2-15. Other Nickel/Zinc Battery Characteristics

Characteristics	Value
Cycle life[a]	600
Relative maintenance,[b] 1 to 5	1.5
Efficiency,[c] %	70
Salvage, $/kWh	10.23
Relative safety,[d] 1 to 10	9

[a]Equivalent full discharges.
[b]Expressed as figure of merit (1 = minimum maintenance).
[c]Based on average 29 miles per 24-hour travel.
[d]Expressed as figure of merit (baseline ICE vehicle-6).

e. Development Assumptions. The "sealed" design of the GM battery is highly desirable in a consumer EV and, as such, will require no service by the operator of the vehicle. However, the battery pack must be watered about once a year by a dealer. This sealed, yet flooded, electrolyte design requires careful charging to keep the gassing rate lower than the internal recombination rate.

Another operational concern of this battery is the low efficiency and low charge acceptance at elevated temperatures. In fact, the GM system includes air cooling (2,200 l/min) to lower the battery temperature below a critical temperature before starting the charge automatically. This could be a problem in hot climates where the ambient temperature is not much lower than that of the battery (i.e., the charger might not turn on in time to charge the battery sufficiently for the next intended use of an EV powered by a nickel/zinc battery).

The GM nickel/zinc battery has proven its performance capabilities, but the practical issues of cost and life must be addressed. The key developments are listed below:

(1) Increased cycle life to at least 600 cycles.

(2) Demonstrate cost characteristics.

(3) Demonstrate reliability and low maintenance.

The important advantages and disadvantages have become evident during the time when the nickel/zinc EV battery has been under active development. Its advantages are specific energy and specific power high enough to be attractive for EV applications, but cost-to-energy and cost-to-power ratios are definitely unattractive. The importance of these high cost figures is magnified by the low cycle life attained to date. The prognosis for cycle life to compensate for the relatively high cost seems to be poor (in comparison with lead/acid).

4. Zinc/Bromine Batteries

a. Introduction. Batteries based on the electrochemical reactions of zinc and bromine have been under development over the past decade by Exxon, GEL, Inc., and ERC (formerly by Gould). The focus of the development work at ERC/Gould has been on stationary batteries. Little detailed performance data on the GEL batteries, which are said to be suitable for EV applications, have been published. As a result, this assessment was focused on the Exxon technology only.

The rationale for developing the zinc/bromine battery as an alternative system for EV applications was primarily based on the use of low-cost reactants, a high cell voltage, a specific energy comparable with that of the nickel/zinc system, and a high degree of electrochemical reversibility.

The principal electrode and cell reactions are as follows:

Negative: $Zn = Zn^{++} + 2e^-$

Positive: $Br_2 + 2e^- = 2Br^-$

Cell: $Zn + Br_2 = ZnBr_2$,..., $E^o = 1.76$ V

During the charge cycle, metallic zinc is deposited as a smooth film onto a carbon-plastic electrode from an aqueous solution of zinc bromide and hydrobromic acid. Bromide ions are oxidized to bromine, which is stored as a proprietary amine complex, a heavy, oily liquid. Complexing greatly reduces the concentration of free bromine in the solution, reducing the self-discharge rate. The bromine electrode is a high-surface-area carbon electrode.

The battery contains pumps for both the positive and negative loops for circulation during both charge and discharge. A valve in the bromine storage tank, which can be shut off when the battery is being charged or is not in use, can reduce the self-discharge rate. This practice limits the extent of self discharge to the amount of bromine contained within the bromine electrodes. A schematic of the system is shown in Figure 2-1.

The separator used to limit bromine diffusion to the zinc electrode is a microporous polyolefin material that is claimed to be low cost. However, even with this material, coulombic efficiencies are substantially less than 100%. The resistivity of the carbon-plastic electrodes is very high, necessitating a bipolar design to obtain adequate power levels. Exxon has developed techniques (shunt-current protection) to alleviate the deleterious effects, such as zinc dendrite growth into flow channels, from the shunt currents that occur in bipolar cell stacks with flowing electrolytes.

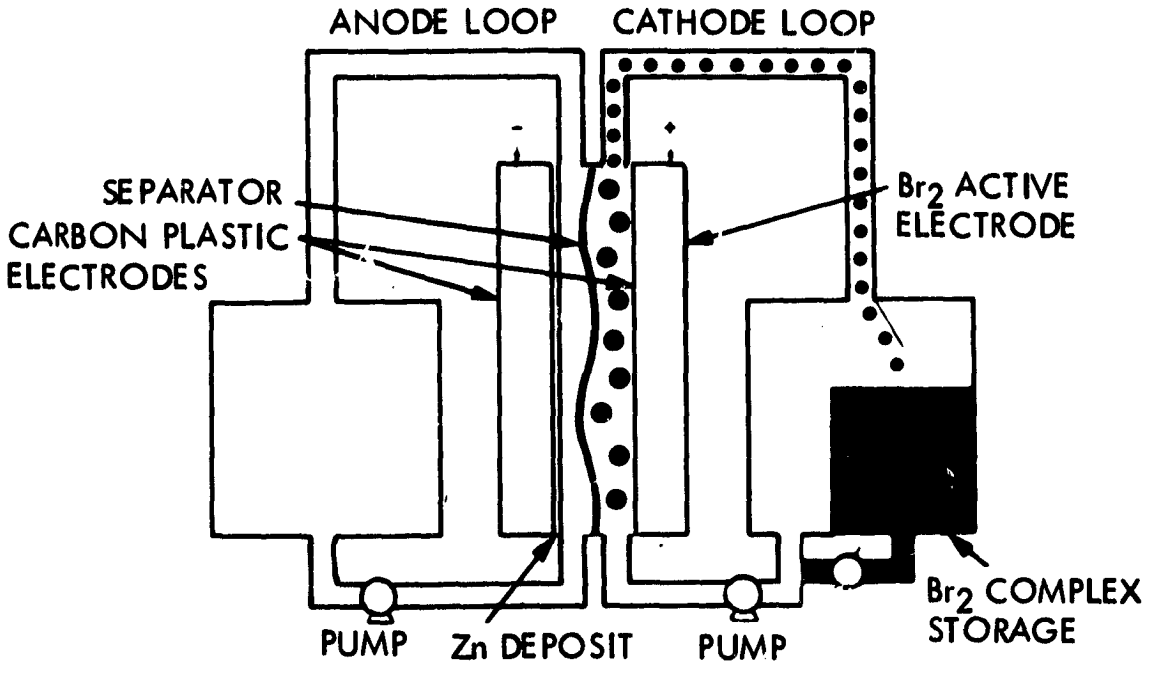

Figure 2-1. Zinc/Bromine Battery (Source: Exxon)

Exxon has been in the process of developing zinc/bromine batteries for almost a decade although their experience with some of the components of the system dates back considerably earlier. This development work has progressed to the point where relatively large zinc/bromine batteries have been assembled and tested. Both 10-kWh and 20-kWh batteries, incorporating somewhat different design details, have been tested during the past 2 years.

Exxon's experience with relatively large batteries makes the task of projecting the performance of improved zinc/bromine batteries somewhat more straightforward than it might otherwise be. However, it should be noted that the batteries that have been built and tested to date have not had the power capabilities that are believed to be needed for advanced EVs.

b. Performance Projections. The discharge characteristics and peak-power capabilities that were projected by the Board for improved zinc/bromine batteries are shown in Tables 2-16 and 2-17, respectively.

Table 2-18 shows projections for the volume of batteries based on the Exxon technology.

c. Original Equipment Manufacturer Cost. The projected cost of the batteries is shown in Table 2-19 for the four applications. The values marked "A" in Table 2-19 represent the projected costs made collectively by the Board. The range of values marked "B" result from a more detailed analysis by one Board member (see paragraph II-A-10).

d. Other Characteristics. Table 2-20 shows the projected values of the other parameters that influence life-cycle costs and acceptance of the zinc/bromine technology.

e. Development Assumptions. Although a few relatively large zinc/bromine batteries have been built by Exxon over recent years, many technology improvements will have to be made before the projections made by the Board can be realized. The key developments required are:

(1) Development of electrodes and other cell-stack components that will give stable energy and power over extended periods.

(2) Development of leak-free cell stacks and ancillary hardware.

(3) Improved power capability, specifically during extended high-rate discharge and at low states of charge.

(4) Improved coulombic efficiency during interrupted discharge.

Table 2-16. Specific Energy (in Wh/kg) as a Function of Power-to-Energy Ratio and Power Density

	Power density, W/kg		
P/E ratio	20	60	100
1.0	67	54	NA
2.1	48	42	32
2.4	49	44	35
3.3	40	36	29

Table 2-17. Specific Power (in W/kg) as a Function of Power-to-Energy Ratio and State of Charge

	State of charge, %		
P/E ratio	50	30	10
1.0	83	69	52
2.1	115	96	72
2.4	135	113	85
3.3	150	125	94

Table 2-18. Battery Volume and Mass Density (in liters/kg per liter)

	Battery size, kWh/kW			
	50/50	12/25	25/60	15/50
Volume, liters	550/1.36	220/1.4	400/1.28	300/1.25

Table 2-19. Initial Battery Cost (OEM Cost in 1982 Dollars)

	Battery size, kWh/kW							
	50/50		12/25		25/60		15/50	
	A	B	A	B	A	B	A	B
Battery cost	2200	2800/ 3500	1190	1800/ 2400	1800	2400/ 3100	1500	2100/ 2750

Table 2-20. Other Zinc/Bromine Battery Characteristics

Characteristics	Value
Cycle life[a]	750
Relative maintenance,[b] 1 to 5	4
Efficiency,[c] %	46
Salvage, $/kWh	2.0
Relative safety,[d] 1 to 10	4

[a]Equivalent full discharges.

[b]Expressed as figure of merit (1 = minimum maintenance).

[c]Based on average 29 miles per 24-hour travel.

[d]Expressed as figure of merit (baseline ICE vehicle-6).

(5) Improved shunt-current protection, especially in high-voltage cell stacks used for EVs.

(6) Development of efficient and reliable mechanical components such as pumps and thermal and electrolyte management systems.

The Board considered that the zinc/bromine system is among the more difficult batteries to develop for EVs. The complexity of the system, its low efficiency and large volume, together with unproven life in practical designs, contribute to the problems of developing this technology for EV applications.

The major positive feature of the Exxon technology is the relatively low projected cost in comparison with other advanced technologies.

5. Zinc/Chlorine Batteries

a. Introduction. The only major U.S. development program on zinc/chlorine batteries for EVs, or indeed for any application, is the one that has been underway since 1968 at Energy Development Associates (EDA), a subsidiary of Gulf & Western, and its corporate predecessors. The Board considered only this technology in making its projections for this system.

The zinc/chlorine electrochemical couple appeared attractive for EV applications because of its high theoretical specific energy, the highly reversible electrode reactions together with the low cost and aburdance of both zinc and chlorine. The electrode, cell, and store reactions are shown below:

$$\text{Negative:} \quad Zn = Zn^{++} + 2e^-$$

$$\text{Positive:} \quad Cl_2 + 2e^- = 2Cl^-$$

$$\text{Cell:} \quad Zn + Cl_2 = ZnCl_2 \text{ ,...., } E^o = 2.12 \text{ V}$$

$$\text{Store:} \quad Cl_2 \cdot xH_2O = Cl_2 + xH_2O \ (x = 6\text{-}8)$$

A schematic of the operation of the system is shown in Figure 2-2. As indicated, no separators are used in this design. During the charge portion of the operating cycle, a pump circulates the electrolyte, a solution of zinc chloride in water, through the unit. Direct current from an external electrical source is passed through the unit, and metallic zinc is deposited on the negative plates as a uniform, non-porous solid. Simultaneously, chlorine gas generated at the positive plates is carried away with the circulating electrolyte. Outside the plate area, the mixture of chlorine gas and electrolyte is cooled, and a pale yellow solid, chlorine hydrate, is formed. The solid chlorine hydrate is retained away from the plates, and the excess electrolyte is returned to the stack. The unit is fully charged when the hydrate store is full.

During discharge, the aqueous, zinc/chloride electrolyte is again circulated. This time it carries chlorine to the positive plates and permits current to be drawn from the system. As the resultant energy is withdrawn, zinc metal reacts at the negative electrode to form zinc ions. The warm electrolyte passes from the stack to the store, decomposing the chlorine hydrate. During discharge, the electrolyte increases in specific gravity due to the concentration of zinc chloride being added, and this sequence maintains the electrolyte concentration within an acceptable range.

Recirculating chlorine-enriched electrolyte to the stack sustains the electric current delivery reactions. Circulation continues until the chlorine hydrate in the store is dissipated, and the unit is discharged.

EDA has adopted a developmental approach that uses graphitic electrode materials that are readily available. Use of these materials has led them to

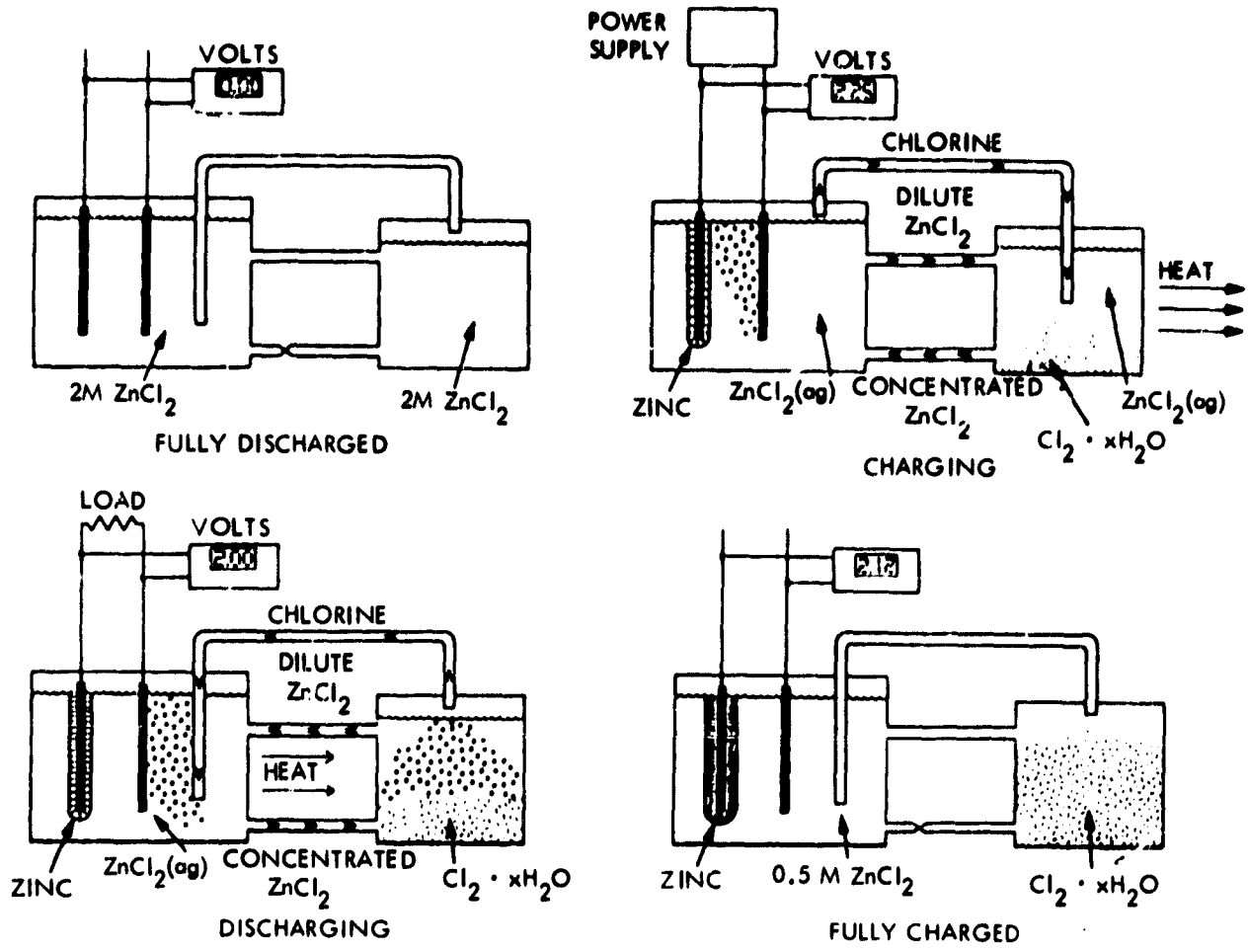

Figure 2-2. Zinc/Chlorine Battery System (Source: Energy Development Associates)

an unusual cell-stack arrangement, referred to as "comb-bipolar" design. In this design, the electrodes are relatively small but are assembled into unit cells that give extended-area bipolar electrodes. This allows shunt currents to be minimized and is said to give a minimum manufacturing cost within the limits imposed by the graphite materials used.

The system is complex, not only because of the chlorine-hydrate formation but also because inert gases must be safely removed for satisfactory operation. However, EDA has built a number of EV batteries and tested them in electric vehicles. Independent test and operational data on zinc/chlorine batteries have yet to be obtained.

b. Performance Projections. The Board projections for the performance of zinc/chlorine batteries for the various missions are shown in Tables 2-21 and 2-22.

Table 2-23 shows projections for the volume of batteries based on the above technology.

Table 2-21. Specific Energy (in Wh/kg) as a Function of Power-to-Energy Ratio and Power Density

P/E ratio	Power density, W/kg		
	20	60	100
1.0	89	78	NA
2.1	54	48	38
2.4	54	49	41
3.3	42	38	31

Table 2-22. Specific Power (in W/kg) as a Function of Power-to-Energy Ratio and State of Charge

P/E ratio	State of charge, %		
	50	30	10
1.0	86	84	80
2.1	110	103	90
2.4	127	121	110
3.3	130	128	115

Table 2-23. Battery Volume and Mass Density (in liters/kg per liter)

	Battery size, kWh/kW			
	50/50	12/25	25/60	15/50
Volume, liters	450/1.25	220/1.01	400/1.16	300/1.19

c. Original Equipment Manufacturer Cost. The projected cost of the battery systems for the four applications is shown in Table 2-24. The values marked "A" in Table 2-24 represent the projected costs made collectively by the Board. The values marked "B" result from a more detailed analysis by one Board member (see Section II-A-10).

d. Other Characteristics. Table 2-25 shows the projected values of the other parameters that influence life-cycle costs and acceptance of the zinc/chlorine technology.

Table 2-24. Initial Battery Cost (OEM Cost in 1982 Dollars)

	Battery size, kWh/kW							
	50/50		12/25		25/60		15/50	
	A	B	A	B	A	B	A	B
Battery cost	3900	4850	2400	2500	4100	4250	3550	3600

Table 2-25. Other Zinc/Chlorine Battery Characteristics

Characteristics	Value
Cycle life[a]	1500
Relative maintenance,[b] 1 to 5	4
Efficiency,[c] %	48
Salvage, $/kWh	0
Relative safety,[d] 1 to 10	4

[a]Equivalent full discharges.

[b]Expressed as figure of merit (1 = minimum maintenance).

[c]Based on average 29 miles per 24-hour travel.

[d]Expressed as figure of merit (baseline ICE vehicle-6).

e. Development Assumptions. The zinc/chlorine battery is one of the most complex battery systems of those under consideration for EV application. It requires many auxiliaries, including a separate storage compartment for chlorine, a refrigeration system, three heat exchangers, an electrolyte pump, a chlorine gas pump, a valve for charge, a valve for discharge, a check valve, and an ultraviolet lamp to prevent hydrogen buildup.

A number of key developments will be necessary before the performance and cost projections can be realized in a practical EV system.

(1) Greatly improved separation of the chlorine hydrate from the electrolyte on charge, giving reduced weight and volume for storage.

(2) Significant improvement in specific power capability without further loss in coulombic efficiency.

(3) Improved coulombic efficiency, especially during interrupted discharge (not so severe as with zinc/bromine).

(4) Development of lightweight, highly efficient auxiliaries.

(5) Verification that electrode material cost projections can be realized in practice.

(6) An appropriate manufacturing technology can be developed for battery production.

(7) Demonstration that the recharge after partial discharge capability of single cells can be scaled up to batteries.

(8) Demonstration that the complex system does not require excessive maintenance.

The Board considered that the zinc/chlorine battery is one of the more difficult batteries to develop for EVs, specifically on the grounds of perceived safety problems. However, this battery does offer a reasonably attractive specific energy with relatively low-cost active materials.

6. Iron/Air Batteries

a. Introduction. Westinghouse Electric Corporation initiated their development of the iron/air battery around 1967, preceding their nickel/iron R&D program by about 2 years. The original concept was a three-electrode system. In this system, separate air anodes and air cathodes were used for the charge and discharge portions of the cycle, respectively. However, it was concluded in the early 1970s that a truly bifunctional electrode would be needed in any practical battery design. By the mid-1970s bifunctional electrodes were indeed delivering 300 to 400 cycles. Later, sub-scale cells (100 cm^2) were operated successfully. The porous

sintered-iron electrode used in this battery is well developed, reliable, inexpensive and is not viewed as a major area of concern. The electrode reactions, cell reactions, and cell potential are shown below:

$$\text{Negative:} \quad 2OH^- + Fe = Fe(OH)_2 + 2e^-$$

$$\text{Positive:} \quad 2e^- + H_2O + 1/2O_2 = 2OH^-$$

$$\text{Cell:} \quad Fe + 1/2O_2 + H_2O = Fe(OH)_2 \text{ ,...., } E^o = 1.28 \text{ V}$$

The interest in the iron/air battery is due to its high specific energy and its use of inexpensive, readily available materials, except for a small amount of silver catalyst. The battery tolerates cell reversal and exhibits very little voltage decline with increasing depth of discharge.

The operating temperature is approximately 40°C and there is a 10% decrease in specific energy at 25°C, due to capacity losses in the iron electrode. Auxiliary heat may be required at ambient temperatures of less than 0°C, but this depends on the internal heating of the battery and the specific system design.

The energy efficiency of the iron/air battery is relatively low at ~50%. This is primarily due to the air electrode, which suffers from high-activation polarization on both charge and discharge, resulting in poor voltaic efficiency. However, the coulombic efficiency is close to 100%.

The iron electrode in the Westinghouse battery is similar to that of the EPI nickel/iron system. The advantages of this electrode include tolerance to overcharge and cell reversal. However, a major disadvantage is the high degree of gassing (as discussed in the section on nickel/iron batteries).

Despite the fact that work has been in progress since the late 1960s, there has been only limited effort on this system compared with other advanced batteries. In the past few years, however, the primary focus of the work has been the continued improvement of the bifunctional air electrode. To date, no full-size cell testing has been performed. However, five-cell, sub-scale modules were built and tested in the late 1970s that demonstrated a specific energy of 110 Wh/kg.

b. Performance Projections. Tables 2-26 and 2-27 show the Board's projections of specific energy and specific power for the iron/air system. It should be emphasized that the confidence level of these projected values is lower than for any other system considered in this study due to the battery's early stage of development.

Table 2-28 shows projections for the volume of complete iron/air battery systems based on the above technology.

c. Original Equipment Manufacturer Cost. The projections for the cost of complete battery systems for the four applications are shown in Table 2-29. The values marked "A" in Table 2-29 represent the projected costs

Table 2-26. Specific Energy (in Wh/kg) as a Function of Power-to-Energy Ratio and Power Density

P/E ratio	Power density, W/kg		
	20	60	100
1.0	109	100	82
2.1	68	63	54
2.4	68	64	56
3.3	52	49	43

Table 2-27. Specific Power (in W/kg) as a Function of Power-to-Energy Ratio and State of Charge

P/E ratio	State of charge, %		
	50	30	10
1.0	110	107	102
2.1	140	131	115
2.4	157	150	136
3.3	165	162	146

Table 2-28. Battery Volume and Mass Density (in liters/kg per liter)

	Battery size, kWh/kW			
	50/50	12/25	25/60	15/50
Volume, liters	338/1.36	158/1.12	338/1.09	274/1.05

Table 2-29. Initial Battery Cost (OEM Cost in 1982 Dollars)

	Battery size, kWh/kW							
	50/50		12/25		25/60		15/50	
	A	B	A	B	A	B	A	B
Battery cost	2400	3500/ 4400	1420	2700/ 3650	2400	3550/ 4450	2070	3300/ 4200

made collectively by the Board. The values marked "B" result from a more detailed analysis by one Board member (see Section II-A-10).

d. Other Characteristics. Table 2-30 shows the projected values of the other parameters that influence life-cycle costs and acceptance of the iron/air technology.

e. Development Assumptions. A number of key developments will have to be successfully implemented before the projections given above can be realized in a practical battery system:

(1) Successful development of long-lived, low-cost bifunctional air electrodes.

(2) Development and demonstration of practical cell designs (essential prior to realistic assessment of technology).

(3) Verification of low-cost production of sintered iron electrodes.

(4) Design, fabrication, and testing of a complete iron/air battery system.

(5) Development of reliable, low-cost auxiliaries.

The iron/air battery is one of the more promising technologies for EV application, but at the present time it is still in an early stage of development. The disadvantages are few but potentially serious. The high energy density is not likely to determine battery size in a system design because of its relatively low volumetric power density, which will also make packaging more difficult than with some other batteries. In addition, the low energy efficiency is unlikely to improve significantly in the near future.

Table 2-30. Other Iron/Air Battery Characteristics

Characteristics	Value
Cycle life[a]	500+
Relative maintenance,[b] 1 to 5	4
Efficiency,[c] %	40
Salvage, $/kWh	0
Relative safety,[d] 1 to 10	6

[a]Equivalent full discharges.

[b]Expressed as figure of merit (1 = minimum maintenance).

[c]Based on average 29 miles per 24-hour travel.

[d]Expressed as figure of merit (baseline ICE vehicle-6).

7. Lithium/Metal Sulfide Batteries

a. Introduction. The lithium/metal sulfide system has been under development by the Argonne National Laboratory, Eagle Picher Industries, Gould, Inc., and Rockwell International since 1972. At the present time, only Gould, Inc., and ANL are actively involved in developing this battery system.

The battery currently under development for EVs uses lithium/aluminum alloy negative electrodes (with small additions of lithium silicon to improve the capacity loading) and iron sulfide (FeS) positive electrodes. The electrolyte composition is currently the ternary mixture of lithium chloride, lithium fluoride, and lithium bromide, which melts at approximately 435°C and thereby defines the minimum operating temperature of the system. The electrode reactions, cell reactions, and cell potential are as follows:

$$\text{Negative:} \quad Li(Al) = Li^{+} + Al + e^{-}$$

$$\text{Positive:} \quad FeS + 2e^{-} = Fe + S^{--}$$

$$\text{Cell:} \quad 2Li(Al) + FeS = Li_2S + Fe + 2Al \ ,\ldots, \ E^{o} = 1.33 \text{ V}$$

The composition of the positive electrode at complete discharge of a stoichiometric cell would be Li_2S and iron, the aluminum remaining in the negative electrode. The lithium reacts with the aluminum on charge at an "underpotential" of approximately 200 mV, preventing the formation of lithium "dendrites" or lithium deposition on current collectors, etc. The result of

the choice of electrode materials is a relatively low open-circuit potential and a greatly reduced theoretical specific energy (460 Wh/kg, as in zinc/chlorine) compared with that of elemental lithium and sulfur. However, the use of the lower performance electrodes greatly simplifies the choice of cell design and the selection of low-cost materials of construction.

The use of the more energetic alternative solid positive electrode material, iron disulfide (FeS_2), is the focus of continuing R&D at ANL and elsewhere. This electrode material offers significant improvements in specific energy and specific power (during the first half of discharge, due to the higher voltage). However, it is less stable at elevated temperatures than FeS, and requires the use of molybdenum (or at least molybdenum-plated) positive electrode current collectors. The present study has made projections for the lower energy couple only, as this is the current focus of battery development activities, both in the United States and abroad.

Recent developments have indicated that the ternary electrolyte LiCl-LiF-LiBr seems more promising than the alternative LiCl-KCl electrolyte because of the problem of lithium chloride freeze-out during periods of high-rate discharge. The ternary electrolyte has the added benefit of preventing the formation of J-phase, a complex, irreversible compound containing potassium. Unfortunately, the ternary electrolyte has a significantly higher melting point than the binary materials (435°C versus 352°C).

The original cell design was a prismatic multi-plate system with a flooded electrolyte and a high-cost boron-nitride ceramic felt separator. Cells of this type fabricated by EPI have demonstrated long cycle lives (~1000 deep cycles) and good specific energy (approximately 90 Wh/kg). However, attempts to build batteries with these cells have shown the difficulty of totally retaining the electrolyte within the individual cells in a series array, resulting in premature short circuiting of the battery.

Developments at Gould, Inc., have demonstrated the attractive characteristics of an alternative immobilized electrolyte design with a high surface-area ceramic powder (MgO) acting as separator and electrolyte retainer. This cell design offers several advantages in terms of cost, improved electrolyte stability, and simplified cell construction. In addition, the operation is independent of orientation and therefore offers a greater flexibility of design. However, the MgO separator cells have yet to demonstrate the excellent cycle life of the earlier BN felt design.

A bipolar battery design is also currently being considered at Gould, Inc., as a means of improving power-density capability. Such a battery would be specifically suited to those applications (e.g., hybrid vehicle) where a high power-to-energy ratio is required. Such a design, also based on the powder separator, offers a marginal improvement in specific energy over the conventional monopolar design.

The main focus of efforts to date has been the development of reliable, low-cost, practical MgO separator cells. The near-term goal at Gould and ANL is to demonstrate battery sub-modules as a first step toward the fabrication and testing of full-size batteries.

The characteristics of this lithium battery are unique in many respects when compared to conventional EV batteries. The prime differences result from the high-temperature operation. The battery cannot operate below the electrolyte eutectic temperature, and the normal temperature is in the range of 425 to 475°C. Using the advanced vacuum multifoil insulation developed by the Linde Division of Union Carbide and by using the stored electrical energy in the battery to operate the internal electrical heaters, the battery should be able to stand for approximately two weeks (initially in the fully charged condition) without the electrolyte freezing.

Alternatively, without expending any of the stored electrical energy, the insulation should keep the electrolyte temperature above the eutectic point for about 2 days. Note that the battery does not "lose" the stored electrical energy by going through a freeze-thaw cycle (the coulombic efficiency remains almost 100%); however, external electrical energy must be used to heat the battery, once the electrolyte is frozen.

The battery also requires special attention for charging. The cells cannot be overcharged without being permanently damaged after only one occurrence. This is due to the irreversible plating of iron on the aluminum when charged above the 1.6-V limit. This requires a charging system that does not allow overcharging under any conditions. ANL has developed a charger that does just that by controlling the charge on a cell-by-cell basis and actually discharges any cell in danger of overcharge. The Li(Al)/FeS_x battery has the capability of accepting a relatively fast charge, with an estimated energy replacement of up to 75% capacity in 1 hour.

b. Performance Projections. The Board projections for the performance of the lithium/metal sulfide (Li/MS) battery system for the various applications are shown in Tables 2-31 and 2-32.

Table 2-33 shows projections for the volume of complete Li/MS battery systems based on the above technology.

Table 2-31. Specific Energy (in Wh/kg) as a Function of Power-to-Energy Ratio and Power Density

	Power density, W/kg		
P/E ratio	20	60	100
1.0	96	83	68
2.1	87	75	61
2.4	87	75	61
3.3	85	75	63

Table 2-32. Specific Power (in W/kg) as a Function of Power-to-Energy Ratio and State of Charge

	State of charge, %		
P/E ratio	50	30	10
1.0	161	126	98
2.1	165	140	90
2.4	165	140	90
3.3	175	137	107

Table 2-33. Battery Volume and Mass Density (in liters/kg per liter)

	Battery size, kWh/kW			
	50/50	12/25	25/60	15/50
Volume, liters	350/1.49	125/1.10	208/1.38	140/1.26

c. Original Equipment Manufacturer Cost. The projections for the cost of complete battery systems for the four applications are shown in Table 2-34. The values marked "A" in Table 2-34 represent the projected costs made collectively by the Board. The values marked "B" result from a more detailed analysis by one Board member (see Section II-A-10).

d. Other Characteristics. Table 2-35 shows the projected values of the other parameters that influence life-cycle costs.

e. Development Assumptions. To date, only single cells of the design assumed in making the projections have been built and tested. A number of key developments will be needed before the projections above will be realized in practical systems:

(1) Improvement in power density, especially toward the end of discharge.

(2) Optimized cell and battery hardware to give a higher specific energy.

Table 2-34. Initial Battery Cost (OEM Cost in 1982 dollars)

	Battery size, kWh/kW							
	50/50		12/25		25/60		15/50	
	A	B	A	B	A	B	A	B
Battery cost	5000	6100	1700	1900	3000	3700	2200	2250

Table 2-35. Other Lithium/Iron-Sulfide Battery Characteristics

Characteristics	Value
Cycle life[a]	750
Relative maintenance,[b] 1 to 5	2.5
Efficiency,[c] %	60
Salvage, $/kWh	2.0
Relative safety,[d] 1 to 10	9

[a]Equivalent full discharges.

[b]Expressed as figure of merit (1 = minimum maintenance).

[c]Based on average 29 mile per 24-hour travel.

[d]Expressed as figure of merit (baseline ICE vehicle-6).

(3) Demonstration that cells can be integrated into full-size batteries without significant loss of performance or reduction in life.

(4) Replacement of present nickel current collectors with lower-cost materials.

(5) Proof that low-cost, active materials (e.g., by assembly in discharged state) can be used to produce practical batteries.

(6) Demonstration of low-cost, high-performance insulation.

A number of advantages and disadvantages of the lithium/metal sulfide technology have emerged during the development programs. The strongest features of this battery are its projected specific energy and specific power in addition to its high volumetric energy density. The negative features are its high operating temperature and its reliance on relatively high cost and somewhat scarce lithium-based materials.

8. Sodium/Sulfur Batteries

a. Introduction. The development of the sodium/sulfur battery, which was initiated at the Ford Aerospace and Communications Corporation (FACC) in the mid-1960s, was based on the finding that β-alumina was a good sodium ion conductor at elevated temperatures. Subsequently, there have been many additional organizations involved in the development of the technology, including CGE, General Electric, Brown Boveri, Chloride Silent Power, British Rail, and the Yuasa Battery Company.

The major interest behind the extensive effort to develop this system into a practical battery is the very high specific energy, offering the promise of a greatly enhanced range capability in advanced electric vehicles.

The Board's evaluation of sodium/sulfur batteries was limited to the only U.S. program directed toward EV applications, i.e., the FACC program. The basic construction of the FACC cell is shown in Figure 2-3. The design incorporates a central sodium electrode configuration. The basic electrode and cell reactions are shown in Figure 2-3. It should be noted that, after the first half of the discharge, the reaction changes to $Na_2S_5 \rightarrow Na_2S_3$ with a declining cell, open-circuit voltage.

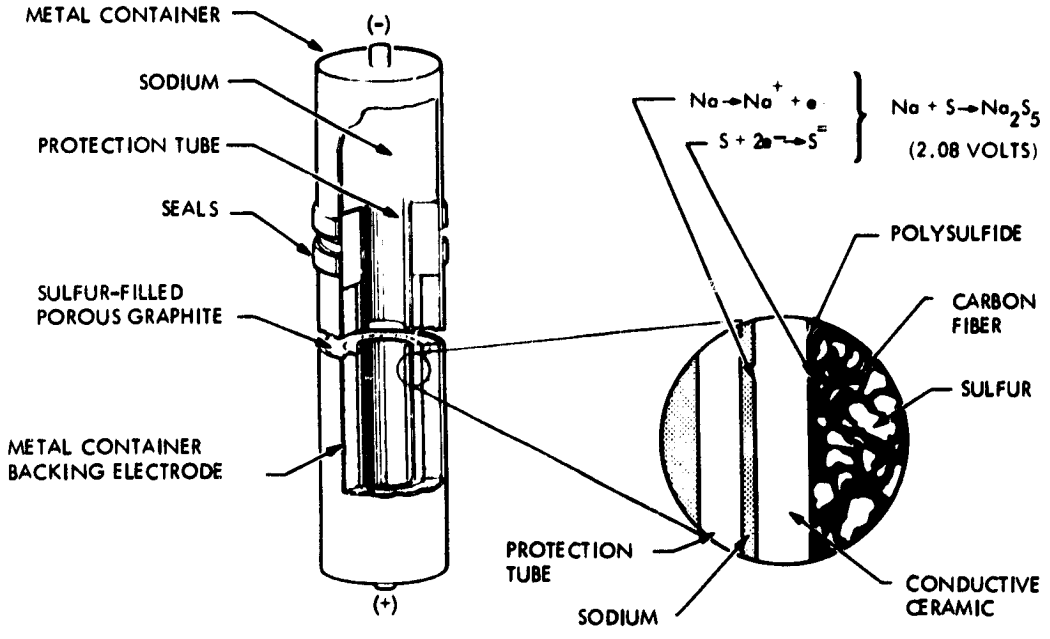

Figure 2-3. Basic Components of the Sodium/Sulfur Battery (Source: Ford Aerospace and Communications Corporation)

FACC has given consideration to the effect of declining open-circuit voltage on power capability and of the difficulty in completely recharging the battery by using a revised definition of the fully charged (F1R) and the fully discharged (F2R) conditions. The sodium/sulfur system has the advantage of significantly higher specific energy than most other batteries, making such an approach (where some capacity is sacrificed) more acceptable. These definitions of state of charge were taken into account by the Board in projecting peak-power values. No similar quantitative approach, allowing for problems at top of charge and end of discharge, was adopted by any of the other battery developers (except for some discussion on top-of-charge gassing problems with Ni-Fe).

As with the Li/MS system, the sodium/sulfur battery must be maintained at elevated temperatures (~350°C versus ~450°C for Li/MS). The same, but somewhat less demanding, considerations (as discussed in the section on the Li/MS battery) are necessary to maintain the battery within its operating temperature range.

The primary focus of the FACC program has been the development of a reliable, high-performance cell. There has been only limited effort expended in the fabrication and testing of batteries. Only one EV battery (35 kWh) has been built to date by FACC, and testing of this battery was inconclusive.

b. Performance Projections. The Board projections for the performance of the NA/S battery system for the various applications are shown in Tables 2-36 and 2-37.

Table 2-38 shows projections for the volume of complete sodium/sulfur battery systems based on the above technology.

c. Original Equipment Manufacturer Cost. The projections for the cost of complete battery systems for the four applications are shown in Table 2-39. The values marked "A" in Table 2-39 represent the projected costs made collectively by the Board. The values marked "B" result from a more detailed analysis by one Board member (see Section II-A-10).

d. Other Characteristics. Table 2-40 shows the projected values of the other parameters that influence life-cycle costs and acceptance of the sodium/sulfur technology.

e. Development Assumptions. The sodium/sulfur battery is currently receiving more support throughout the world than any other battery system for EV applications. The primary reasons for this are that the system offers both high performance and low cost. However, many developments will be required before the promise suggested by the projections can be realized in a practical system:

(1) Development of reproducible, strong, and low resistance β-alumina tubes produced from low-cost starting materials and using potentially low-cost processing methods.

Table 2-36. Specific Energy (in Wh/kg) as a Function of Power-to-Energy Ratio and Power Density

	Power density, W/kg		
P/E ratio	20	60	100
1.0	121	109	95
2.1	87	82	76
2.4	83	78	73
3.3	73	69	64

Table 2-37. Specific Power (in W/kg) as a Function of Power-to-Energy Ratio and State of Charge

	State of charge, %		
P/E ratio	50	30	10
1.0	148	141	129
2.1	199	192	180
2.4	224	210	180
3.3	244	234	220

Table 2-38. Battery Volume and Mass Density (in liters/kg per liter)

	Battery size, kWh/kW			
	50/50	12/25	25/60	15/50
Volume, liters	380/1.09	128/1.08	272/1.11	192/1.07

Table 2-39. Initial Battery Cost (OEM Cost in 1982 Dollars)

	Battery size, kWh/kW							
	50/50		12/25		25/60		15/50	
	A	B	A	B	A	B	A	B
Battery cost	4500	6100	2425	3000	4325	4100	3625	3300

Table 2-40. Other Sodium/Sulfur Battery Characteristics

Characteristics	Value
Cycle life[a]	750
Relative maintenance,[b] 1 to 5	3.5
Efficiency,[c] %	66
Salvage, $/kWh	0
Relative safety,[d] 1 to 10	5

[a]Equivalent full discharges.

[b]Expressed as figure of merit (1 = minimum maintenance).

[c]Based on average 29 mile per 24-hour travel.

[d]Expressed as figure of merit (baseline ICE vehicle-6).

(2) Demonstration that the cycle lives of such tubes exhibit good Weibull-shape factors.

(3) Demonstrated ability to undergo repeated freeze-thaw cycling without cell failures.

(4) Successful demonstration of low-cost, corrosion-resistant construction materials and positive electrode-current collectors.

(5) Demonstration that batteries can be developed that are tolerant to on-the-road conditions without ceramic failure (safety considerations).

The sodium/sulfur battery is one of several batteries under development that has the capability of yielding considerably higher energy-to-weight ratios than any of the near-term batteries. A negative feature, however, is that the volumetric ratios are significantly less attractive.

Despite intensive, worldwide development activity to date, the battery system must still be considered in its early stages of engineering development. It is not yet clear that the inherent advantages of this system can be realized in commercial EV batteries.

9. Aluminum/Air Batteries

a. Introduction. The aluminum/air battery is the result of a search for an electrochemical fuel. Early R&D focused on sodium and lithium electrodes in aqueous systems but shifted to aluminum for cost, availability, and safety reasons. DOE support of the aluminum/air battery began in 1978 at the Lawrence Livermore National Laboratory (LLNL). The primary interest in this battery system is based on the promise of developing an electric vehicle capable of long-range and rapid refueling. This battery provides the high-energy density needed for long range through the use of consumable aluminum anodes and fuel-cell-type air cathodes.

The aluminum/air battery consists of two essential components: a galvanic cell stack and a fluidized bed crystallizer. The cell consists of two air cathode cassettes held at an angle of 3 to 6 deg. These are designed for ease of replacement during maintenance. Current collection is affected by parallel tracts of copper that make contact with the aluminum at the electrolyte interface. Refueling is accomplished by the continued feeding of new plates and water. During operation, the aluminum, water, and air react, forming a powder of hydrargillite (aluminum trihydroxide).

The electrode, cell, crystallizer, and battery reactions are as follows:

$$\text{Anode:} \quad Al + NaOH + 3OH^- = NaAl(OH)_4 + 3e^-$$

$$\text{Cathode:} \quad 3e^- + {}^3/_2H_2O + {}^3/_4O_2 = 3OH^-$$

$$\text{Cell:} \quad Al + NaOH + {}^3/_2H_2O + {}^3/_4O_2 = NaAl(OH)_4$$

$$\text{Crystallizer reaction:} \quad NaAl(OH)_4 = NaOH + Al(OH)_3$$

$$\text{Battery reaction:} \quad Al + {}^3/_2H_2O + {}^3/_4O_2 = Al(OH)_3$$

Schematic diagrams detailing the cell and crystallizer operation are shown in Figures 2-4a and 2-4b.

Until the present time, the emphasis of the development program has been on the air electrodes and cell design. Small-scale systems have been built and evaluated to identify critical problem areas. Current emphasis is on aluminum-alloy development (especially to improve coulombic efficiency and to broaden the operating temperature range) and improvements to the crystallizer.

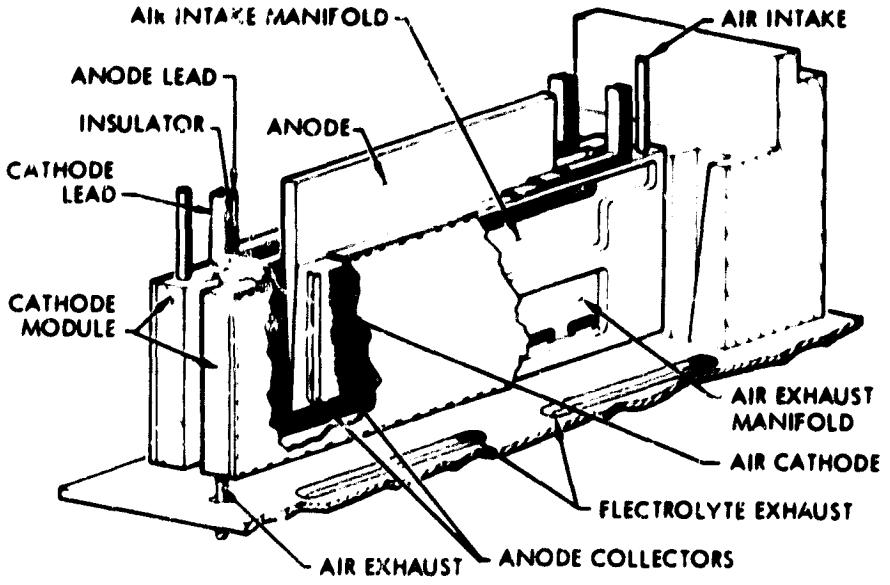

Figure 2-4a. Wedge-shaped cells are formed by positioning two air-electrode cassettes at an angle of 3 to 6 deg. Individual cassettes can be removed and replaced following disfunction or failure. (Source: Lawrence Livermore National Laboratory)

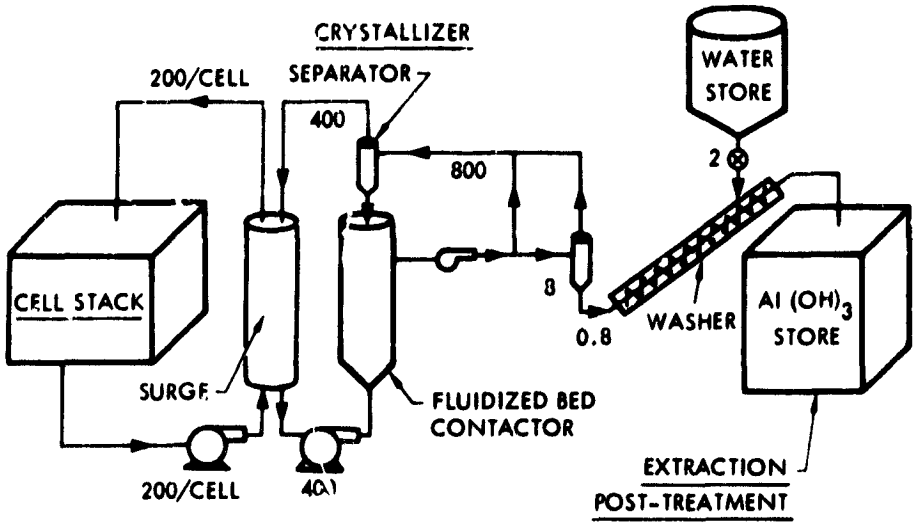

Figure 2-4b. Electrolyte is circulated between cell stack and crystallizer. Particles are retained in the crystallizer by means of a hydrocyclone separator, which may also be used selectively to remove mature particles for storage. Numbers indicate approximate volumetric flow rates (ml/s). (Source: Lawrence Livermore National Laboratory)

b. Performance Projections. Because the aluminum/air system is a primary battery, the only mission considered was for the full-performance EV, i.e., the equivalent of a 50-kWh/50-kW battery. The discharge characteristics projected for this battery are shown in Table 2-41. The nature of the electrochemical reactions is such that the peak-specific power does not depend on the state of charge; indeed, state of charge has no meaning for this system.

The Board's projection for the volume of the full-performance battery was 528 liters, with a mass density of 0.6 kg per liter.

c. Original Equipment Manufacturer Cost. The projected cost for this battery (not subject to detailed analysis) was $2100. However, it must be recognized that this cost relates to cell hardware and auxiliaries because the active materials are used as "fuel." Projections of aluminum-alloy costs did not form part of this study.

d. Other Characteristics. The other factors influencing life-cycle costs (with the exception of the aluminum fuel) and acceptance of aluminum/air technology are shown in Table 2-42.

e. Development Assumptions. It is difficult to make projections for the aluminum/air battery in the absence of a successful demonstration of a full-size battery system or even full-size engineering cells. The Board considered the following key developments to be necessary before the projections can be realized in a practical system:

(1) Development of a low-cost aluminum alloy with reduced self discharge while maintaining electrochemical and system performance.

(2) Demonstration of cathode life, under realistic operating conditions.

(3) Demonstration of lightweight, reliable, and low-cost device to separate hydrargillite.

(4) Design development and life test of high-performance, manufacturable cell stacks that minimize shunt currents throughout battery use.

(5) Design, fabrication, and testing of full-size battery system, including low-cost, reliable, and efficient auxiliaries.

The main advantage of the aluminum/air battery for EV application is its unique characteristic of virtually unlimited range. However, its low energy efficiency and system complexity are significant factors to be considered in selecting this battery for commercial EVs.

Table 2-41. Specific Energy (in Wh/kg) as a Function of Power-to-Energy Ratio and Power Density

P/E ratio	Power density, W/kg		
	20	60	100
1.0	158	158	151

Table 2-42. Other Nickel/Iron Battery Characteristics

Characteristics	Value
Cycle life	NA
Relative maintenance,[a] 1 to 5	4.5
Efficiency,[b] %	18
Salvage, $/kWh	0
Relative safety,[c] 1 to 10	6

[a]Expressed as figure of merit (1 = minimum maintenance).

[b]Source efficiency combining discharge and charge (alumimum production) efficiencies.

[b]Expressed as figure of merit (baseline ICE vehicle-6).

10. Assessment of Battery Selling-Price Estimates

a. Introduction. This section summarizes subjective estimates for the OEM selling prices for the batteries considered by the JPL Board. These estimates have drawn on related information and methods developed in earlier and current projects.

Table 2-43 presents an outline of the major segments of the method used in making the subjective estimate from the developer's estimate and related information. The term "Investigator's Estimate" is used to identify this

subjective estimate.[5] A more detailed exposition of the method of analysis is presented in the Appendices (Volume V).

The extent to which this method can be fully implemented varies widely, depending on the amount of information published and the extent to which the developer wishes to participate in the process of clarifying the issues raised. The greater the cooperation between developer and investigator, the less is the subjective element in the Investigator Estimate.

For each battery, a comparison is made of the estimates from the developer, JPL Board estimate, and the Investigator Estimate generated in this section.

Included in the comparison charts for each battery are letter-labeled data points. These are values extracted or derived from earlier projects. The lines connecting the data points on a chart are not intended to indicate a continuum of values but, rather, the profile of the values for the four batteries.

All values of the battery OEM selling prices are in 1982 dollars unless otherwise noted. The derivation of the selling price estimates is based for

Table 2-43. Outline for Determining Investigator Estimate

(1)	Definition of technology, especially in relation to battery design, materials and components, and performance specification assumed in the design for the cost estimate
(2)	Definition of process flowsheet and process-and-equipment development needs for manufacturing assumed battery design for cost estimate
(3)	Analysis of developer's estimates for material and component costs, direct labor hours, and installed equipment costs for the production rate specified
(4)	Discussion with developer to clarify issues raised in the above analysis
(5)	Evaluation of developer's "overall capability" at the time of generating his developer selling-price estimate
(6)	Determination of Investigator's Estimate by making subjective adjustments to item (3) parameters in conjunction with evaluation made in item (5)

[5]The Investigator's Estimate represents that of J.A. Consiglio, Solva-Tek Associates. The JPL Board estimates represent those of the remaining members of the AV Battery Review Board (B.A. Askew, P.C. Symons, and W.J. Walsh). This section of the report was prepared in April 1984.

the most part on Electric Power Research Institute/A.D. Little, Inc. (EPRI/ADL) guidelines. The aluminum/air battery was not considered because a developer estimate had not been received at the time of preparation of this section. A summary comparison and discussion is presented at the end of this section.

As indicated in Table 2-43 (item 5), an important element in making the subjective determination of an Investigator Estimate is the evaluation of the developer's overall capability at the time he generates his cost or selling price estimates. A summary of this capability evaluation for the developers being considered is listed in Table 2-44.

The capability rankings are divided into four groups with group A representing the highest overall capability and group D representing the lowest capability. The order in a given group is not significant. The column in Table 2-44 labeled "Impression" is the Investigator's impression of the developer's approach in making and presenting the results of his estimate. As a general rule (but with exception) an estimate made by a group D developer is likely to underestimate the future realized cost or price by a wide margin. This phenomenon has been documented in other prototype projects (Reference 2-1).

For some battery developers in group D, future realized prices can be two to three times the values projected in their early estimates. Some explanation is required for Exxon's placement in group D. At the time initial estimates were prepared, Exxon had not built a prototype stack or system. This fact, in addition to the lack of definition in the technology [item (1)], process flowsheet and equipment-development needs placed Exxon in the lowest capability group. Further definition has taken place since that time, although further evaluation is not possible.

Table 2-44. Developer Overall Capability Assessment: Relative Order by Groups

Group	Battery	Developer	Impression
A	Pb/Acid	No specific developer assessed	Conservative
	Ni/Fe	Eagle Picher Industries	Conservative
B	Zn/Cl	Energy Development Associates	Optimistic
	Na/S	Ford Aerospace and Communications Corp.	Conservative
C	Li/MS	Gould, Inc.	Conservative
		Argonne National Laboratory	Optimistic
D	Zn/Br	Exxon	Optimistic
	Fe/Air	Westinghouse	Optimistic

A closing comment on the evaluation of the developer's capability: This procedure is used as a working tool to treat the information from the various developers in a more consistent manner. There is no claim that it is foolproof in eliminating error or uncertainty.

b. Lead/Acid Battery. The comparison of the selling-price estimates for the ISOA/Pb/Acid battery is shown in Figure 2-5. The JPL Panel's values are represented by Phil Symons' Equation values. Point labelled A is an Investigator Estimate (following ADL guidelines) generated in an earlier study (Reference 2-2). It is for an EV battery at a production rate of 100,000 batteries per year with lead at 40¢/lb. The battery performance specification was not defined in terms of the JPL Panel's performance parameters. The specification is a low power-to-energy ratio and is closest to the specification for a full-performance vehicle battery.

The assumptions concerning the battery production facility were that it was a modern, highly automated plant. Fabrication in a typical automated plant would increase the selling price by 15 to 20%. For lead at 30¢/lb, the selling price would decrease approximately 15%.

The Investigator Estimate 1980 DOE Study is contoured to the JPL Panel (Symons Equation values) line, starting at point A. No changes were made in the estimate to reflect 1980-1982 cost changes. Under these conditions, the estimate should be viewed as optimistic for 40¢/lb lead.

c. Nickel/Iron Battery. The comparison of the selling-price estimates for the nickel/iron battery is shown in Figure 2-6. Points labelled A and B are based on an Investigator's Estimate (generated by Phil Symons and Joseph Consiglio) for an EPRI project (Reference 2-3). This estimate was based on Eagle Picher Industries, Inc., data and is expressed in 1982 dollars per revised EPRI/ADL/Symons guidelines. Point A was derived by converting the EPRI Investigator's Estimate from 20,000 to 100,000 batteries per year production, using extrapolation factors developed and used in the EPRI study. Point B was derived from Point A by applying approximate adjustment factors to materials, equipment, and rent values to raise the energy content from 23 to 50 kWh.

This estimate is optimistic because the materials-cost reductions applied in the extrapolation procedure is not likely to be realized for the nickel costs. EPRI Study values represent the Investigator estimates for the various batteries.

d. Zinc/Chlorine Battery. The comparison of the selling-price estimates for the zinc/chlorine battery is shown in Figure 2-7. Points labelled A, B, and C are based on a Synthesized Developer Estimate and an Investigator's Estimate (generated by Symons and Consiglio) for the EPRI project (see Reference 2-3). Energy Development Associates provided the developer data used in these estimates. All estimates are in 1982 dollars.

Point A was derived by applying extrapolation factors to the Investigator's Estimate to convert the production rate from 20,000 to

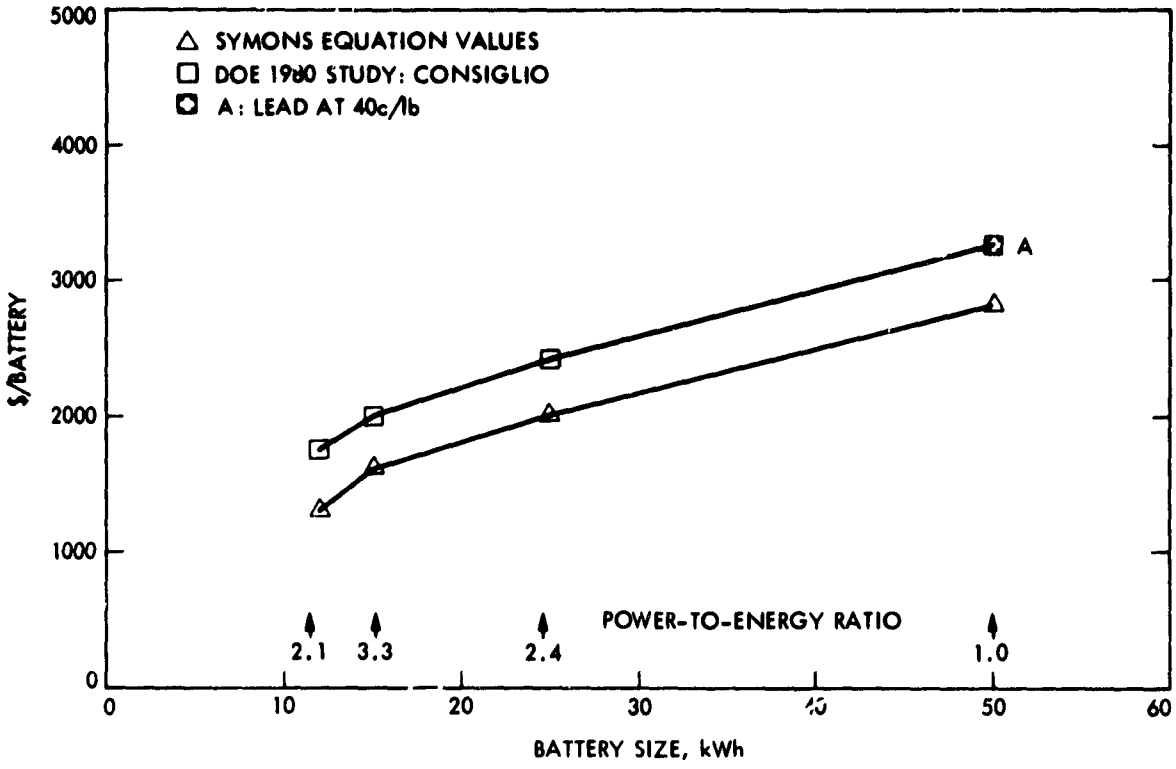

Figure 2-5. Comparison of Pb/Acid Selling-Price Estimates

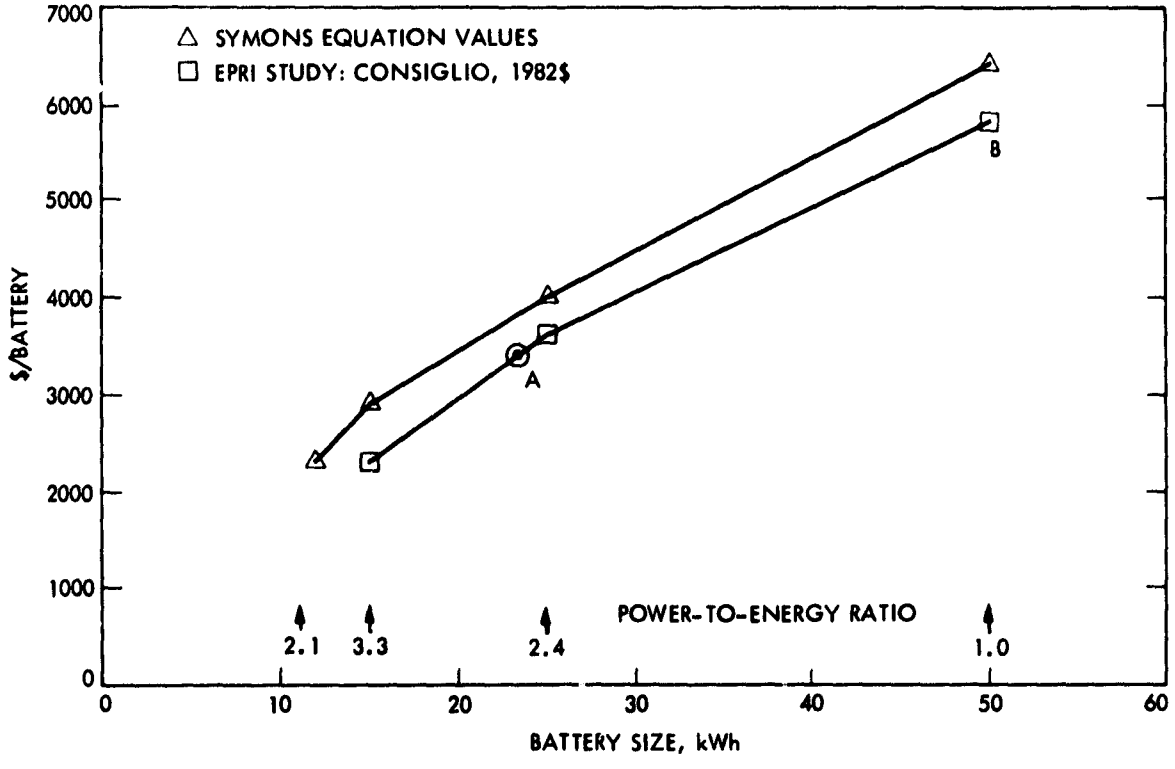

Figure 2-6. Comparison of Ni/Fe Selling-Price Estimates

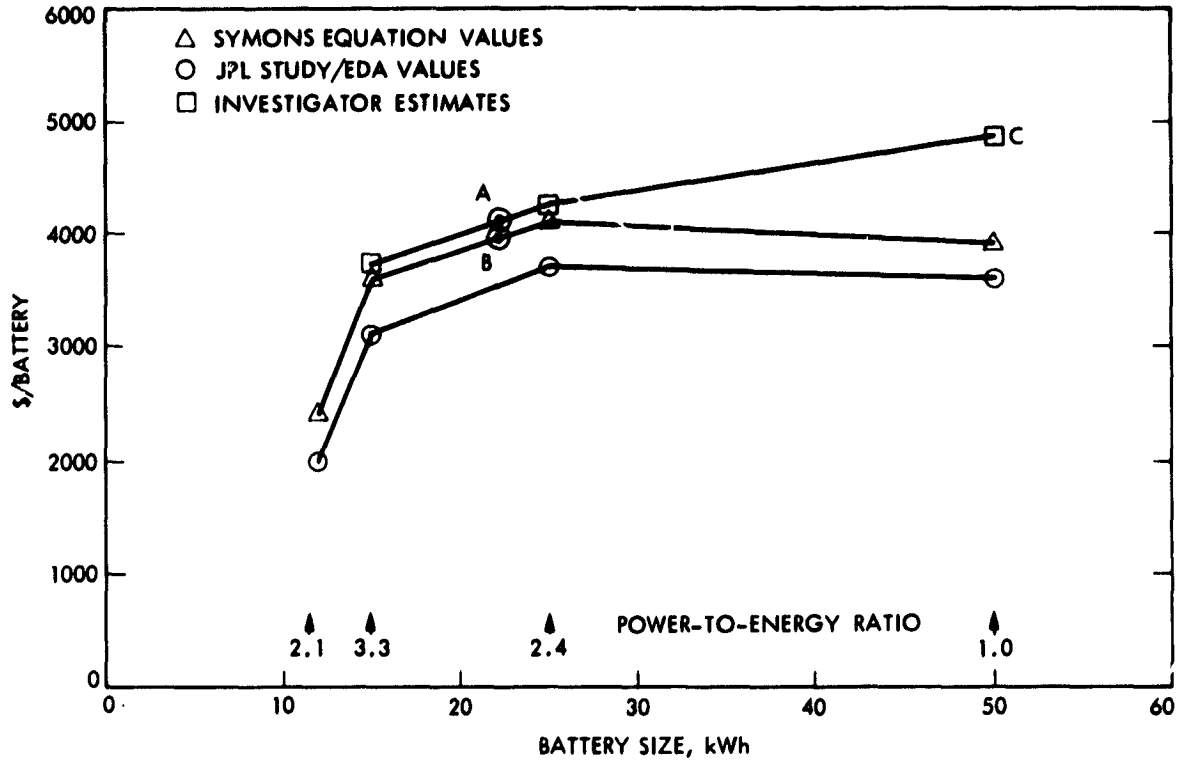

Figure 2-7. Comparison of Zn/Cl Selling-Price Estimates

100,000 batteries per year. Point B was derived from the Synthesized Developer estimate by applying extrapolation factors to convert the production rate from 50,000 to 100,000 batteries per year. Point C was derived from Point B by applying adjustment factors to the power-related components and energy-storage-related components. A value of 1.14 (50 kW/44 kW) for power adjustment and 1.64 $[(50/22)^{0.6}]$ for energy storage adjustment was used.

The Investigator Estimates are optimistic with respect to achieving the cost reductions in graphite, projected by the extrapolation factors used for materials. These estimates are conservative for the amount of graphite used for the zinc electrodes and comb buses.

e. Sodium/Sulfur Battery. The comparison of the selling-price estimates for the sodium/sulfur battery is shown in Figure 2-8. This figure contains two sets of selling price information: cells and battery.

The cell OEM selling-price estimates provided by Ford for the JPL Study is the lower solid line (Reference 2-4). Point B is also a cell OEM price estimate (discussed below). The balance of the lines and data points in the figure pertain to battery estimates. All estimates are based on Ford-supplied data. Symons Equation values are presumed to be 1982 dollars, values labeled EPRI or Ford 1980 cost model are in 1980 dollars.

Ford projections for cell OEM selling price in $/battery are given by the lowest line. Point B is the cell price derived from the Ford 1980 cost

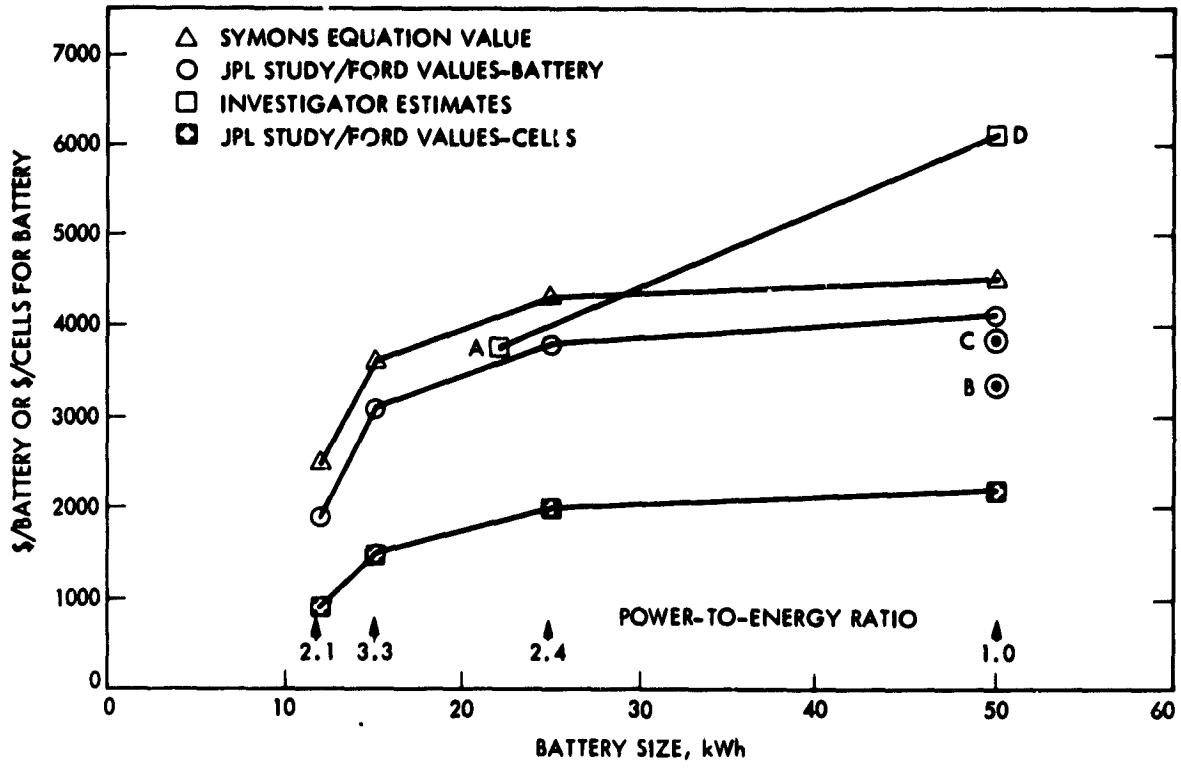

Figure 2-8. Comparison of Na/S Selling-Price Estimates

model (Reference 2-5) for a cell having the same volume as the cell used in the full-performance vehicle battery for the JPL Study. These values are for a production rate of 36,000,000 cells per year equivalent to 100,000 batteries per year. On a per-cell basis, the cell prices have a JPL Study value of $6.13 and 1980 cost model of $9.54. A one-on-one comparison of the two cases shows a major difference in equivalent cell-assembly costs:

OEM price	JPL study	1980 cost model
Tube	$3.46	$3.23
Cell assembly	2.67	6.31
Cell total	$6.13	$9.54

There is an excellent correspondence in electrolyte tube OEM selling price of $3.46 versus $3.23 between the two estimates. However, there is a significant change projected in the cell assembly OEM selling price equivalent: $2.67 versus $6.31. This is a projected 58% reduction based on the Ford 1980 cost model. The factors contributing to this projected cost reduction are not evident from an analysis of the available information. Ford, in their JPL study Table 3-1 (see Reference 2-4), suggest reductions to be achieved by using sodium at $1/kg, sulphur electrode graphite at $10/kg, and utilizing a highly automated plant. However, these items have already

been factored into the Ford 1980 cost model (see Reference 2-5): sodium at $0.45/kg, graphite at $9.09/kg, and the plant was assumed to be highly automated. There seems to be insufficient information to justify Ford's projected cost reduction in the cell-assembly stage.

The upper portion of Figure 2-8 shows the estimated selling prices based on Ford's JPL Study and the JPL Panel values. Points labeled A, C, and D are values generated in part from the EPRI study (see Reference 2-3).

Point A is a Synthesized Developer Estimate (Ford 1980 cost model) for a van battery using 240 cells. Tube and cell dimensions for this battery are of different dimensions than those used in the Ford JPL Study. Point C is a Synthesized Developer estimate using Ford's JPL cell price and Ford's 1980 cost model for cell-to-module assembly. Component costs were increased by $500/battery to bring this item in line with Ford's range of $600 to $1000/battery used in the JPL Study. Point D, based entirely on the Ford 1980 cost model, uses the cell price corresponding to Point B. The line joining points A and D represents Investigator Estimates until there is better documentation on how Ford intends to achieve the projected cell-assembly costs.

f. Lithium/Metal Sulfide Battery. The comparison of the lithium/metal sulfide battery estimates is shown in Figure 2-9. The Gould and ANL estimates are not based on a detailed design and manufacturing cost study. The projected lower costs by ANL are based, in part, on manufacturing all lithium components (rather than market purchased) from a lower-cost, abundant material such as lithium carbonate. Projected lithium compound cost reductions would be approximately 50%. Further studies are needed to verify the magnitude of the projected cost reduction.

Pending more detailed studies, the Investigator Estimate is placed below Gould's estimate, at a value equal to 25% of the difference between the Gould and ANL lines.

g. Zinc/Bromine Battery. The comparison of the zinc/bromine battery selling-price estimates is shown in Figure 2-10.

Exxon has published an estimated selling price of approximately $38 to $40/kWh for a 20-kWh, self-contained battery (based on ADL guidelines). This estimate was prepared prior to any significant experience with building stacks or learning experiences of identifying and resolving problems since stacks have been built.

A few problems currently exist concerning electrode warpage, deformation of separator bosses, and life of the activated carbon layer for electrodes. Costs are expected to increase as these problems are resolved.

An analysis of some of the material cost items, direct labor hours, and equipment cost items shows the following:

(1) Factory costs for selected injected molded items range from $1.55 to $2.74/kg, compared with 1977 costs for high and low density polyethylene at $4.00/kg (Reference 2-6).

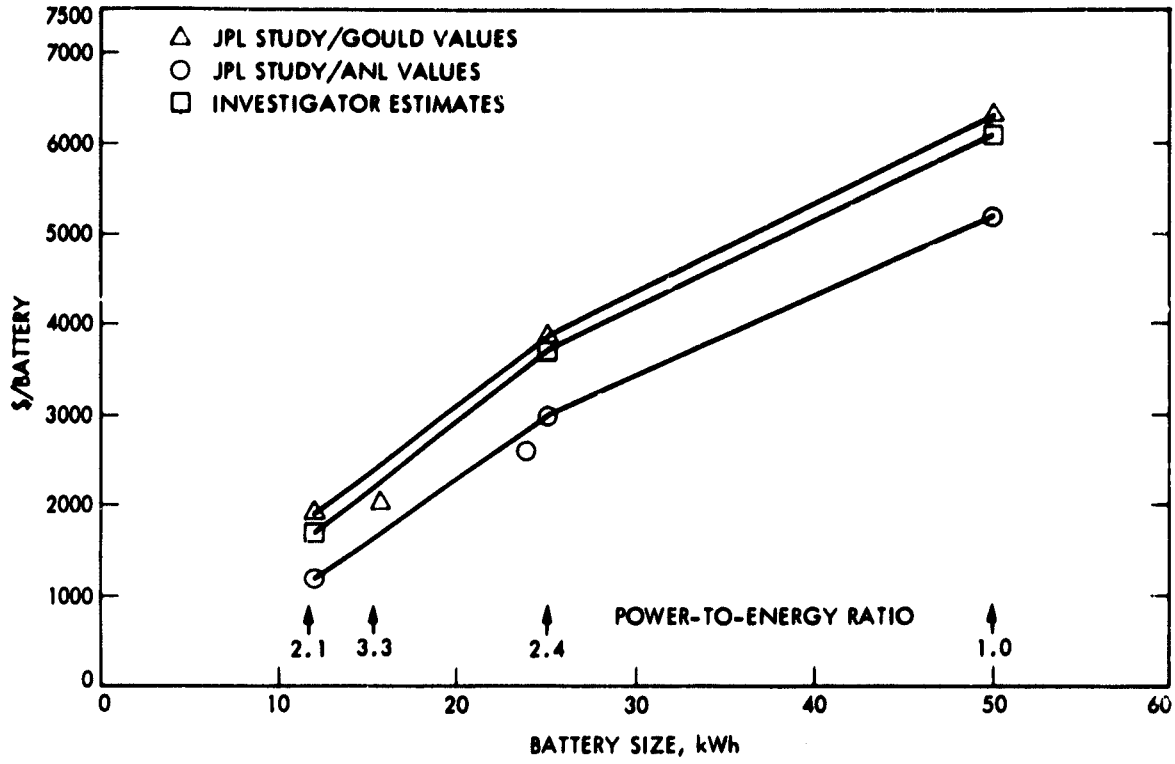

Figure 2-9. Comparison of Li/FeS Selling-Price Estimates

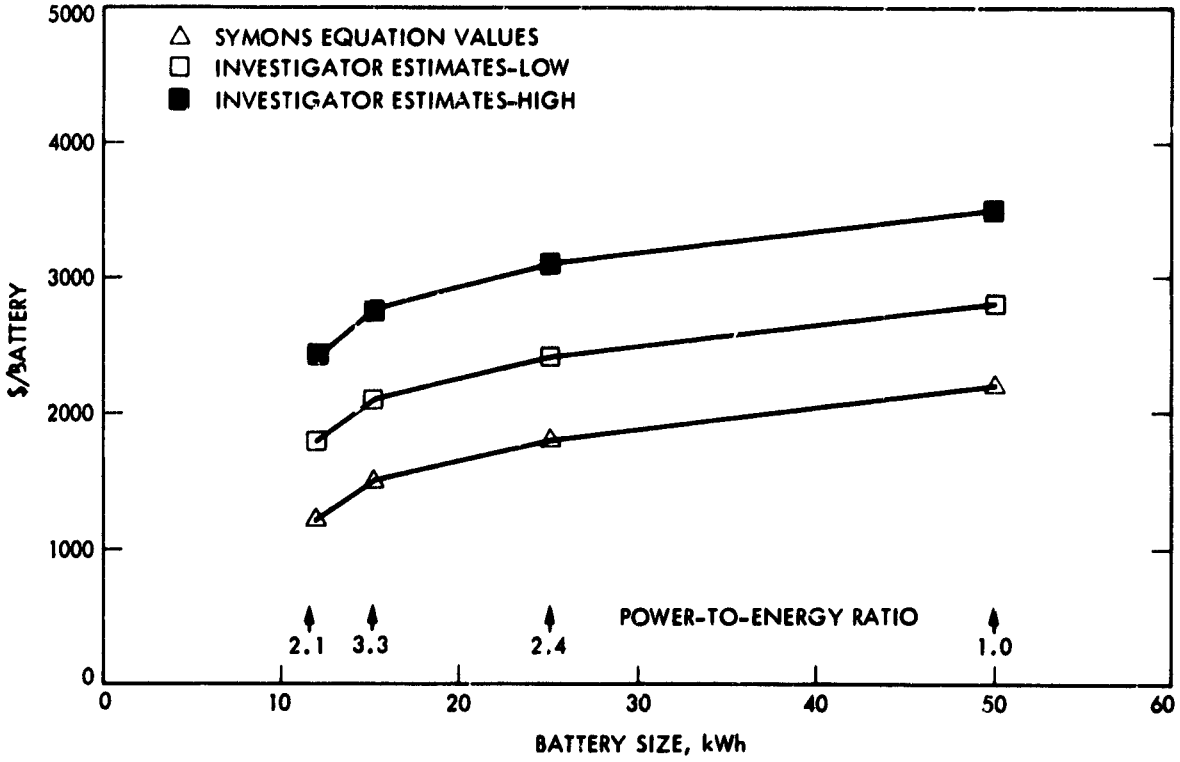

Figure 2-10. Comparison of Zn/Br Selling-Price Estimates

(2) Direct labor hours and installed equipment cost comparisons, with a generalized comparison referenced to the lead/acid battery, indicates direct labor hours at 39% of the correlating value and equipment costs at 53% of the correlating value (see Reference 2-3).

The Exxon estimate is for a battery, presumably rated at 20 kWh/30 kW. This battery was adjusted to a 50 kWh/50 kW battery by use of the following factors: power-related factor value of 1.67 (50/30) and an energy-storage-related factor value of 1.73 $[(50/20)^{0.6}]$. The Investigator used an average value of 1.70 and derived an estimated selling price of $1400 for a 50 kWh/50 kW battery.

In this case, a subjective estimate is that the realized selling price is likely to be between 100 to 150% greater than the derived value of $1400 per battery. A major consideration in this instance is that Exxon was judged to have a low capability at the time they generated their estimate. The range of the Investigator Estimate is shown in Figure 2-10.

h. Iron/Air Battery. A comparison of the iron/air battery estimates is shown in Figure 2-11. The information to document and support the cost projections made in Westinghouse's report to JPL is essentially non-existent.

The evident status of the development is in the research phase with no evidence of scaling up cells to a prototype device level. A preliminary cost estimate, based on a cost model that is not described, did not raise the Investigator's level of confidence. For these reasons, Westinghouse is placed in the low capability group D in Table 2-44. The Investigator's subjective estimate under these circumstances is that Westinghouse's realized selling price is likely to be between 100 and 150% greater than their current estimates. The range of estimates is shown in Figure 2-11.

i. Summary Comparisons. The range of cost estimates are summarized in Table 2-45 (relative to the Board values), including those batteries that were not addressed in the previous discussions. These factors are based on the previous figures although some adjustments and extrapolation were necessary to encompass all the AV applications in a consistent form for the ensuing vehicle-battery calculations.

The highest degree of uncertainty exists with the bipolar lead/acid, zinc/bromine, iron/air, and aluminum/air. This is understandable for the bipolar lead/acid and iron/air, which are largely undefined. Aluminum/air is at an early stage of development as well although cells have been demonstrated. The zinc/bromine battery has been demonstrated in developmental batteries; however, the manufacturing experience of the developer was relatively low at the time of their cost estimates.

The estimates of battery costs by the developers, Review Board, and Investigator are shown in Figure 2-12 (a, b, c, d), including all the batteries in the assessment. Note that the ANL estimate was chosen to represent the developer estimate for Li/FeS (the only case with two subcontractors).

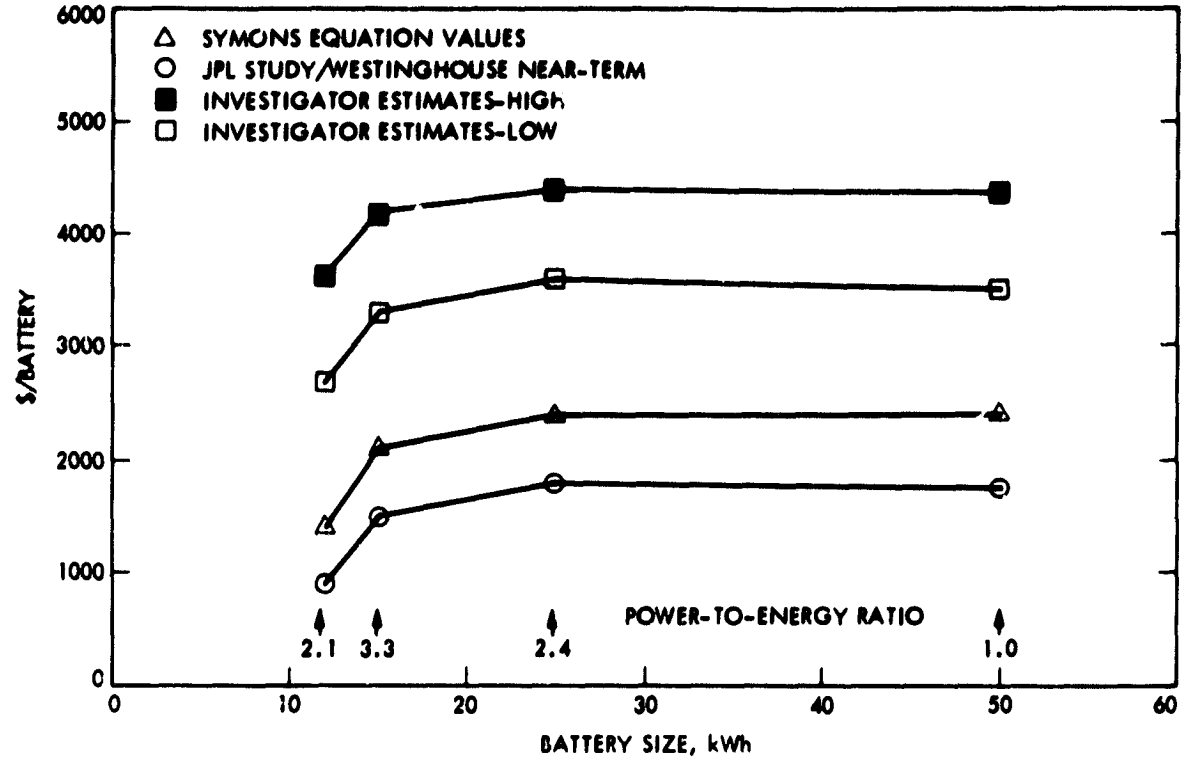

Figure 2-11. Comparison of Fe/Air Selling-Price Estimates

Table 2-45. Cost-Range Factors as a Function of Power-to-Energy Ratio

Battery	Power-to-energy ratio			
	1.0	2.1	2.4	3.3
Pb/Acid	1.16	1.35	1.20	1.27
Bipolar Pb/Acid[a]	1.50	1.50	1.50	1.50
Ni/Fe	0.91	0.87[b]	0.90	1.00
Ni/Zn[a]	1.10	1.10	1.10	1.10
Zn/Br	1.59	2.02	1.72	1.83
Zn/Cl	1.24	1.04[b]	1.04	1.01
Fe/Air	1.83	2.57	1.83	2.03
Li/FeS	1.28	0.93	1.19	0.98
Na/S	1.36	1.24[b]	0.95	0.91[b]
Al/Air[a]	1.50			

[a]Arbitrary range considering the state of development.

[b]Extrapolation from previously presented curves.

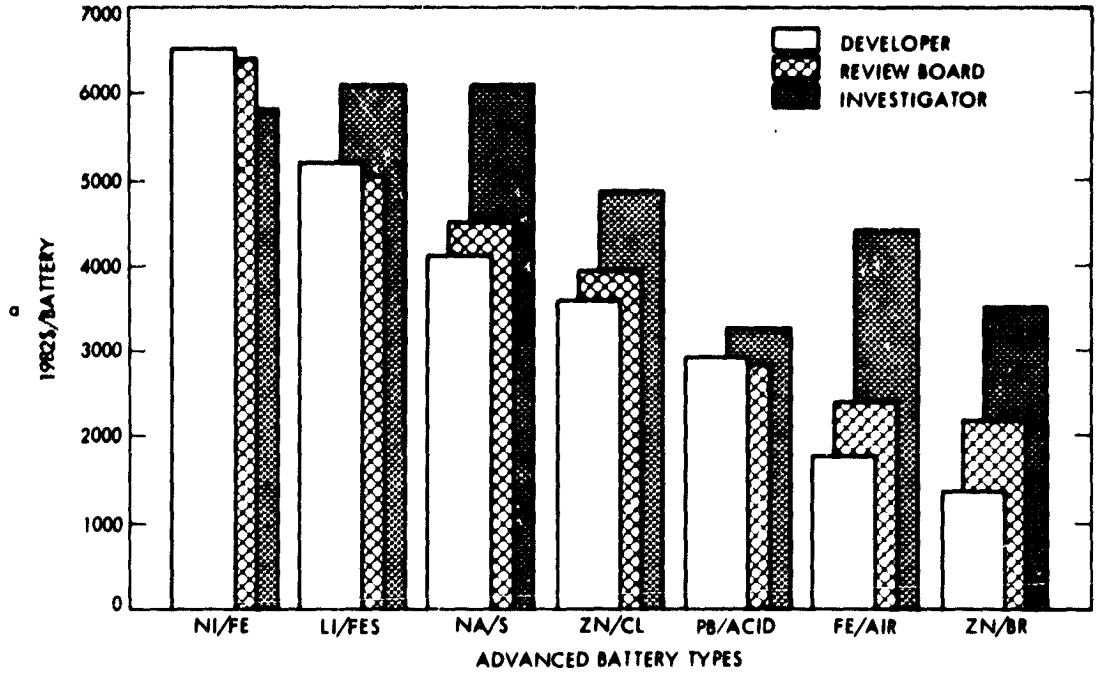

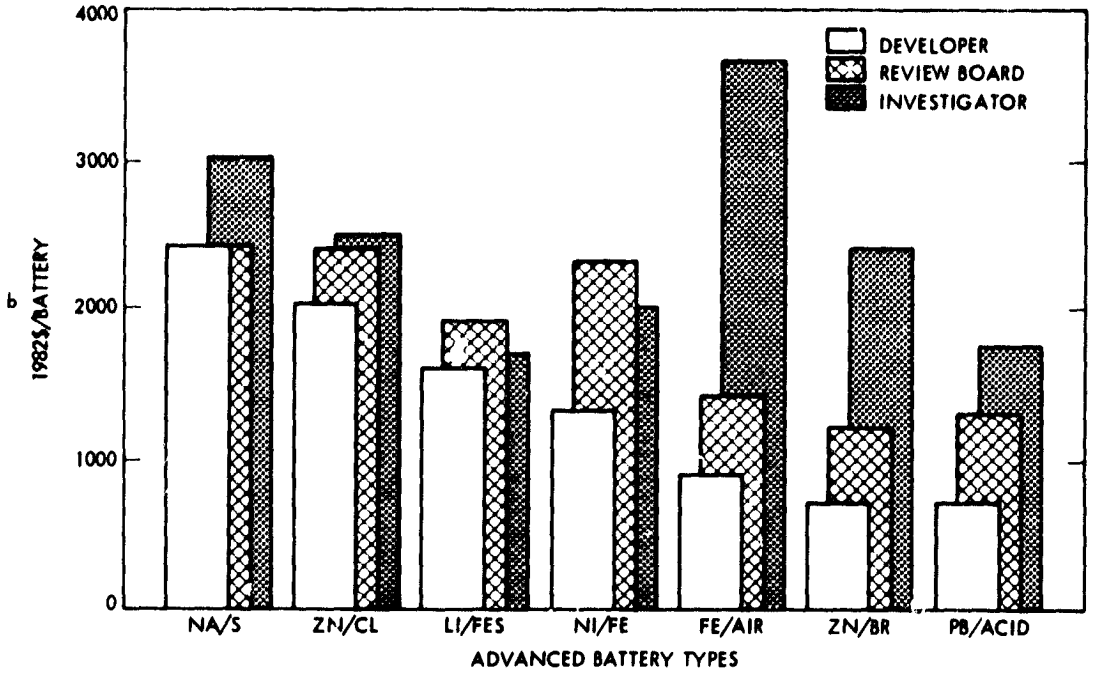

Figure 2-12. Original Equipment Manufacturer Price Estimates
(a) 50 kW/50 kWh, P/E = 1.0
(b) 25 kW/12 kWh, P/E = 2.1

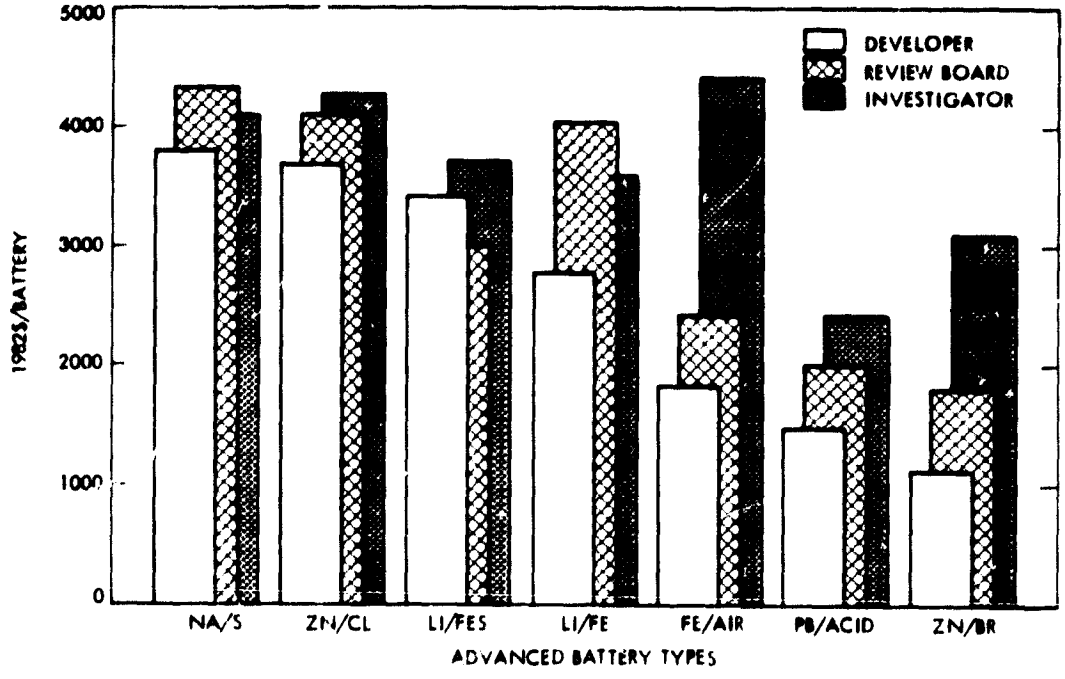

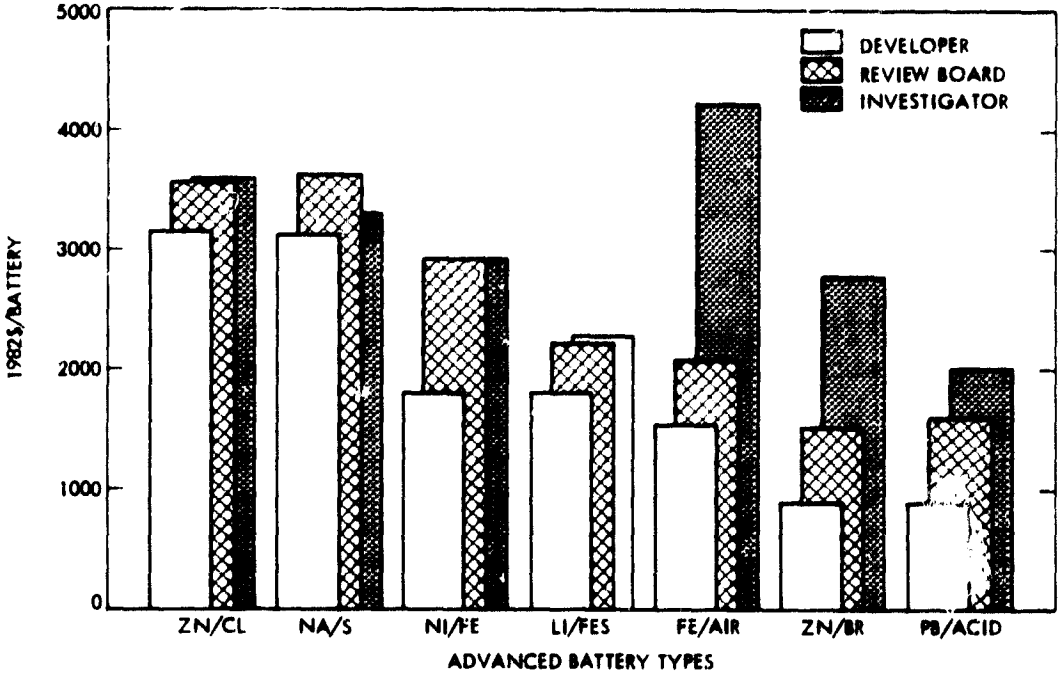

Figure 2-12. Original Equipment Manufacturer Price Estimates
(c) 60 kW/25 kWh, P/E = 2.4
(d) 50 kW/15 kWh, P/E = 3.3

B. MECHANICAL POWER-PEAKING DEVICES

While power-peaking devices include chemical and electrochemical as well as mechanical devices, this review is limited to mechanical energy storage only because chemical and electrochemical energy storage are considered separately as potential subsystems for the AVs in other parts of this report.

Because the AV is a vehicle that is to be competitive with the future contemporary ICE vehicle in terms of range (among others), the mechanical energy storage was not considered sufficiently attractive for routine consideration with other energy sources. The rationale was that, while mechanical storage adds significantly to the instantaneous power capability, it adds little to the total on-board energy storage capability for long-range requirements.

However, this characteristic of a high power/energy ratio can potentially reduce the power/energy requirements of some battery couples sufficiently to make them candidates for the advanced EV where otherwise they would not be. In addition, several of the battery candidates operate at relatively low efficiencies when they are being charged or discharged at high rates (high power). Under these circumstances it is possible to increase the overall energy efficiency by using a mechanical energy-storage device to absorb part of the power during deceleration regeneration and to provide part of the power needed for acceleration.

Finally, because in many cases the battery replacement cost is the largest single factor in life-cycle costs, any means of extending battery life can be beneficial. Because battery life is often related to depth of discharge and/or typical maximum power demands, mechanical energy storage has the potential, for some batteries, of reducing life-cycle battery replacement costs.

In summary, the use of mechanical power-peaking devices seems to offer the following advantages:

(1) Potential improvement in EV overall energy efficiency.

(2) Possible reductions in EV life-cycle costs.

(3) Potential of compensating for power/energy deficiencies of some battery candidates.

Based on these potential advantages, it was decided a brief review and assessment of mechanical energy-storage devices was justified. Mechanical energy-storage devices have been in use for centuries in the form of flywheels for machines, springs for clocks, and counterweights for doors or windows. More recently, compressed air to operate lifts and air hammers, hydraulic accumulators for heavy machinery, liquid springs such as used in shock absorbers, and elastomers for items like spear guns and toys, have come into wide use. Only steel flywheels have had automotive applications where appreciable levels of energy was stored. And, with the exception of a few recent experimental projects, the specific energy-storage capability was almost insignificant compared to the needs of any AV.

The mechanical energy storage devices that have received recent attention for possible automotive application are considered in this review as power-peaking candidates are; these devices are:

(1) Flywheels.

(2) Compressed air.

(3) Hydraulic accumulators.

(4) Elastomers.

(5) Linear elastic materials.

(6) Liquid springs.

1. Flywheels

a. Energy Considerations. The flywheel is the only mechanical energy-storage device considered that stores the energy in kinetic form, which has both advantages and disadvantages. The most significant advantage is the extremely high specific energy and power theoretically possible. There are two important disadvantages:

(1) Because of continuing motion, there are continuous losses due to such conditions as friction, aerodynamic drag, and imbalance that are analogous to self discharge in a storage battery. Methods of minimizing these losses are complicated and costly.

(2) As energy is added or removed, the rotating speed is changed. This feature almost demands a continuously variable transmission (CVT) for a mechanical drive or a sophisticated control system for an electric drive.

Basically, there are two types of materials used in flywheels: isotropic and composite. The isotropic material is usually a high-strength steel while the composites usually include Kevlar and/or fiberglass and/or carbon fibers because of their high strength-to-weight ratio. The isotropic flywheels have been in use much longer and are usually easier to fabricate. However, the composite materials have the advantage in terms of energy-storage capacity due to their higher strength-to-weight ratio in the direction of the maximum stresses. Thus, the isotropic material has the capability of withstanding the same level of stress in any direction although it is lo primarily in one direction. In a sense a weight penalty is paid to provide strength in a direction that is unimportant. The composite material is designed to provide nigh strength only in the directions needed.

The important factors in the flywheel from an energy standpoint are:

(1) The failure governing stress, which determines how much energy per particle can be stressed. For a given rotor, this will occur at the maximum allowable revolutions/minute.

(2) The rotor configuration that determines how efficiently the material in the rotor is being used to store energy.

(3) The range of rotational speed through which energy can be effectively removed because this determines the portion of stored energy that can be recovered.

It is of interest to note that with an ideal rotor, the maximum theoretical specific energy storage for known isotropic materials is only about 50 Wh/kg, and for composite materials the theoretical limit is nearly an order of magnitude greater. Thus, composite materials have a significant theoretical advantage over isotropic materials.

b. Power Considerations. The limitations associated with the maximum rate of energy addition or energy removal (i.e., the maximum power that can be put into or taken out of the flywheel system) are usually not determined by the flywheel but by the shaft and other hardware. For example, if the flywheel stores 1 kWh of energy and is removed in 10 seconds, the average power available during this time is 360 kW. Thus, the shaft, gears, belts, or whatever is involved in the conversion and transmission of this power would have to be sized accordingly.

c. Hardware Considerations. Flywheels have been used in some form for centuries, but especially since the beginning of the Industrial Revolution. Many early machines required massive flywheels (e.g., single-cylinder steam or internal-combustion engines) to smooth out power strokes and permit continuous operation by conserving angular momentum. These early flywheels were usually made of an isotropic metal and were either constant cross section or of the hub-web-rim configuration. The rim tangential velocities were low as was the typical specific energy, but the specific power under some conditions was high.

From the automotive power-peaking standpoint, the early and significant work was related to the flywheel-powered buses of Zurich, Switzerland, in operation 20 to 30 years ago. These steel flywheels typically were about 1.6 m in diameter, 1360 kg, and operated up to about 3,000 rev/min, giving a stored energy of about 9 kWh and a specific energy of about 6 Wh/kg (rotor only).

In the last decade there have been many experimental flywheel system programs in the United States involving both isotropic materials and composite materials, as shown in Table 2-46.

Recently, the composite flywheel rotors and other non-steel rotor concepts have begun receiving considerable attention, and a number of experimental rotors have been built. The Lawrence Livermore National

Table 2-46. Experimental Flywheel Systems

Flywheel rotor type	Total rotor weight, kg	Max speed, rev/min	Specific energy, Wh/kg
Four Steel-stacked discs[a]	309	14,000	5.17
Counter-rotating steel discs[b]	592	15,000	25.3
Aluminum hub Kevlar/ Fiberglass rim[c]	27.3	25,000	36.7
AISI 4340 steel forging[d]	20	20,000	5.0
Laminated steel[e]	90	10,000	5.6
Pierced steel disc[f]	82	8,000	3.5

[a]Garrett AiResearch - developed for New York City subway car.

[b]Rockwell International - developed for U.S. Army Mobility Equipment R&D Center (MERDC).

[c]Garrett AiResearch - developed for ETV-2.

[d]General Electric Company - developed for laboratory studies of Regenerative Flywheel Energy Systems.

[e]University of Wisconsin - developed with AiResearch for prototype vehicle power plant.

[f]Kinergy Research and Development - one of several systems built and adapted to automobiles for demonstration.

Laboratory tested thin-rim rotors fabricated from various materials with specific energies approaching 200 Wh/kg at failure. AiResearch tested thin multi-rim rotors exhibiting over 80 Wh/kg without failure. These figures show the enormous energy-storage potential of flywheel rotors, especially for composite materials. However, it should be noted that a great deal of supporting hardware is needed in the form of housings, vacuum pumps, oil pumps, shafts, and some system of efficiently removing the energy from the rotor. Also, the rotor cannot be allowed to operate at or near the failure stress levels, nor can all of the stored energy be removed from the rotor. Thus, for the complete flywheel assembly, in the 0.5 to 1.0 kWh sizes, the anticipated specific energies are expected to be around 10 to 20 Wh/kg for isotropic rotors and 20 to 40 Wh/kg for composite rotors. Including energy removal and conversion components, the anticipated specific energies are about 1/4 the values shown above, or about 5 to 10 Wh/kg for composite systems.

d. Safety Considerations. At the rotational speeds used to approach the peak-design, energy-storage levels, the rotor tangential velocity may be 600 to 900 m/s, which is similar to bullet velocities of a high-powered rifle. Thus, the hazard associated with large metal fragments moving at bullet velocities is apparent. Consequently, some type of effective containment is required, especially for the isotropic rotor. Indications are that, if properly designed, the composite rotor will not fail catastrophically with resulting high velocity fragments, but in a more controlled manner by unwinding, stretching, breaking of fibers, etc. Even with the catastrophic failure, tests have shown that the composite fragments are much easier to contain.

The lower susceptability of the composite rotor to catastrophic failure can be interpreted as an important advantage. This is because it is extremely difficult to contain the particles of an isotropic flywheel failure, resulting in a near-prohibitive increase in weight and cost. The alternative is to maximize the reliability of the rotor (also costly) and to accept the consequences of a few partially contained failures. With the composite flywheel, if the catastrophic failure can be totally avoided, neither the expensive and heavy containment nor the consequences of an uncontained failure are likely concerns.

A recent study concludes that it is indeed easier to contain glass composites than steel of equal kinetic energy by a factor of 2.5. The estimates for a 0.8-kWh steel flywheel weighing 18 kg projected that 18 kg of containment is needed for a disc-type flywheel, as opposed to 48 kg for a rim type.

There are other safety factors to be considered, including the adverse effect of gyroscopic forces and the potential fire/explosion hazard, which is associated with dust from composite rotors and with penetration of the hot interior of the housing by flammable liquids or other materials. Most of the safety questions have not been adequately answered with many of the projections coming from experience with aircraft jet engine rotors. Safety must receive much more attention before flywheels are even seriously considered for mass-produced automobiles.

e. Performance Characteristics. Available energy depends on the type and size of the flywheel rotor. A comparison for a 1-kWh system with the estimates for S-glass and Kevlar rotors reported by LLNL is summarized in Table 2-47.

The system specific energy is not a constant over a wide range of system sizes because many of the components do not scale linearly. This is especially true for the smaller units where accessories and certain fixed-weight components are a greater percentage of total weight. Therefore, as a first approximation at 0.5 kWh design energy, the specific energies might more realistically be 14.5 Wh/kg and 20.0 Wh/kg, respectively. It is also likely that the design rev/min would be somewhat higher, perhaps 30,000 rev/min.

The self-discharge rate is important for an extended period of non-use overnight (or longer) or possibly for constant-speed operation (for some

Table 2-47. Comparison of 1-kWh S-Glass and Kevlar Flywheel Systems

Characteristics	S-Glass	Kevlar
Flywheel assembly weight, kg	57	38
Design rev/min x 1000	25	25
Housing diameter, m	0.6	0.71
Housing width, m	0.23	0.18
Mass moment of inertia, $kg-m/s^2$	0.10	0.10
Time to reach design speed, s	360	360
Accessory weights, kg		
Lubrication pump	1.8	1.8
Vacuum system	3.6	3.6
Others	0.2	0.2
System weight, kg	62.6	43.6
System specific energy, Wh/kg	15.6	22.9

systems). During this period of non-use, energy is continuously being lost due to:

(1) Windage (aerodynamic).

(2) Bearing friction.

(3) Vacuum seals.

(4) Vacuum pump.

(5) Oil pump.

(6) Others.

In addition, there will be losses associated with the power-conversion system. The flywheel system spin losses for the AiResearch ETV-2 are shown in Figure 2-13 (Reference 2-7). The data show good agreement between the predicted losses and the JPL test data, with the deviation attributed to variations in flywheel windage due to the vacuum-pump cycling.

The combination of losses represents a significant energy drain that continues whenever the flywheel is in operation. The losses increase with increasing energy-storage capacity, which provides one of the arguments for minimizing the size of the flywheel system. Other arguments are that recharge time can be reduced (assuming a limited power source), and that noise, safety problems, and cost can be minimized. In other words, the flywheel system

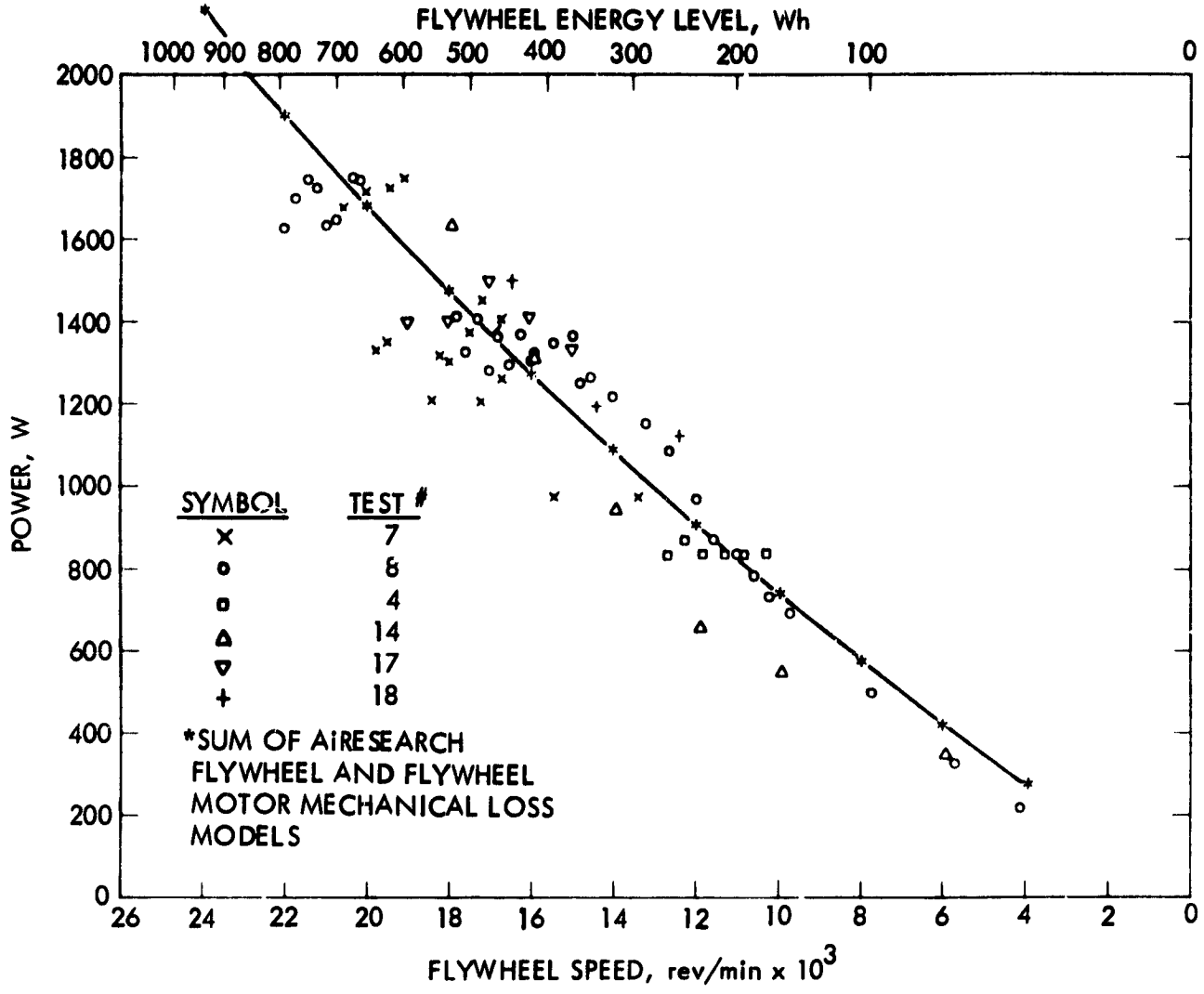

Figure 2-13. ETV-2 Flywheel-System Spin Losses (see Reference 2-7)

should be used primarily as a power-peaking device, not as an energy-storage device.

f. Cost Considerations. Because there are no mass-manufactured flywheel systems to use for comparison, costs are necessarily speculative. Estimates made by the LLNL panel for the flywheel system including rotor, housing, and vacuum pump are shown below.

Using isotropic rotors	$10.65 per kg (1977 dollars)
Using composite rotors	$ 6.60 per kg (1977 dollars)

g. Other Considerations. Since the first analyses of electric or hybrid vehicle applications, flywheels have looked attractive. This is due, in part, to the ease of the analysis and confidence in the results, as compared to a complex electrochemical or thermal system. Within limits, these analyses were accurate. It is indeed possible to build flywheels that have impressive values of specific power and specific energy. The problems are:

(1) Getting the energy into and out of the flywheel (a CVT is almost inevitable).

(2) Maintaining the stored energy over a reasonable time period (i. e., minimizing self discharge).

(3) Achieving reliability in spite of highly loaded bearings, close tolerances, a hostile environment, etc.

(4) Minimizing noise associated with high tangential wheel speeds, high rotational speeds, and high gear ratios.

(5) Minimizing the size and weight of all of the auxiliary and conversion systems.

(6) Minimizing the safety hazard associated with a rotor failure.

In spite of these concerns, the flywheel has definite promise as a power-peaking system. However, the energy capacity should be only as large as necessary for power peaking through urban driving cycles, probably 250 to 500 Wh. This size would still yield most of the advantages of the flywheel system while minimizing the concerns listed above.

2. Compressed Air

Compressed air has proven to be an effective means of storing energy to be used later in high-power applications such as air jack hammers, impact tools, and automobile lifts. It is a free-working fluid that is non-toxic, colorless, odorless, and available in unlimited quantities. However, it has the disadvantage of being noisy at high velocity, having significant losses associated with transferring, requiring large storage containers, needing appreciable heat transfer for efficient operation, and potentially presenting a safety hazard.

Conceptually, operation of the system in a vehicle is quite simple: during deceleration, regeneration is achieved by driving an air compressor and storing the compressed air in a pressure vessel. During power peaking, the compressed air is passed through an air motor, which provides useful power. Unfortunately, this conceptually simple system would be neither efficient nor effective, due to the behavior of the air as it is being compressed for storage and expanded to produce useful work. A schematic of the compressed air system is shown in Figure 2-14.

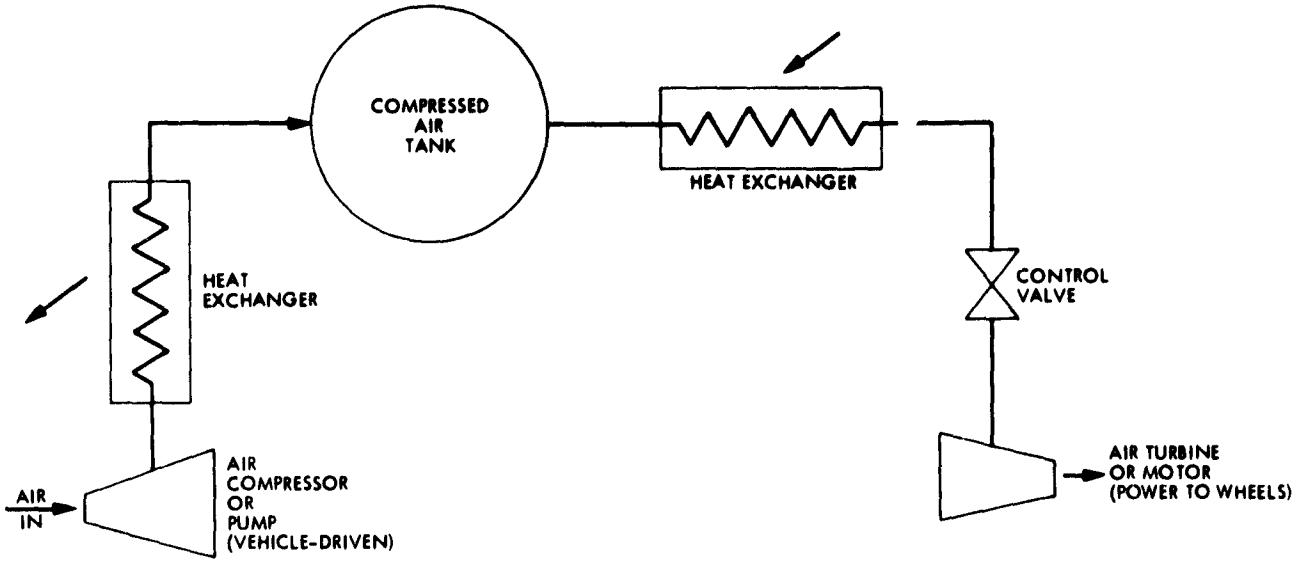

Figure 2-14. Compressed-Air, Power-Peaking System

a. Energy Considerations. When air is adiabatically compressed, there is an increase in temperature corresponding to the increase in pressure; for example, if an ideal compressor raises the pressure of standard air to 10 atm, the resulting temperature will rise to 284°C. A non-ideal compressor will raise the temperature even higher.

One of the major problems with the high temperature is that the corresponding density is increased much less than the pressure, thus increasing the volume required for a given mass storage. In the example cited, the density would have increased by only a factor of 5.18 (even less for non-ideal) instead of 10, corresponding to an isothermal compression; this means double the required storage volume and at least double the storage tank weight.

The situation is reversed as the air is being bled from the tank to produce useful work. For an adiabatic expansion in the tank, the stored air temperature decreases. This works against system efficiency for two reasons: (1) The airflow required to produce a given power is directly proportional to the absolute temperature of the air entering the turbine (air motor). (2) The amount of usable air in the storage tank decreases as the temperature decreases. Therefore, to produce a given horsepower, the airflow rate would have to be continually increased as the tank temperature and pressure decreases.

Ideally, the air should be cooled after compression before storage and heated after leaving the storage tank, but before expansion through the turbine. Cooling is the lesser of the problems because ambient air makes an effective heat sink, and with a reasonable heat exchanger the air could be cooled to within 10° or 20° of ambient (note that the air in the tank must also continually reject heat as the pressure is being raised by the once-cooled air). Heating air leaving the tank is more of a problem because without an external heat source, the maximum possible temperature is ambient,

and a much higher temperature is desirable. Some possible heat sources are from heat-engine radiators or exhaust, electric motor excess heat, or the air-conditioning condenser. Of course, heat can be provided by burning a combustible fuel, but then many of the complexities of another heat engine are added, and the original intent of a simple power-peaking device is diminished or lost.

For an electric vehicle with no reliable heat source, the probable system is one that is near-isothermal. Using the assumption of isothermal operation and ideal compressor and turbine, comparisons can be made of various alternatives for the compressed air system and the compressed air system can be compared with other system alternatives.

The main variables involved for the isothermal system are:

(1) The maximum power required.

(2) The total stored energy required (without regenerating).

(3) The maximum tank storage pressure.

(4) The turbine-design pressure ratio.

The power required determines the required air flow rate for a given pressure ratio across the turbine. The flow rate decreases with an increasing pressure ratio, but it is not linear. For example, Table 2-48 shows the air-flow rate to produce 1 hp with various ideal turbine pressure ratios. Also shown is the decease in flow required with the increasing pressure ratio; note the diminishing return.

Table 2-48. Ideal Turbine Performance and Required Airflow per Produced Kilowatts[a] in a 0.5-kWh Isothermal System

Turbine Pressure Ratio,[b] P_{in}/P_{out}	Required airflow, kg/s	% Change
2	1.419×10^{-2}	NA
4	0.783×10^{-2}	-81%
8	0.575×10^{-2}	-36%
16	0.468×10^{-2}	-23%
32	4.090×10^{-3}	-13%

[a]Turbine inlet temperature is assumed to be 15°C.

[b]Turbine discharge pressure is assumed to be atmospheric.

At first glance it seems that the optimum system would be the one with the highest turbine-pressure ratio. However, this is not necessarily true for the following reasons:

(1) The higher the required turbine inlet pressure, the more unusable air the storage tank will contain.

(2) A higher tank storage pressure means thicker tank walls to maintain a given stress level.

(3) More work per mass of air is required to compress the air to the higher tank pressures. That is, even though the turbine uses fewer pounds of air for given work, the compressor uses more regeneration energy to compress it.

As a comparison, Table 2-49 also shows the total amount of air needed to produce 0.5 kWh of energy. The size of the tank and the weight of the total system can then be estimated for various storage-tank pressures (Table 2-50). For an isothermal system the ratio of final-to-initial storage-tank pressure will equal the ratio of final-to-initial air mass in the storage tank.

Tables 2-49 and 2-50 show the various parameters for several ideal isothermal-system designs, using storage pressure from 16 to 64 atm and turbine inlet pressure from 2 to 8 atm. Because each system represents a

Table 2-49. Comparison of Compressed Air Storage Volume Requirements[a]

Maximum storage-tank pressure, atm	Turbine inlet pressure, atm	Usable air from tank, kg	Maximum air in tank, kg	Required tank volume, l
16	2	34	39	1031
32	2	34	37	481
64	2	34	35	232
16	4	19	25	671
32	4	19	22	286
64	4	19	20	134
16	8	14	28	730
32	8	14	19	243
64	8	14	11	104

[a]Available stored energy = 0.5 kWh, isothermal.

Table 2-50. Weight Comparison of Compressed Air Storage System[a]

Maximum storage-tank pressure, atm	Turbine inlet pressure, atm	Storage-tank volume, l	Spherical tank radius, m	Storage-tank weight, kg	Tank plus air weight, kg
16	2	1031	0.63	61	100
32	2	481	0.49	57	94
64	2	232	0.38	54	89
16	4	671	0.54	39	64
32	4	286	0.41	34	56
64	4	134	0.32	31	51
16	8	730	0.56	43	71
32	8	243	0.39	29	48
64	8	104	0.29	25	36

[a]Available stored energy = 0.5 kWh, isothermal.

usable 0.5 kWh of energy, the range of specific energy using the given assumptions range from about 5 to 13 Wh/kg. If a tank material with a greater assumed strength-to-weight ratio [very possible because the assumed values were for aluminum with an allowable stress of 114 MN/m^2 (16.6 ksi) or steel with an allowable stress of 345 MN/m^2 (50 ksi)] is used in conjunction with a heat source for the air, these values could easily be tripled. Consequently, with a mature design, the range of values for stored energy, including the weight of air and storage tank, would be about 20 to 40 Wh/kg.

The stored energy for the system is comparatively high in mass, but it is rather low in volume. The storage tank for the example system has volume requirements of about 100 to 1000 liters. However, for optimized pressures, pressure ratio, and mature technology, the expectations would be 5 to 15 Wh/l.

b. Cost Considerations. The cost for the storage system is low because the working fluid is free; the tank is light and comprises a simple technology. The example system has a higher weight storage tank but a lower cost-per-unit weight than a mature system. As the tank sophistication increases, the weight goes down; but the cost per weight goes up. A reasonable mature storage system cost is about $200/kWh (1977 dollars).

Note that although the cost for the energy-storage system is low, the costs for the auxiliary and conversion systems will be high. In addition

to the storage, there are four major subsystems required for a complete working system:

(1) Heat exchangers.

(2) Control valves/regulators.

(3) Air compressor or pump.

(4) Air turbine or motor.

A system designed to produce 20 kW and absorb even higher power levels and which uses near-ambient temperature air will be relatively large and expensive; most of the components would have to be developed. Heat exchangers that must contain fluids at 10 to 100 atm of pressure are difficult to build inexpensively. The high pressures require thick walls, in contrast to the thin walls needed for effective heat exchange. Thus, the surface area, weight, and cost go up dramatically with increasing pressure.

Similar problems will exist with the compressor. At these high pressure ratios, a multi-stage piston-type compressor with intercoolers is probably the only viable alternative, which means a sophisticated, high-strength device in a small package (and a corresponding high price). Unlike turbocharger turbines (which use a low-pressure ratio, high-temperature gas to produce a few kW of power), the high-pressure ratio will probably require a multi-staged, pressure-compounded, or velocity-compounded impulse wheel, which again is an expensive, sophisticated device.

Although accurate estimates have not been made concerning these additional component costs, a consumer cost for the 20 kW, 0.5-kWh system could easily be $2,000 to $5,000. Furthermore, there could be appreciable maintenance costs and reduced reliability, especially with the rotating machinery. These factors will probably combine to make the system an unattractive option as compared to the flywheel system.

3. Hydraulic Accumulators

Like compressed air systems, hydraulic accumulators have been used for years for energy storage and have proven effective for many applications. The primary use has been in conjunction with hydraulic systems in which fluid motors or actuators are used, usually on an intermittent basis, for slow-moving, high-power applications. A schematic for this type of system is shown in Figure 2-15.

a. Energy Considerations. The energy in the hydraulic accumulator is stored almost entirely in the compressed gas contained within the accumulator. The hydraulic fluid provides a means of compressing the gas and of transforming the stored energy within the gas to useful work (via the hydraulic motor). The mass of gas contained in the accumulator is typically constant, usually separable from the hydraulic fluid by a bladder. The pressure is equalized across the bladder, and work is performed by passing the high-pressure accumulator hydraulic fluid through a fluid motor and into the low-pressure reservoir. The pressure in the compressed gas, and correspondingly

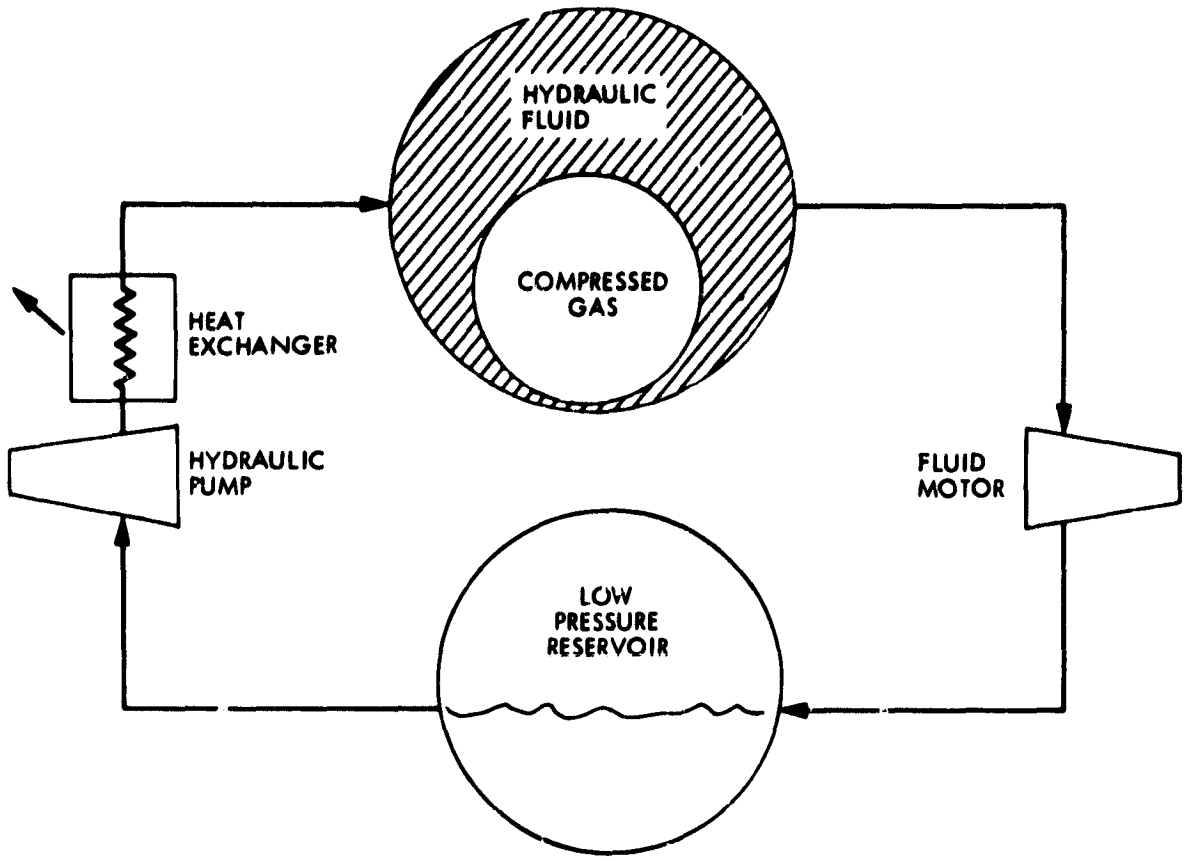

Figure 2-15. Hydraulic Accumulator Energy-Storage System

the potential for work from the hydraulic fluid, depends on the volume of the gas relative to the overall accumulator volume and the thermodynamics of the gas during expansion. Because the energy storage media is the same as for the compressed-air system (assuming air in the accumulator), the theoretical work capability will be the same in both cases with the same mass of air and the same thermodynamics. Thus, with these assumptions, the hydraulic accumulator will always have a lower specific energy than the compressed-air system, both in volume and mass. The hydraulic fluid is basically incompressible and, therefore, stores no appreciable recoverable energy - it simply acts as a working fluid to convey the energy.

b. Power Considerations. Although the stored energy is contained almost entirely in the compressed gas, the utilization is quite different from the compressed-air system. The probable operation would be over a rather limited range of pressure (isobaric would be ideal) at high absolute pressure levels (200 to 400 atm). Thus, the required air and fluid storage volumes are determined by the total fluid flow at the design pressure to produce the desired energy. The flow rate is determined by the power demand. For example, if the working fluids are assumed to be air and

hydraulic fluid with a specific gravity of 0.8, and the working pressure range is 200 atm to 1 atm, then the ideal power is 0.02 kW per cm^3/s of fluid flow (0.44 hp per $in.^3/s$).

Because the power produced is directly proportional to the pressure drop through the ideal pump, the required flow will increase or decrease as the working pressure is decreased or increased. Table 2-51 shows the volume flow requirements of hydraulic fluid for various assumed inlet pressures.

The storage system will not be isobaric but will depend on the relative change of the air volume during expansion (and the thermodynamics of the process). Without deliberate heat exchange the actual process the gas experiences will probably be between isentropic and isothermal. In either case, the gas initial volume would need to be several times the hydraulic fluid volume to minimize the pressure change during operation. If the initial ratio is assumed to be 3.0, then volume and weight requirements are estimated as shown in Table 2-52.

As was true with the compressed-air systems, the values shown for tank weights represent conservative state of the art. If higher strength-to-weight materials (composites, for example) are used and some heat exchange is included, the projected values of mass specific energy would increase by at least a factor of 3, corresponding to about 3 to 5 Wh/kg.

c. Cost Considerations. The cost of the hydraulic accumulator system is uncertain, but the storage system with fluid would be about 8 times the compressed air system, or about $1,600 per kWh. The remainder of the system, for a 20-kW power capability, would probably be in the range of $500 to $1,500, thereby putting the system cost at about $2,000 to $3,000 per kWh.

Table 2-51. Ideal Hydraulic Motor Flow Requirements

Pump motor inlet pressure, atm	Required volume flow per kW, cm^3/kW	Fluid volume for 0.5 kWh, l	Fluid weight for 0.5 kWh, kg
50	200	360	288
100	100	180	144
200	50	90	72
400	25	45	36

Table 2-52. Weight Comparison of Ideal Hydraulic Accumulator Storage Systems for 0.5 kWh Stored Energy (Isothermal)

Input pressure, atm	Air volume, l	Air weight, kg	Tank volume, l	Spherical tank radium, m	Tank weight, kg	Tank + air + fluid + weight, kg
50	1080	182	1440	0.70	260	730
100	540	182	720	0.56	270	596
200	270	182	360	0.44	262	516
400	135	182	180	0.35	264	491

d. Other Considerations. The advantages of the hydraulic accumulator as compared to a compressed-air system are:

(1) A smaller volume flow rate of working fluid for a given power.

(2) Less noise generation.

(3) Lower rotational speed of the motor (turbine).

(4) Closed system, less dependent on ambient conditions.

(5) Hydraulic pumps and motors of various capacity are already in widespread usage.

(6) Easier to obtain higher pressures with incompressible fluid.

Disadvantages of this system as compared to compressed air include:

(1) Lower specific energy on mass and volume basis.

(2) System fluid leaks are much more of a problem.

(3) Cost per unit of stored energy is higher.

(4) Hydraulic motors in existence are usually designed for intermittent duty.

4. Elastomers

Elastomers are materials that have low values of modulus of elasticity and have elongation capabilities of several hundred percent. A rubber band is an example of a simple elastomeric energy storage device, which in the "stretched" position has the capability of performing useful work. Natural rubber, polyurethane, and latex are among the most likely candidates for larger-scale energy storage.

Unfortunately, for the purposes of large-scale energy storage, elastomers have two major problems:

(1) The ultimate tensile strength is low compared to most solid materials (usually 2000 to 5000 psi).

(2) The energy-storage capacity is greatly diminished through repeated cycling, typically 50% to 75% after 100 or fewer cycles.

Conceptually, the storage system is simple: The elastomer is stretched during the energy absorption phase and relaxed during the energy release. The actual mechanism could be purely mechanical (such as a rubber band to power an airplane) or hydraulic. An example of a hydraulic system as suggested by United Technologies Corporation is shown in Figure 2-16. The elastomer has a specific energy of about 6.6 Wh/kg; the whole system is about 1.5 Wh/kg. The energy capacity of this device was projected to be 207 Wh.

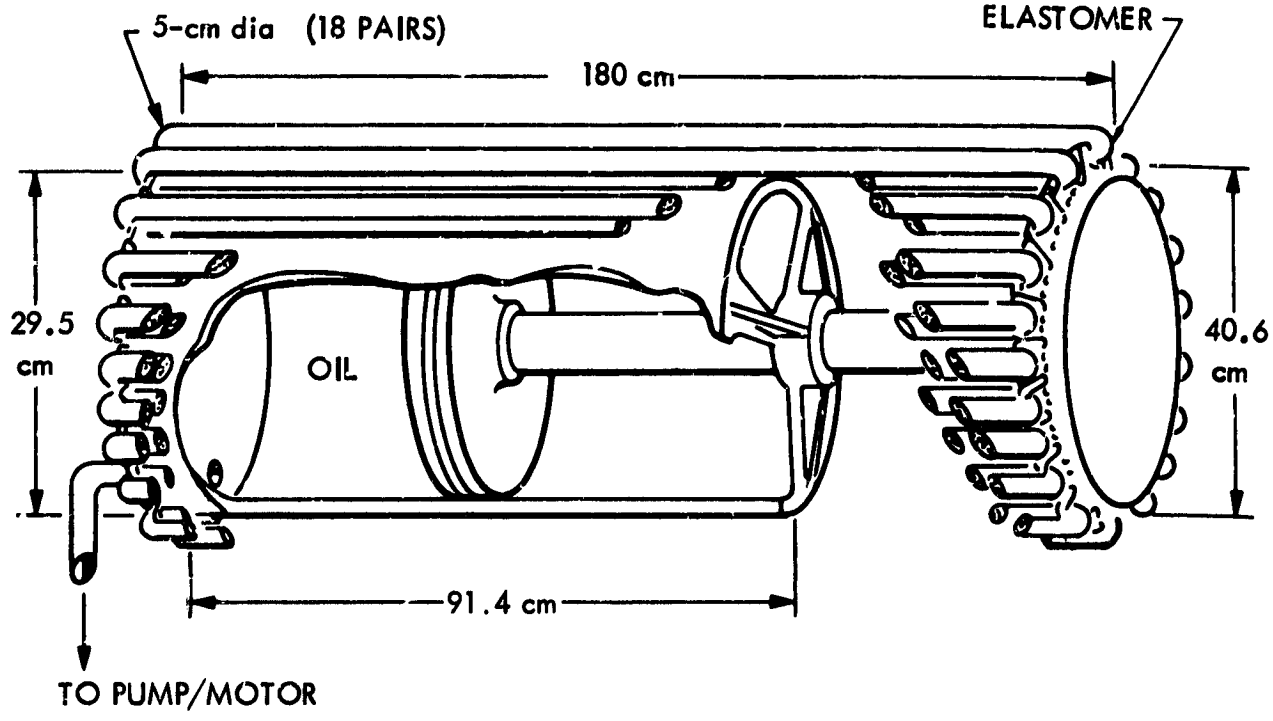

Figure 2-16. Elastomer/Hydraulic Energy-Storage System (Source: Lawrence Livermore National Laboratory)

Thus, the elastomeric energy-storage system has the advantages of simplicity, low noise, low cost, and good safety characteristics, but the almost insurmountable disadvantage of extremely low energy density. It has potential applications for cases in which only a low level of energy storage is required (perhaps less than 100 Wh), and specific energy is not a major consideration.

5. Liquid Springs

Liquid springs are based on the compressibility of liquids, which is low. Consequently, a system of this type would use extremely high pressures (1000 to 5000 atm) to cause sufficient fluid deformation for even low levels of energy storage. Even with pressures of this magnitude, the specific energy values (based on fluid and container only) are only about 0.5 to 1.0 Wh/kg.

The liquid-spring storage system is relatively simple: a liquid in a sealed, high-strength container is compressed (as a shock absorber) as energy is absorbed. However, because of the small displacements involved, it is unclear what type of auxiliary systems would be used to convert the stored energy into useful propulsion power. This, along with the low expected values of specific energy, make liquid springs unlikely candidates for power peaking.

6. Linear Elastic Solids

When a solid material is deformed some amount (but below the elastic limit), it has the capability of doing work as it returns to its original configuration. Spiral springs in watches and clocks provide the most familiar example of this method of energy storage, but other types of solids could perform the same functions. For example, helical springs, leaf springs, or even straight sections of metal rods can store recoverable energy.

A major advantage of a spring over a solid rod is that the amount of deformation allowable is significantly greater, which simplifies the recovery of the energy for most applications due to the smaller force moving through a greater distance.

The primary advantages of linear elastic solids are relative simplicity, low cost, low noise, and relative safety. However, the major disadvantage of low specific energy (1-5 Wh/kg for elastic solid and about 0.1 to 1 Wh/kg for storage system) essentially precludes the system from consideration.

7. Summary

Six potential candidates for power-peaking systems were reviewed:

(1) Flywheels.

(2) Compressed air.

(3) Hydraulic accumulators.

(4) Elastomers.

(5) Linear elastic materials.

(6) Liquid springs.

All of these systems have the common characteristic of being capable of absorbing high power levels without excessively large comp nts. However, with the exception of the flywheel, the energy-storage capability is extremely limited as compared to a storage battery.

There are significant differences in the various systems with respect to the state of development of critical hardware. For example, the turbo-machinery for a compressed-air system is almost nonexistent, while the hydraulic pumps and motors for a hydraulic accumulator system are almost state-of-the-art. Others, like the flywheel system, are currently under active development; liquid springs and linear elastic materials are scarcely more th n concepts.

For the immediate future the flywheel system would seem to be the only reasonable alternative for EHV power peaking. The flywheel rotor development has been active and succes l, as has been the case with CVTs. The projected costs an specific energy values are not prohibitive, certainly for a 0.25 to 0.5 kWh energy capacity and 20 to 30 kW of power capability. There are problems yet to be resolved, such as noise and high self-discharge rates; but for the time reference associated with this study, those are considered expected development problems.

SECTION II REFERENCES

2-1. "Bringing Plant Cost Estimates Closer to Reality," Chemical Week, pp. 30-33, August 4, 1982.

2-2. Consiglio, J. A., "Cost Analysis - Lead/Acid Batteries," Solva-Tek Associates, Topsfield, Massachusetts, November 20, 1978.

2-3. Symons, P. C., and Consiglio, J. A., Evaluation of Developmental Battery Cost Estimates, Solva-Tek Associates, Topsfield, Massachusetts, January 10, 1984.

2-4. Battery Design Analysis, [Sodium/Sulfur Batteries], Final Report, ARD 8181, Ford Aerospace and Communications Corporation, Aeronutronic Division, Newport Beach, California, February 1984.

2-5. "Sodium/Sulfur Battery Development Economic Analysis," Phase IV Topical Status Report, Ford Aerospace and Communications Corporation, Newport Beach, California, September 1980.

2-6. Preliminary Energy Use and Economic Analysis of Aluminum/Air Battery for Automotive Propulsion, Report R7908, Interplan Corporation, Santa Barbara, California, April 1980.

2-7. DeGrey, S. P., "Test and Evaluation of the DOE Flywheel-Electric Vehicle ETV-2," JPL Internal Report 5030-539, July 1982.

SECTION II BIBLIOGRAPHY

Barlow, T. M., et al., Mechanical Energy Storage Technology Project: Annual Report for Calendar Year 1980, LLNL Report UCRL-50056-80, Lawrence Livermore National Laboratory, Livermore, California.

Evaluation of Filament - Wound Kevlar - 49/Epoxy Fatigue Properties, LLNL Report UCRL 15264, Lawrence Livermore National Laboratory, Livermore, California, June 3, 1980.

Kay, J. F., Compression Molded Energy Storage Flywheels, LLNL Report UCRL-15324, Lawrence Livermore National Laboratory, Livermore, California, October 1980.

O'Connell, L., et al., Energy Storage Systems for Automotive Propulsions Final Report, Vol. II, UCRL-53053-80, December 1980.

Regenerative Flywheel Energy Storage System, Vol. II, Final Report, SRD-79-148-2, General Electric Company.

Regenerative Flywheel Energy Storage System, Vol. III, SRD-79-148-3, General Electric Company, June 27, 1980.

Sapowith, A. D., et al., State-of-the-Art Review of Flywheel Burst Containment, UCRL-15257, May 15, 1980.

Strauch, S., "Flywheel Systems for Vehicles," PAPER presented at the Electric and Hybrid Vehicle Advanced Technology Seminar, December 8-9, 1980.

SECTION III

ENERGY-CONVERSION SUBSYSTEMS

A. FUEL CELLS/METHANOL

1. Introduction

The purpose of this task was to provide an assessment of fuel-cell technology as a candidate power source for advanced vehicle systems. This task stemmed from the need to authenticate the potential of fuel-cell systems, to identify what must be done to make fuel cells compatible with advanced vehicles, and to establish fuel-cell power-system technology priorities. This effort builds upon findings from previous fuel-cell studies and from discussions with government and industrial personnel involved in the development of fuel-cell technologies.

The range and performance requirements of the advanced vehicle virtually dictate the inclusion of some type of "open" power source where propulsion energy can be stored as a liquid or gas in a separate container from the energy-conversion device. The "open" system energy converters are typically taken to be heat engines such as the conventional spark-ignition and compression-ignition engines, or the longer-range Brayton (gas turbine) or Stirling engines. All of these heat engines have in common mechanical work produced by the expansion of a gas heated by the combustion of a fuel.

A more direct and more efficient means of converting the fuel energy into useful work is the fuel cell, which for many years has been considered an alternative means of producing electrical energy from hydrogen or hydrogen-bearing fuels. It offers the potential advantages of high efficiency, low pollution levels, and a small number of moving parts (resulting in low noise levels and high reliability). The corresponding disadvantages have been viewed as high initial cost, large volume and weight (resulting in a low specific power), and a long start-up time required to reach rated output. Because of this combination of advantages and disadvantages, the fuel-cell applications thus far primarily have been limited to space systems and relatively large industrial power units. However, a number of recent activities by various private firms, institutions, and national laboratories have produced results indicating that fuel cells, in fact, could prove to be feasible for transportation systems.

The history of fuel cells dates back to 1802 when Sir Humphrey Davy experimented with a cell using carbon and nitric acid. However, Sir William Grove, another Englishman who in 1839 used crude cells as a means of providing electricity to decompose water, is usually given credit for the fuel-cell concept. In 1889 Ludwig Mond and Carl Langer developed a device (which they actually called a fuel cell) that produced a current of about 6 A/ft^2. F. T. Bacon demonstrated a working hydrogen/oxygen cell in 1932, but by then the development of generators and power plants had progressed to the point where there was little interest in the fuel cell. The space activities of the 1950s and 1960s revived fuel-cell activity, especially alkaline electrolyte hydrogen/oxygen cells. Since then, most efforts have been aimed at large phosphoric acid units (40 kW to 4.8 MW) for load leveling, apartment

complexes, other industrial uses, and work with smaller phosphoric acid (1.5 to 5 kW) units for the military. Only since the recent shortage and price increase of motor fuels has a serious interest developed in possible automobile applications, and as yet, no hardware development has been achieved in this area.

Fuel cells have an efficiency advantage because they convert chemical energy directly to electrical energy. Thus, the transfer of mechanical energy is eliminated from the system, as is not the case in high-temperature combustion processes. As a result, the amount of waste heat rejected is dramatically reduced, and many pollutants associated with high-temperature combustion products can be completely avoided. There are no moving parts in the cell itself, but auxiliary equipment in the form of pumps and blowers are required for steady-state operation. The curves of Figure 3-1 show the possible efficiency of fuel cells compared to other power sources.

Basically, there are three types of fuel-cell systems: direct, indirect, and regenerative. The direct system combines the fuel and oxidizer (usually, hydrogen and oxygen) from their separate storage tanks to produce the oxidized fuel (usually water), electricity, and waste heat.

The indirect system decomposes a substance containing hydrogen into hydrogen gas and other chemical species and combines the hydrogen with oxygen from the air. In this case, in addition to water, electricity, and waste heat, there are discharged gases, including the unused part of the air and the unused portions of the decomposed fuel. Typically, a "reformer" or catalytic "cracker" are used to obtain hydrogen from the fuel. Fuels potentially include all hydrogen-bearing substances, but from a practical standpoint only a few are viable candidates. They include hydrocarbon fuels (methane, naptha, gasoline, and fuel oils), alcohols (ethanol and methanol), and other hydrogen-bearing compounds, such as ammonia.

Regenerative fuel-cell systems are much like secondary storage batteries because they are electrically rechargeable. The most likely couples are hydrogen and chlorine or hydrogen and bromine. They are not "open" power sources because the fuel and oxidizer are permanent parts of the system. However, because of the potentially high specific power and specific energy (over 100 Wh/kg), they are of long-range interest for electric vehicles.

Another classification of specific importance in fuel cells relates to the type of electrolyte. For cells using a liquid electrolyte, it will be either alkaline or acid. The alkaline/electrolyte cells have many advantages, the major one is their proven performance using non-noble-metal catalysts. This is an extremely important consideration because the projected cost of the platinum catalyst is 20 to 30% of the overall system cost. However, the alkaline electrolyte is not compatible with carbon dioxide, which will be present both in the air and in the decomposed (or reformed) hydrocarbon fuels and alcohols. This problem is alleviated somewhat by using non-carbon-bearing fuels, such as ammonia. But even then, an air-scrubber would be required, as air is composed of about 0.03% carbon dioxide.

Other electrolyte types include solid polymer electrolytes (SPE) and molten carbonate electrolytes. Of these, the molten carbonate is not a likely automotive candidate because the electrolyte must be constantly maintained at

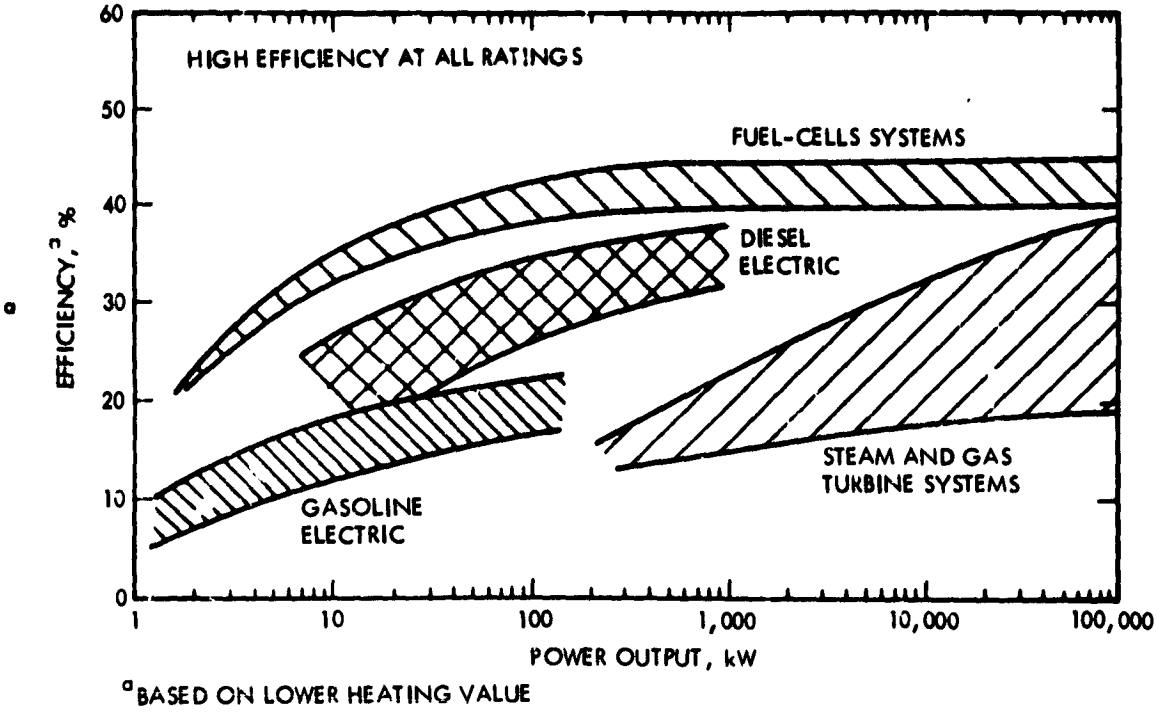

[a]BASED ON LOWER HEATING VALUE

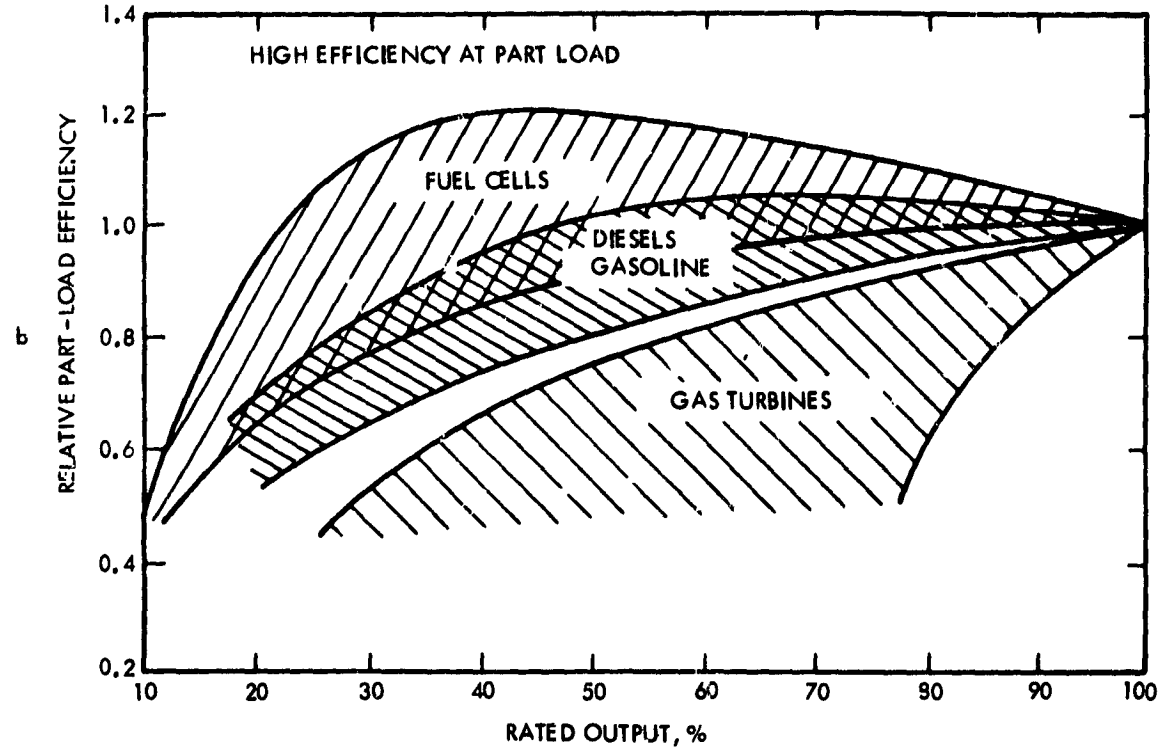

Figure 3-1. Fuel-Cell System Efficiency Comparison
(Source: Los Alamos National Laboratory)

a very high temperature (approximately 650°C), and bulky, expensive components are required.

2. Fuel-Cell Principles

A simple schematic (Figure 3-2) shows how a hydrogen/oxygen alkaline electrolyte cell operates. The electrodes are necessarily porous because they are required to bring gaseous reactants into contact with the electrolyte. At the electrodes, an electron interchange occurs that results in an external load current so that the electron exchange associated with direct contact of the molecules in a combustion process is avoided. In the case shown, the fuel (H_2) combines with hydroxyl ions in the electrolyte (OH^-) at the anode to give water and the electrons that travel through the external load. At the cathode, the electrons and the O_2 from the air combine with water to form the hydroxyl ions.

The net reaction is the same as that for stoichiometric combustion of hydrogen and oxygen, requiring 1 mole of hydrogen gas and 1/2 mole of oxygen gas for the formation of one mole of water.

Each molecule of hydrogen gas oxydized by the electron transfer through the external circuits results in a charge transfer corresponding to two electrons. Therefore, for 1 mole of hydrogen gas, the total charge transfer is

$$Q = q_{total} = 2e\,N_a$$

$$= \left(2\ \frac{\text{electrons}}{\text{molecule}}\right)\left(1.602 \times 10^{-19}\ \frac{\text{Coulomb}}{\text{electron}}\right)\left(6.023 \times 10^{23}\ \frac{\text{Molecule}}{\text{g-mole}}\right)$$

$$= 1.93 \times 10^5\ \text{Coulomb/g-mole}$$

where e is the electron charge and N_a is Avogadro's Number. Thus,

$$Q = 1.93 \times 10^8\ \text{Coulomb/kg-mole}$$

$$= 1.93 \times 10^8\ \text{A-s/kg-mole}$$

The useful electrical work delivered depends on the potential

$$W_{electrical} = q\,V$$

where V is the voltage potential.

The fuel cell also may be considered thermodynamically as a steady flow process, which has electrical energy as its work output as shown in Figure 3-3.

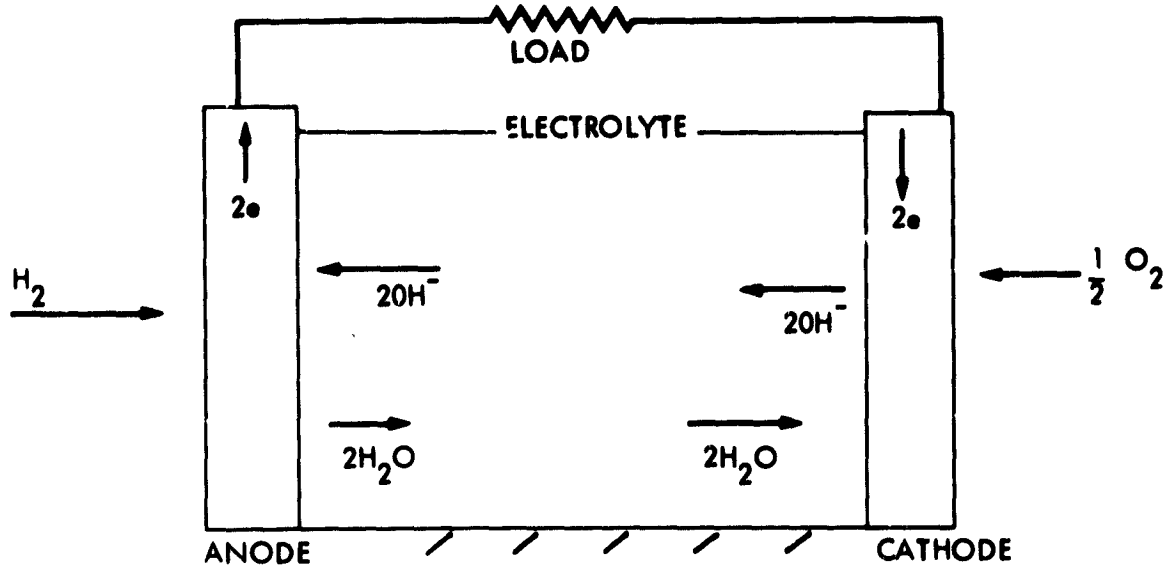

Figure 3-2. H_2/O_2 Alkaline Electrolyte Cell Schematic

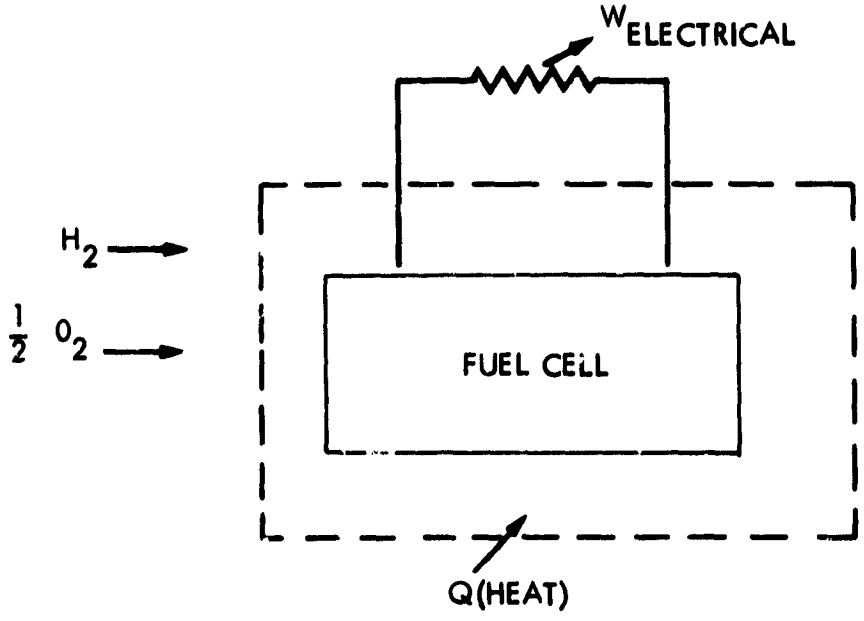

Figure 3-3. Simple Thermodynamic Model

For a steady-flow system

$$h_{reactants} + Q = h_{products} + W_{electrical} \text{ or}$$

$$W_{electrical} = h_{reactants} - h_{products} + Q$$

The Gibbs free-energy function also may be used to calculate electrical energy produced for an isothermal reversible constant-pressure process. At 25°C, the electrical energy produced may be represented as follows:

$$W_{electrical} = G_1 - G_2 = 56.7 \times 10^6 \ \frac{\text{Cal}}{\text{kg-mole of } H_2}$$

$$= 2.37 \times 10^8 \ \frac{\text{Joule}}{\text{kg-mole of } H_2}$$

Then, because $V = W_{electrical}/Q = \dfrac{2.37 \times 10^8}{1.93 \times 10^8}$

$$V = 1.23 \text{ V}$$

The potential of 1.23 V calculated by this method neglects all losses and as such may be used to compute the maximum possible efficiency:

$$\eta_{max} = \frac{G_1 - G_2}{H_1 - H_2} = \frac{W_{electrical}}{H_{combustion}}$$

$$= \frac{2.37 \times 10^8}{2.86 \times 10^8} = 0.83$$

In the equation above, the denominator of the fraction represents the energy of combustion per mole of hydrogen gas. Thus, for the conditions assumed, the hydrogen/oxygen fuel cell will have a maximum efficiency of 83%, with 17% of the energy being rejected as heat. The process described here is ideal, however, and the actual efficiency of the cell will be considerably lower because of losses inherent in the system. There will be the irreversible voltage drops that occur in the cells. Also, in computing the efficiency of the system, one must consider the motor/controller efficiency and the power required to operate all of the auxiliary systems. A more reasonable peak efficiency for the hydrogen/oxygen cell propulsion system would be on the order of 45 to 50% (including the controller/motor combination), which is still extremely good compared to even the best of the conventional heat-engine energy conversion systems.

The use of a hydrogen/oxygen/air fuel cell for automotive applications does not seem likely at the moment because of a number of factors. Among

these are the high cost, packaging problems, the inability to store significant quantities of hydrogen safely and inexpensively on a vehicle, the lack of hydrogen at a competitive price, and the lack of an infrastructure system to distribute the hydrogen. Of more potential interest is the use of a hydrocarbon fuel, such as methane gas or methanol. Of these two, methanol seems to be the more attractive because it can be produced from many sources such as wood, refuse, and garbage, but specifically because it can be produced from coal and stored as a liquid. Ammonia is also a potential fuel candidate because of the enormous manufacturing capability already in existence. There is, however, an obvious safety problem associated with ammonia as well as the infrastructure problem. It is also clear that an indirect fuel-cell system using hydrogen-bearing fuels will be somewhat less efficient than the direct system using only hydrogen. The overall efficiency will be reduced due to the energy associated with fuel decomposition and lower potential on the electrodes, even though some of the exhaust energy is recovered in the reforming process.

3. Fuel-Cell Alternatives

Obviously, there are a number of fuel-cell types along with a number of alternate fuels that could be considered candidates for automotive applications. However, under the guidelines of the Advanced Vehicle Assessment, petroleum-based fuels are eliminated, as are fuels that could not meet the requirements for widespread, fast refueling (infrastructure consideration). Consequently, it was determined that the most likely fuel candidate was methanol, which essentially eliminated the alkaline fuel cell from further consideration. In the event that the carbon dioxide incompatiblity of alkaline cells is eliminated, they would become prime candidates. Also, the possibility of ammonia as a viable fuel must be borne in mind, as that would also ease the problems of the alkaline cell.

The most comprehensive recent work concerning automotive fuel-cell applications has been done by Los Alamos National Laboratory (LANL) and their contractors, United Technologies Corporation (UTC), General Electric Company (GE), and the Energy Research Corporation (ERC) (References 3-1, 3-2, and 3-3). This work has focused on methanol fuel using phosphoric acid, advanced acid, and solid polymer electrolytes. Preliminary design studies were performed by the contractors for a fuel-cell system that would meet certain goals and requirements specified by LANL. Because these design studies are the most recent and comprehensive, they were used to represent the prime candidates for the present assessment. The LANL goals and requirements are shown in Table 3-1.

An abundant data source of fuel-cell performance does not exist to provide a sound basis for a detailed assessment for advanced vehicle applications. Analyses have been dependent upon data from three basic sources, namely, that generated for electric utilities, that which provides total energy data, and that developed for military and space applications. Although the military application comes closest to resembling vehicular operations, the military fuel cells were usually of the 3- to 5-kW size. The data from the utility sources were usually larger than the 40-kW size. The total energy data were generated under idealized conditions of continuous rather than the intermittent vehicle duty-cycle conditions. The deficiency of data also exists in areas of thermal management and fuel-flow management, especially as it relates to integrated fuel-cell stack and fuel-processor systems.

Table 3-1. Fuel-Cell Design Goals and Requirements

Item	Goal/requirement
Weight,[a] kg	318
Volume,[a] m^3	0.34
Continuous power,[a] kW	20
Peak power,[a] kW	60
Start-up,[b] min	0.5
Fuel	Methanol

[a]Lawrence Livermore National Laboratory.

[b]Jet Propulsion Laboratory.

a. Solid Polymer Electrolyte Fuel Cell. The SPE fuel cell has been under development for over 2 decades. It has been established as a successful power plant for space applications. More recently, it has found terrestrial applications in such devices as data buoys, air samplers, and mobile transmitters. The same basic technology has been adapted for hydrogen production from water electrolysis.

The basic elements of an SPE unit cell are shown in Figure 3-4. As in the phosphoric acid (PA) and trifluoromethane sulfonic acid (TFMSA), the SPE unit cell is a hydrogen/oxygen fuel cell with catalyzed anode and cathode but with a solid polymeric electrolyte. The various functional elements (fuel-cell stack, fuel processor, and electrolyzer) in the fuel-cell power plant are shown in Figure 3-5.

General Electric Company has described the operation as follows: Pure methanol is pumped from the fuel tank to the vaporizer where it is evaporated by steam produced from fuel-cell waste heat. The methanol (gas) is further heated in the super-heater and then is fed to the methanol reactor (cracking reactor). There, the methanol is converted to H_2/CO at 300°C according to the reaction

$$CH_3OH\ (g) \longrightarrow 2H_2 + CO$$

Heat for the exothermic reaction (90,250 kJ/kg mol CH_3OH) is provided at 343°C by 1450°C flue gas derived from burning excess fuel leaving the fuel-cell chambers. The H_2/CO stream leaves the reactor, exchanges heat with the incoming methanol stream in the preheater, and enters the anode exhaust dryer. At that location, most of the water vapor of the fuel-cell anode exhaust is reclaimed across the water transport membranes. The vapor exchange ensures system water balance and provides water for the ensuing CO shift. Additional water is added to adjust the steam-to-carbon ratio (S/C) to

C-2

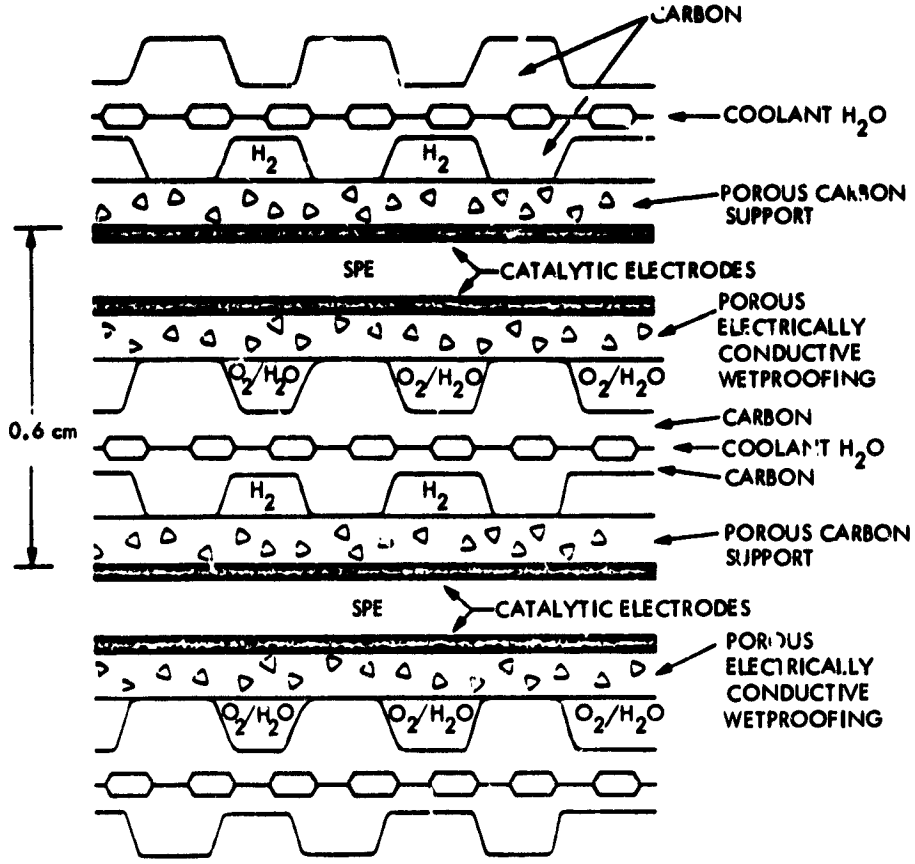

Figure 3-4. Basic Solid Polymer Electrolyte Structure in the Fuel-Cell Module (Source: General Electric Company)

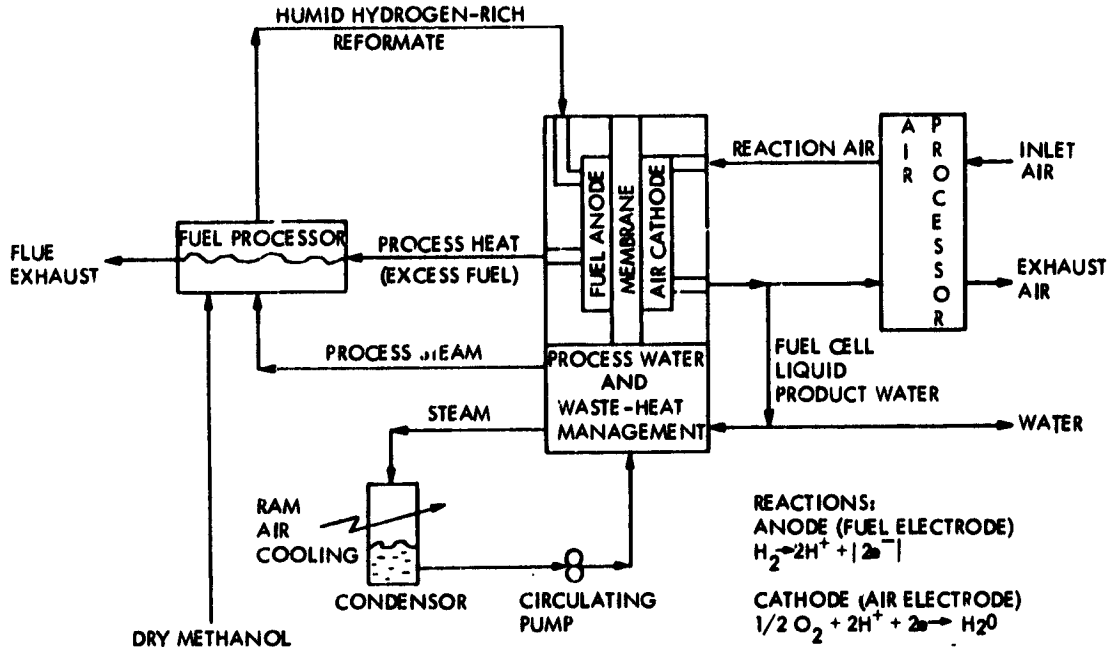

Figure 3-5. Indirect Methanol/Air Solid Polymer Electrolyte Fuel-Cell System (Source: General Electric Company)

3.0 in the shift reactor. The water added in the reformate humidifier is produced in the vaporizer from fuel-cell waste heat.

The fuel stream enters the shift preheater where its temperature is increased and then into the CO shift reactor. The CO shift is exothermic and is used to produce high-pressure steam. This steam provides part of the power for the air compressor. The final reformate leaves the preheater and enters the anode humidifier, wherein some of the water used in the shift reactor is replaced by vapor exchange with steam from the vaporizer. Final trimming of the water content in the fuel-cell feed is achieved by injecting liquid water into the stream, which lowers the temperature and saturates the feed stream.

The fuel charge enters the fuel-cell anode chambers and produces electrical power. At each point along a cell, the fuel stream remains saturated. As hydrogen is used, water vapor condenses from the gaseous stream onto the membrane electrode assembly (M&E). The liquid water is protonically pumped across the M&E from the fuel side to air side, where it appears as liquid water. After the fuel exhaust stream leaves the fuel cells, it passes through the anode exhaust dryer. It now contains the excess hydrogen, product CO_2, and some water vapor. It is mixed with stoichiometric air, preheated, and burned to form hot flue gas, which supports the cracking reaction. The flue gas leaves the system at moderate temperature with about 40% of the system product water.

Reaction air is compressed to about 10 atm abs. Some of the heat of compression is removed by exchanging with exhaust air. The reaction air is then humidified by absorbing water from the exhaust air via water vapor transport membranes. It is not necessary to saturate the feed air completely because condensing water from the fuel side and reaction product water form at a rate high enough to saturate the air stream and prevent membane drying. The air reacts in the air chambers and leaves saturated with water vapor and carrying liquid product water. The product water is separated from exhaust air in the separator. Exhaust air completes the path to the exhaust air water economizer and reaction air cooler. It leaves that component with maximum temperature and low humidity for use in the expander. Net power for the compressor/expander is provided by the steam expander.

The cooling system and waste-heat conversion operates as follows: Liquid water enters the fuel-cell boilers where it is evaporated to steam. The steam enters the vaporizer where it provides heat for methanol vaporization. Some of the steam is directed to the fuel humidifiers. Remaining low pressure steam is fed to the compressor/expander to provide work for air compression. A condenser provides the heat sink for the steam expansion in the expander. Condensate from the vaporizer is sub-cooled to prevent flashing before return to the circulation pump, which feeds back to the cooling loop. Some product water taken from the separator is added to the coolant stream to compensate for the water used in the humidifiers.

An electrolyzer subsystem is used to manufacture hydrogen and oxygen during off-peak loads; these gases are stored in pressure vessels. For start-up and peak power, pure hydrogen and oxygen are admitted to fuel and oxidant chambers, respectively. Enough hydrogen and oxygen is stored for the expected 1-minute warm-up, which would bring the fuel cell to a

self-sustaining temperature and the fuel processor to essentially steady-state temperature.

Performance Characteristics. The baseline power plant layout is shown in Figure 3-6, and some projected characteristics are given in Table 3-2.

The performance polarization curves established for the baseline SPE design are shown in Figure 3-7. These voltage-current curves are based upon the performances of (1) a pure hydrogen/oxygen cell and (2) a reformate/air cell. In the baseline design for a vehicle, the fuel-cell stack can draw its reactants from the pure hydrogen/oxygen source, the reformate/air source, or a mixture of the two, depending upon the power level and drive mode. Based on these curves, LANL has developed a composite curve (Figure 3-8) that shows voltage and fuel consumption versus current density. A mathematical model describing the voltage-current and voltage fuel consumption relationships must consider the effects of the power/voltage level transitions of the baseline power-system design.

Prior reformate/air SPE fuel-cell tests were conducted using a simulated reformate with a fixed carbon monoxide concentration level of 0.3%. For the feasibility study, a design point yielding 0.17% CO was used. Because the CO level will vary in a practical system (without precise control), a carbon monoxide tolerance map should be developed either empirically or theoretically early in the design of the power plant.

The electrolyzer subsystem manufactures the hydrogen and oxygen used during start-up and peak power. The pressurized gas vessels are sized to

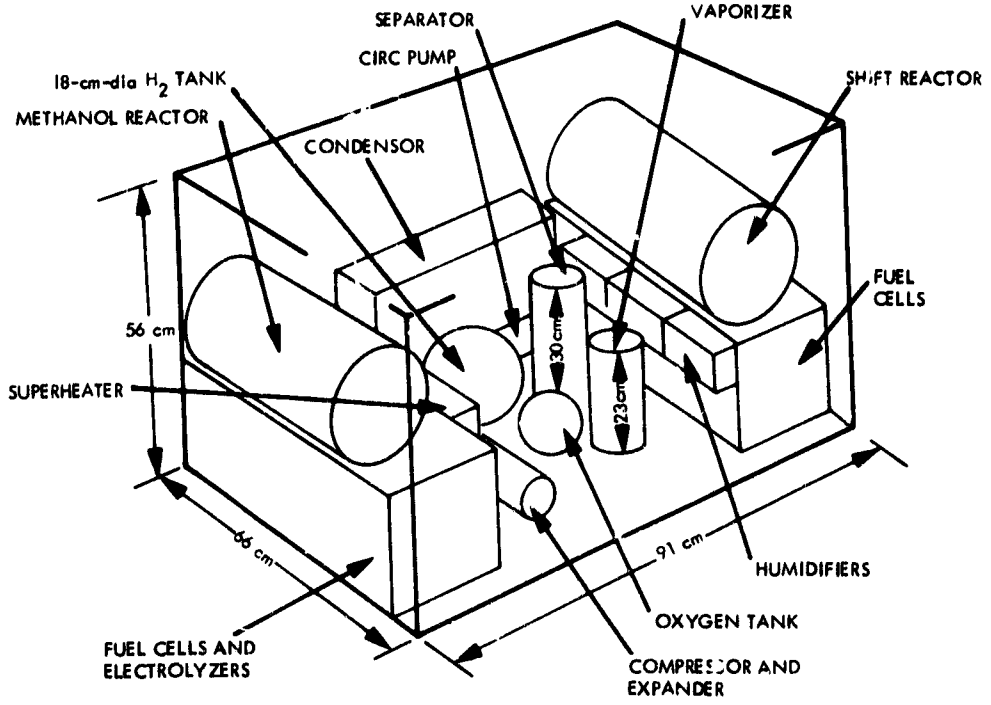

Figure 3-6. Projected Solid Polymer Electrolyte Power Plant Layout

Table 3-2. Projected SPE Fuel-Cell System Characteristics[a]

Characteristics	Value
Specific power, W/kg	
Continuous	131
Peak	431
Power density,[b] W/l	
Continuous	59
Peak	194
Operating pressure and temperature	10 atm cathode, 2 atm anode, 104°C
Efficiency at continuous rating, %	51
Cold start-up time, min	1 to 3[c]

[a]Based on 96-Vdc, 20-kW (continuous rating) GE system design.
[b]Based on 0.12-m^3 component volume with 34% packing factor.
[c]Time required on reformate, instantaneous start on H_2/O_2 possible.

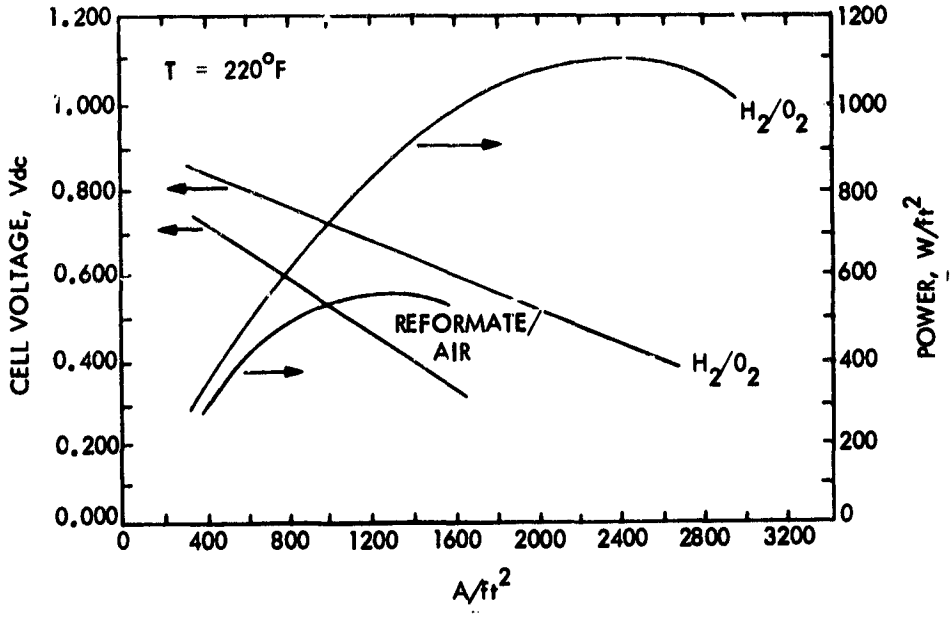

Figure 3-7. H_2/O_2 and Reformed Methanol/Air Performance Polarization Curves (Source: General Electric Company)

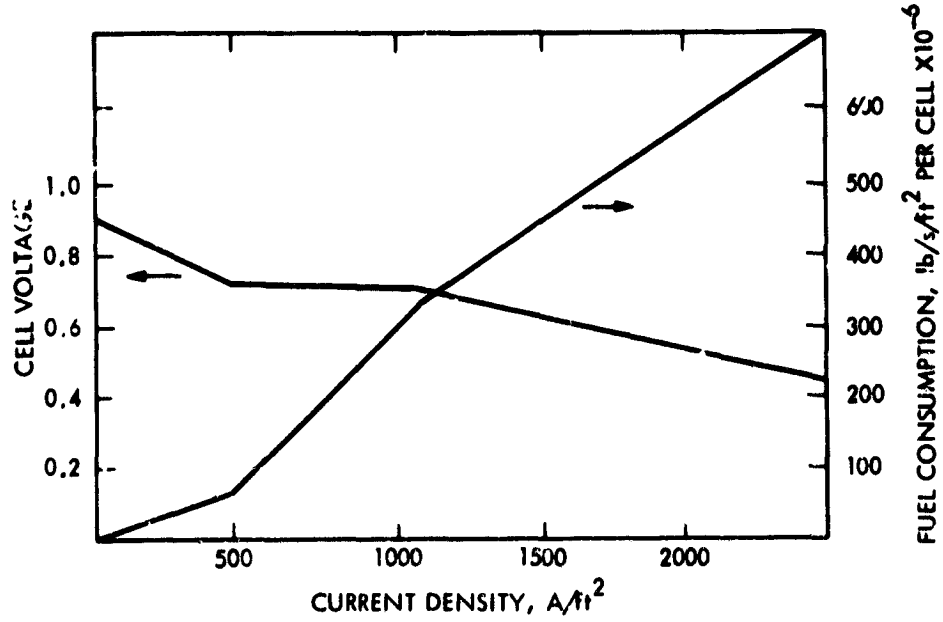

Figure 3-8. Composite Fuel-Cell Characteristics, Reformate/Air, H_2/O_2 (Source: Los Alamos National Laboratory)

provide the necessary power until the fuel cell reaches a self-sustaining temperature and the fuel processor reaches a steady-state temperature. The effect of temperature on rapid start, on/off, start/stop should be investigated. The problem of freeze-thaw is a more catastrophic phenomenon, and although it has been examined for other applications, it should be analyzed in the context of vehicular power plant design.

The baseline power plant incorporated a graphite ring, free-piston approach for compressor-expander design, and assumes an 82% steam expander efficiency. The efficiency value is questionable in view of the relatively poor design of the baseline configuration. The brittleness of the graphite rings and the replacement of the free piston with a vane-type-pump approach should be considered. A parasitic power loss of 700 W is possible in the baseline design.

Sensitivity analyses to determine the effect of component efficiency on system output should be conducted to optimize the design and verify the parasitic power loss levels.

The claims for the SPE fuel-cell system seem to satisfy the gross requirements and goals shown in Table 3-1; however, the assessment indicates large uncertainties in attaining cost reduction and in actual performance.

Cost and Life. The manufacturing cost has been projected by GE to be about $3300 for a 20-kW unit in production quantities of 100,000 per year. Therefore, the selling price would be expected to be about $6600 or $330/kW. GE has estimated the recoverable platinum cost to be $960 for the 0.72 Vdc per cell baseline plant.

The cost of the SPE membrane accounts for a large portion of the cost of the SPE power plant. The assumption that future membranes could conceivably cost about $\$65/m^2$ compared to existing $\$320-430/m^2$ will depend upon (1) technical direction in establishing a use life of the membrane specific to vehicles, i.e., replacing the 40,000-h utility application requirement with a 4000-h vehicular-use life and (2) directed research and development to focus recent worldwide interest in low-cost, efficient membranes on vehicular applications.

The cost of the platinum catalyst accounts for another major portion of the cost of the SPE power plant. There seems to be no inherent technical reason why the platinum loading cannot be reduced from the present level of $86\ g/m^2$. However, a projection of an order of magnitude reduction to $8\ g/m^2$ without more substantiating evidence seems somewhat suspect. An immediate test to verify loading versus performance would be in order.

b. Phosphoric Acid Fuel Cell. LANL contracted with two organizations for phosphoric acid fuel cell (PAFC) designs and their study approaches varied accordingly. United Technologies Corporation (UTC) identified their most attractive near-term design choice, evaluated the system deficiencies for vehicular applications, and designed an advanced system that specifically addressed the near-term system deficiencies (see Reference 3-2). The UTC advanced design met the goals of the LANL contract, and the performance described in this report deals strictly with that design. Energy Research Corporation (ERC) projected PAFC performance characteristics based on parametric analyses of the effects of current density, catalyst loading, and pressurization on system efficiency (see Reference 3-3). ERC contrasted the PAFC system with an advanced acid system, which is described in Section IV of this report.

The phosphoric acid cell has a more extensive design and manufacturing base than the SPE system previously discussed. It has been under development for years, and the technology demonstrated in current technology systems is well documented. However, the bulk of the information concerns constant-load operation, and the performance in cyclic-load vehicular applications is largely unknown.

The most apparent challenge with the PAFC is one of scaling down (weight and volume) to a size acceptable for a vehicle. UTC has attacked this problem by physically and thermally integrating the cell stack and reformer (i.e., internal reforming) as well as proposing specifically designed ancillary components. Other key features of the advanced power plant are atmospheric pressure operation, improved cell performance compared to existing power plants, and the ability to operate at elevated temperatures for short periods. The basic elements of a PAFC (UTC) unit cell are shown in Figure 3-9. Besides the catalyzed anode and cathode, the key element is the ribbed substrate that functions as gas reaction distribution channels, current conductor, heat transfer, and phosphoric acid electrolyte storage media.

The various functional elements for the UTC advanced design are shown in Figure 3-10. The operation of the system has been described by UTC as follows: The fuel-water mix is pumped through cooling passages in the cell where it is partially vaporized by stack reject heat. (Another option with slightly

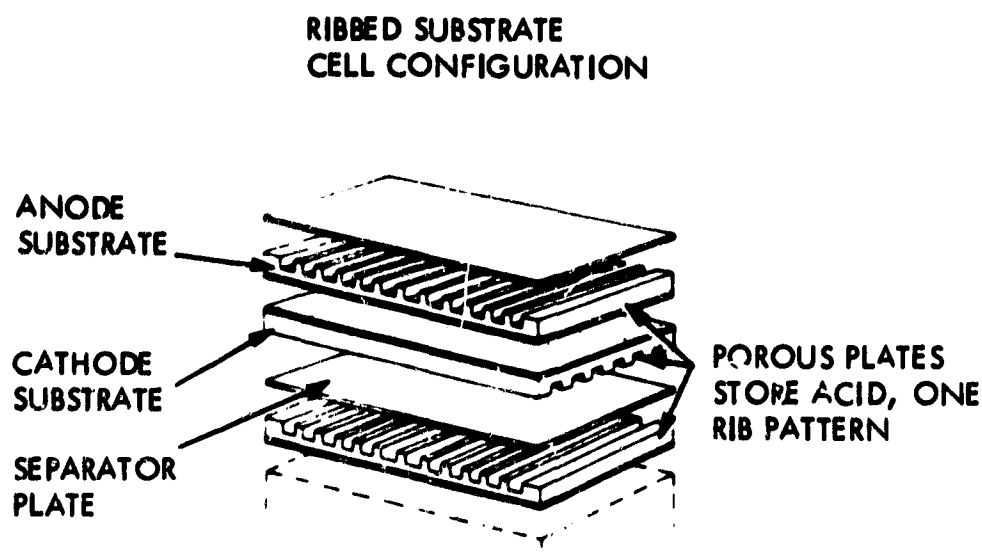

Figure 3-9. Phosphoric Acid Fuel Cell Ribbed Substrate Cell Configuration (Source: United Technologies Corporation)

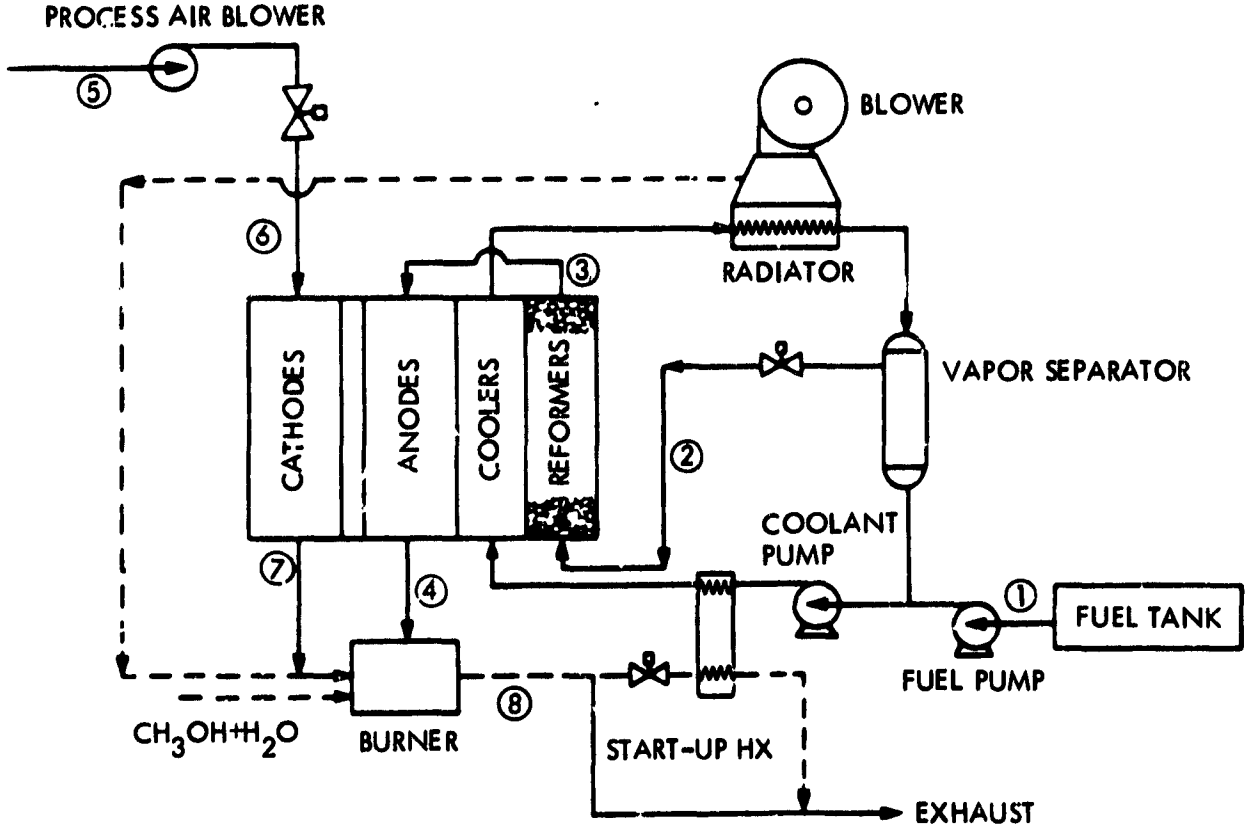

Figure 3-10. United Technologies Corporation Advanced Phosphoric Acid Fuel Cell Power Plant (Source: United Technologies Corporation)

increased complexity uses water cooling of the stack as in present power plants; heat is subsequently transferred to vaporize the methanol-water mix. This option has the advantage of reducing fuel inventory and retains the advantage from use of stack heat.) The vapor is separated and returned to separate passages within the cell stack where the methanol and water vapor react over a reform catalyst to produce the hydrogen-rich gas used in the anode (fuel electrode) reaction. The phosphoric acid cell operates at 204°C, and vaporization and reforming has been demonstrated at these temperatures. Use of cell stack reject heat to provide heat for vaporization and reforming in this manner reduces requirements on ancillary components, such as radiators, cooling pumps, and fans. Placing reform catalyst in the cell stack improves packaging. Both effects reduce power-plant weight and volume.

The hydrogen-rich gas is passed over the anode where 85% of the hydrogen is consumed. The remaining hydrogen is burned to provide additional heat to the system and then exhausted. Excess heat at high power is rejected through the radiator or to the vehicle heater (not shown). The radiator fan also provides air to the anode exhaust burner during start-up. A process air blower provides oxygen to the cathode (air electrode).

The advanced power plant design is based on improved cell performance. Improved performance reduces stack area and increases efficiency, which reduces requirements on ancillary components. Improved performance also increases overload capability, which reduces the need for a battery during acceleration transients. Figure 3-11 compares phosphoric acid fuel-cell performance demonstrated in power-plant cell stacks to future expectations for this technology. A modest improvement in performance can be achieved by structural and material changes that reduce both resistance and diffusion losses. Achieving further improvements requires changes to the cathode reaction or higher pressure operation. Concept feasibility has been established for two approaches that change the cathode reaction: (1) imposition of a reduction/oxidation (redox) process at the cathode by changing the cathode catalyst and (2) changing the electrolyte.

Increased pressure can also be used to improve cell-stack performance and to reduce the size of piping and heat exchangers. UTC's electric utility power plants operate at elevated pressure. Further study of this option is recommended for the vehicle power plant, with special consideration being given to the performance of turbocompressors or positive displacement expander-compressors to achieve the pressure increases at high efficiency. UTC has used improvement of performance based on cathode redox catalysts as the basis for this study because it provides the simplest system concept.

Energy Research Corporation chose a pressurized system to improve performance, and described the operation of their system (shown in Figure 3-12) as follows:

The fuel mixture is vaporized in the reformer by the waste heat of the fuel cell, then reformed. The reforming reaction is represented by the following equation:

$$CH_3OH + 1.3\ H_2O \longrightarrow CO_2 + 3H_2 + 0.3\ H_2O$$

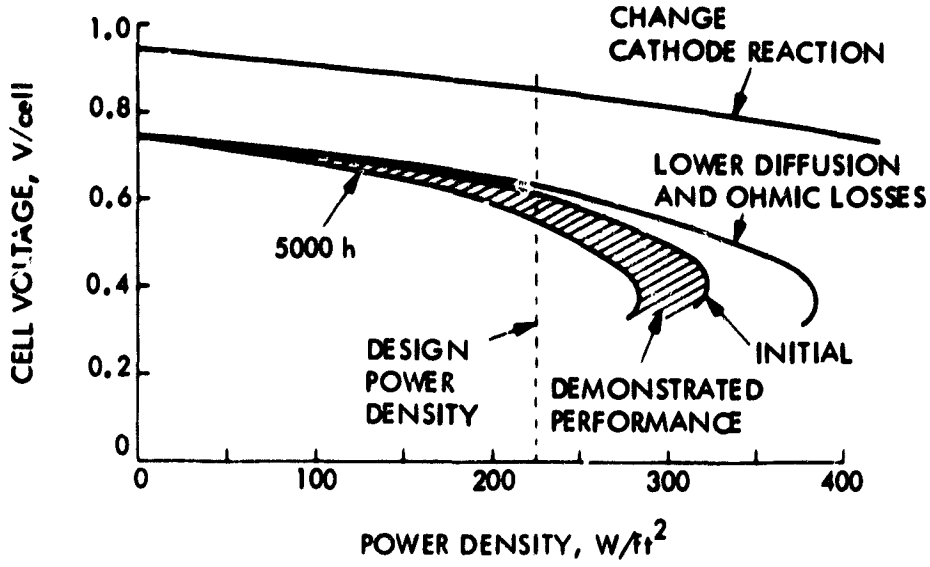

Figure 3-11. Improved Phosphoric Acid Fuel Cell Performance Projections (Source: United Technologies Corporation)

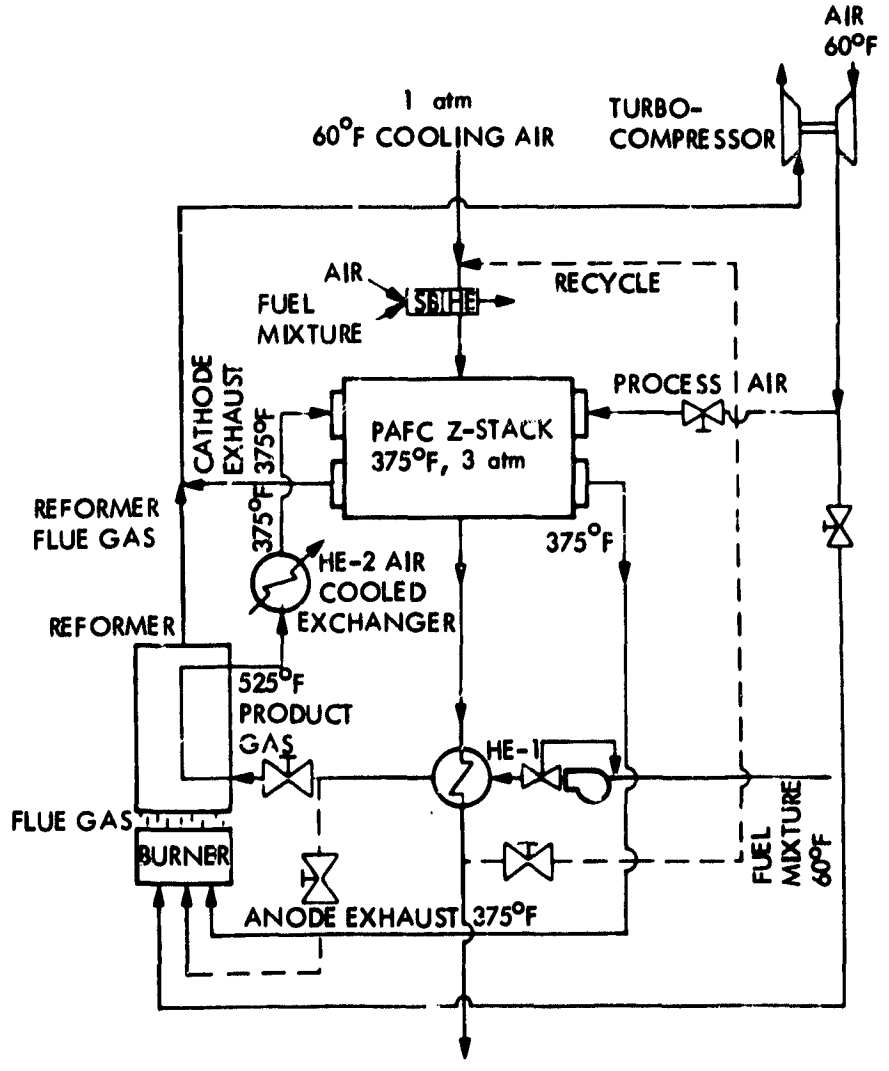

Figure 3-12. Energy Research Corporation Polymer Acid Fuel Cell Power Plant (Source: Energy Research Corporation)

The product gas is shifted toward the top of the reformer where the temperature is low. The shifted product gas at 274°C is cooled down by an air-cooled exchanger. The fuel is fed to the fuel-cell anode. The unspent fuel is returned to the reformer burner where it is combusted with fresh air. The heat energy in the flue gas is used to vaporize the fuel mixture and to provide the endothermic heat of reaction. The system is operated at 3.16 atm. A turbocompressor compresses the air for the fuel-cell cathode and the reformer burner. To save fuel, the cooling air for removal of fuel-cell waste heat is not pressurized. The reformer flue gas and the cathode exhaust are expanded in the turbocompressor to provide energy for compression. For the turbocompressor to be energy self-sufficient, it should be 80% efficient. This suggests that substantial development is required to improve the efficiency of the turbocompressor to 80% (because typical turbocompressors are about 50% efficient).

During start-up, a part of the fuel mixture is combusted in the reformer burner. The flue gas provides the latent heat of vaporization and the endothermic heat of reaction. Also, a part of the fuel mixture is combusted in the start-up burner to heat up the cooling-loop air. The heated air passes through the stack, transferring the heat to the cold stack. Most of the exiting air is recycled, mixed with ambient air, and circulated, thus rapidly heating up the stack.

An automatic control unit (ACU) measures the output current (load) and accordingly controls the fuel-flow rate to the reformer. Similarly, it also controls the temperatures of the reformer and the fuel-cell stack by measuring the exit temperatures.

Performance Characteristics. The UTC and ERC designs do not differ substantially in projected specific power capabilities, although their design approaches and operating conditions are quite different. The characteristics are summarized in Table 3-3. Substantial developments are required to achieve this projected performance. UTC considered a number of alternatives, including internal reforming, lowering diffusion losses, system pressurization, and changing the cathode reaction (redox couple). The resulting performance differences are summarized in Figure 3-13.

UTC can meet the LANL requirements (and perform as described in Table 3-3) only through a combination of internal reforming, the development of a redox couple, and specific designs of ancillary components. UTC estimated that 8 to 12 years would be required for the development. ERC assumed a pressurized system with better oxidant utilization as well as improved catalyst utilization and estimated 4 years to system readiness.

Cost and Life. UTC estimated the costs of the vehicular power plant from its experience with high-production estimates for the natural gas/fuel, 40-kW unit. Manufacturing cost estimates range from $150 to 250/kW continuous (1981 dollars) for large production quantities of 100,000 units per year. The cost range is a function of cell improvement and whether or not noble metals can be eliminated from the cathode. A life of greater than 5000 hours is projected for the system (as opposed to 40,000 hours for the utility system).

Table 3-3. Projected Polymer Acid Fuel Cell System Characteristics[a]

Characteristic	UTC[b]	ERC[c]
Specific power, W/kg		
Continuous	80	88
Peak	240	269
Power density,[d] W/l		
Continuous	59	59
Peak	176	179
Operating pressure and temperature, atm, °C	1.0, 204	3.0, 191
Efficiency at continuous rating, %	56	60
Cold start-up time, min	5 to 7	10 to 12

[a]Based on 96-Vdc, 20-kW (continuous rating) system designs.

[b]United Technologies Corporation.

[c]Energy Research Corporation.

[d]Based on 0.23-m^3 component volume with 60% packing factor.

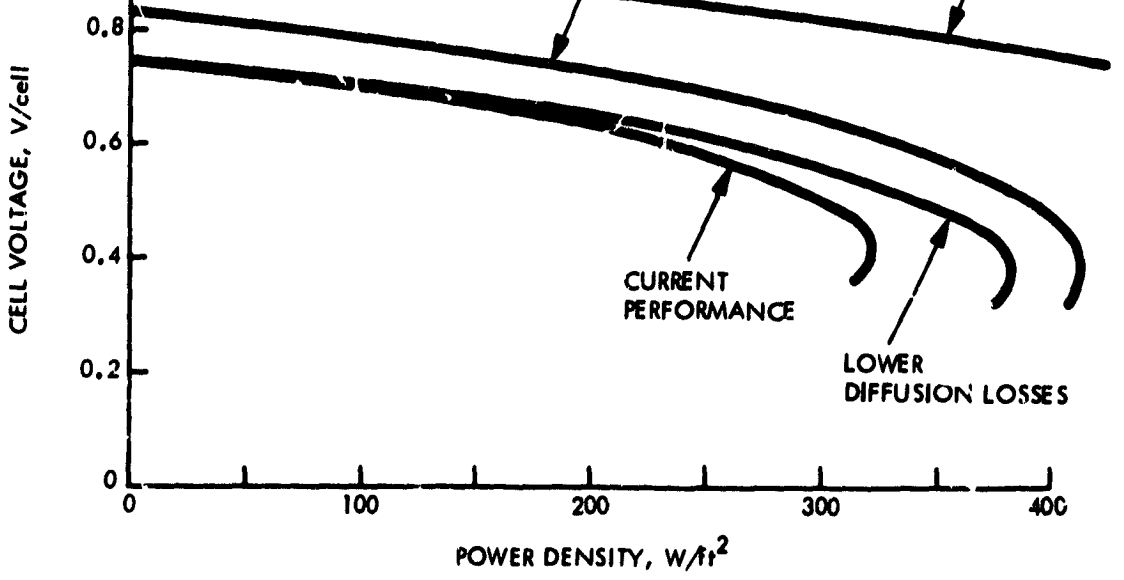

Figure 3-13. Comparison of Advanced Performance Alternatives (Source: United Technologies Corporation)

ERC estimated the manufacturing cost to be $100/kW continuous (1981 dollars) in quantities of 100,000 units per year. The life expectancy is about 4000 hours. This includes an assumption of 0.375 mg/cm^2 (electrode area) of platinum catalyst.

The ERC and UTC cost estimates are significantly different, especially considering that the UTC estimate for a near-term fuel cell with 0.375-mg/cm^2 platinum loading is $250 to 300/kW (1981 dollars). These numbers should be considered in light of the lack of production experience and development uncertainty.

c. Trifluoromethane Sulfonic Acid Fuel Cell. The basic elements for a TFMSA fuel cell are essentially the same as the ERC phosphoric acid fuel cell. The various functional elements of the ERC fuel cell power plant are shown in Figure 3-14.

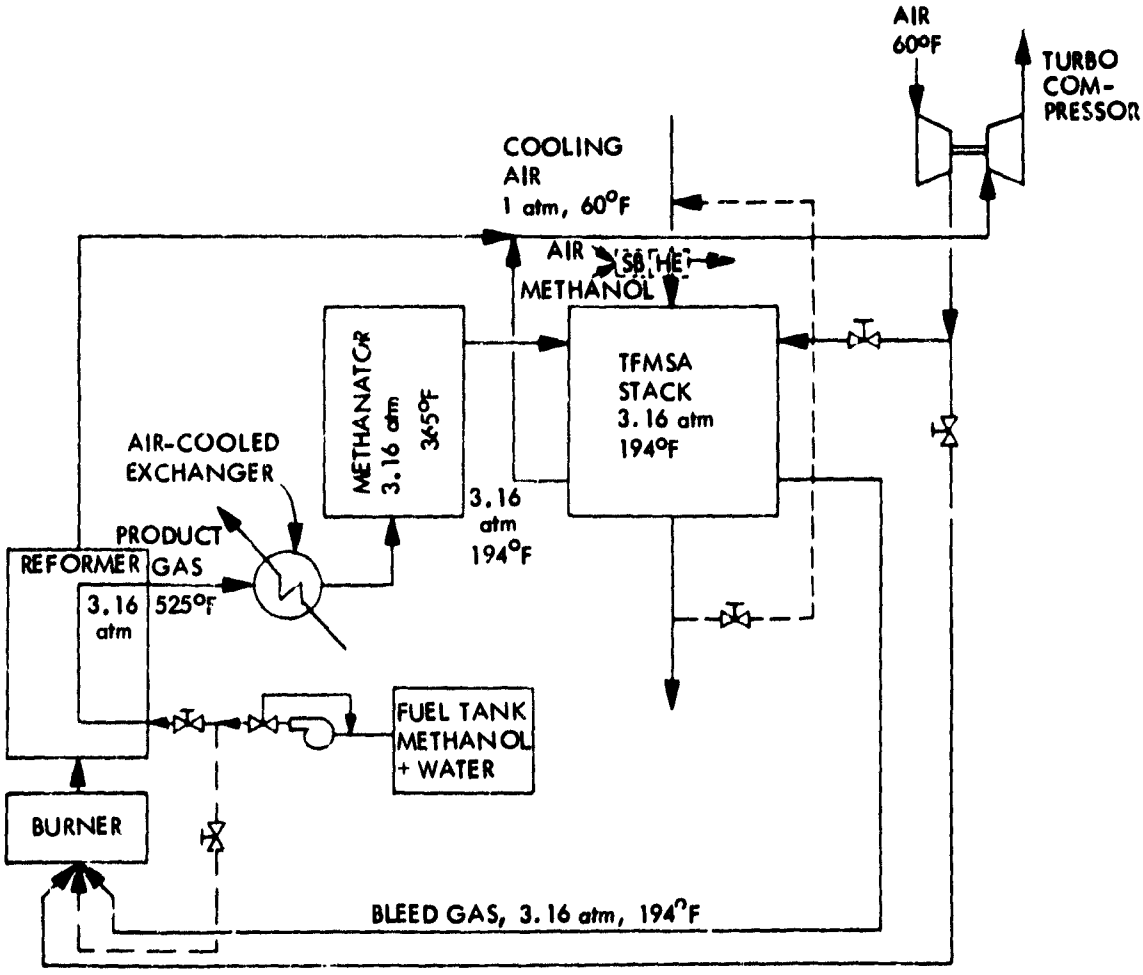

Figure 3-14. Energy Research Corporation 20-kW Trifluoromethane Sulfonic Acid Fuel Cell Power Plant (Source: Energy Research Corporation)

ERC described the operation as follows: The fuel mixture is vaporized in the reformer, then reformed. The reforming reaction is represented by the following equation:

$$CH_3OH + 1.3\ H_2O \longrightarrow CO_2 + 3H_2 + 0.3\ H_2O$$

The product gas is shifted toward the top of the reformer where the temperature is low. The shifted product gas at 274°C is cooled down by an air-cooled exchanger. It then enters the methanator to reduce the CO level. The methanation reaction occurs at about 185°C. The methanated fuel is fed to the fuel-cell anode. The unspent fuel is returned to the reformer burner where it is combusted with fresh air. The heat energy in the flue gas is used to vaporize the fuel mixture and to provide the endothermic heat of reaction. The system is operated at 3.16 atm. A turbocompressor compresses the air for the fuel-cell cathode and the reformer burner. The cooling air for removal of fuel-cell waste heat is not pressurized to save fuel. The reformer flue gas and the cathode exhaust are expanded in the turbocompressor to provide energy for compression. For the turbocompressor to be energy self-sufficient, it should be 80% efficient. This is a questionable assumption because typical compressors operate around 50% efficiency.

During start-up, a part of the fuel mixture is combusted in the reformer burner. The flue gas provides the latent heat of vaporization and the endothermic heat of reaction. Also, a part of the fuel mixture is combusted in the start-up burner to heat up the cooling-loop air. The heated air passes through the stack, transferring the heat to the cold stack. Most of exiting air is recycled, mixed with ambient air, and circulated, thus rapidly heating the stack.

An automatic control unit (ACU) measures the output current (load) and accordingly controls the fuel-flow rate to the reformer. Similarly, it also controls the temperatures of the reformer and the fuel-cell stack by measuring the exit temperatures.

Performance Characteristics. The projected performance of the TFMSA in comparison to the PAFC is given in Figure 3-15. The specific system characteristics are shown in Table 3-4.

The data show that the TFMSA can meet the physical constraints and exceed the peak-power goals but apparently still fall short of the acceptable start-up requirement, in spite of the reduced energy requirements due to its lower operating temperatures (90°C vs. 191 to 204°C for PAFC). The efficiency is somewhat lower than that of the PAFC because of the required methanator. The methanator is required to reduce the carbon monoxide level to a few parts per million. Unfortunately, unless the reaction conditions are carefully controlled, CO can react with the hydrogen to reduce the efficiency (forming methane in methanator).

In addition to its sensitivity to fuel purity, the TFMSA has the problem of water management and the related control of the electrolyte concentration

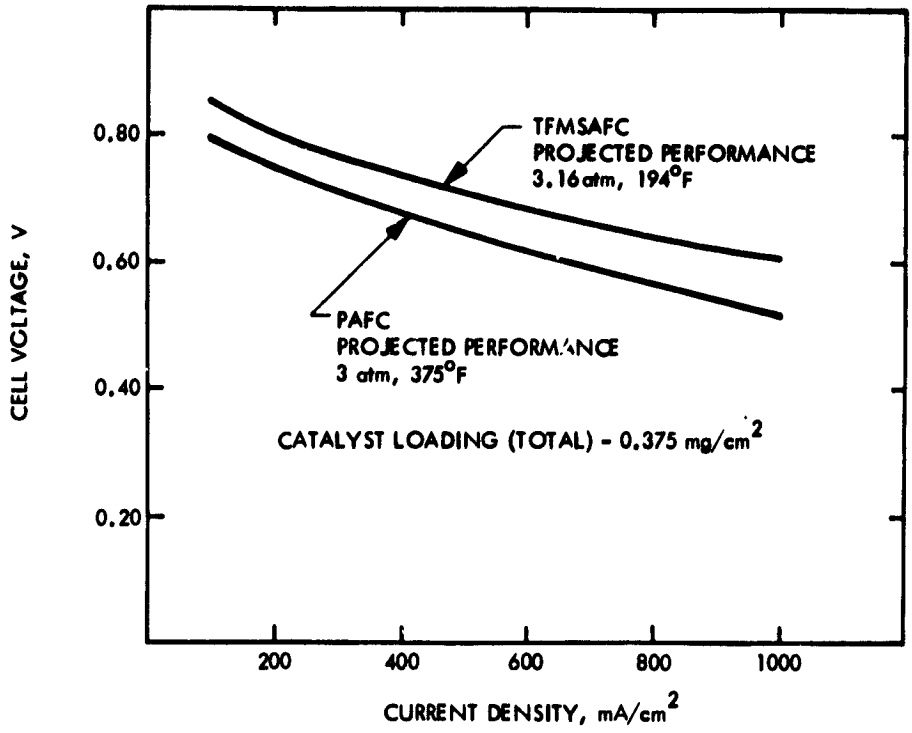

Figure 3-15. Comparison of the Polymer Acid Fuel Cell and Trifluoromethane Sulfonic Acid Fuel Cell Performance Projections (Source: Energy Research Corporation)

Table 3-4. Projected TFMSAFC System Characteristics[a]

Characteristics	Value
Specific power, W/kg	
Continuous	93
Peak	329
Power density,[b] W/l	
Continuous	46
Peak	162
Operating temperature and pressure, atm, °C	3.16, 90
Efficiency at continuous rating, %	40 to 45
Cold start-up time, min	3

[a]Based on 96-Vdc, 20-kW (continuous rating) ERC system design.

[b]Based on 0.26-m^3 component volume with 60% packing factor (consistent with UTC assumption).

between 3 and 6 molarity; accurate temperature measurements are absolutely essential in controlling and ensuring optimal performance versus concentration.

ERC has conceptualized a vehicle system, which is shown in Figure 3-16.

Cost and Life. ERC has estimated the manufacturing cost to be $190/kW continuous (1981 dollars) for a system with a life expectancy of more than 4000 h. This includes an assumption of 0.375 mg/cm^2 (electrode area) of platinum catalyst.

4 Conclusions

If the assumption is made that methanol is the nonpetroleum fuel for the advanced vehicle power sources, then the fuel-cell candidates are the following:

(1) Solid polymer electrolyte.

(2) Phosphoric acid.

(3) Advanced acid (e.g., TFMSA).

Of these, the phosphoric acid (PA) system has the greatest probability of technical success. This is because PA systems have the most extensive data

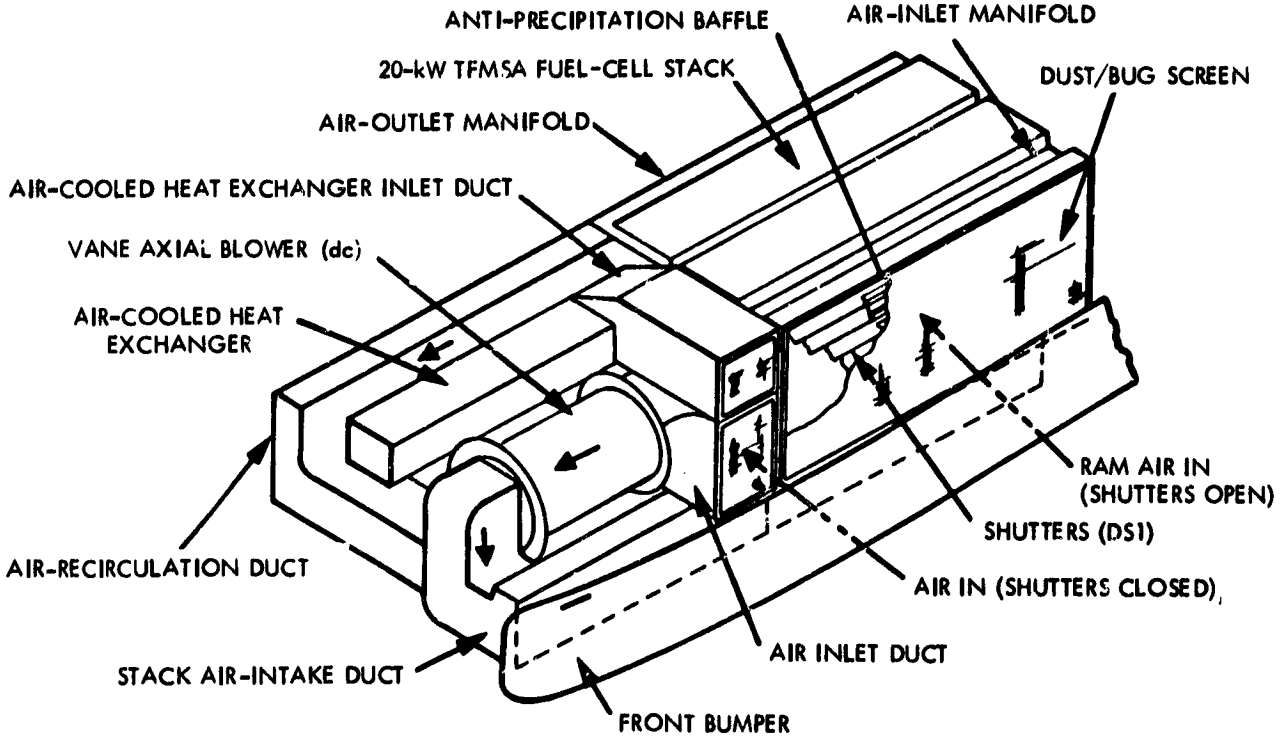

Figure 3-16. Projected Layout for a Trifluoromethane Sulfonic Acid Fuel Cell (Source: Energy Research Corporation)

upon which to build. However, substantial development is required in the areas of redox cathode reduction and operation at lower temperatures (for start-up). Next in line are the advanced acid cells because the technology is quite close to that of the PA cells. However, it should be recognized that the step from phosphoric acid to one of the advanced acids is a significant one with no guarantee of success.

The SPE system, while on a firm foundation based on water-electrolysis systems, is the farthest from reality. None of the major components has ever been built on a technology level compatible with that projected for the vehicle application. Enormous reductions from state-of-the-art catalyst loadings and cost reductions of the solid polymer material are necessary even to approach the quoted costs.

The generic problem of parasitic power losses for all three fuel-cell power plants continues to be questionable but apparently not unresolvable. Losses are quoted to range from 192 to over 800 W based on past utility and military system data. The frequent start/stop, warm-up/cool-down, and off/on operations associated with passenger-vehicle driving cycles may well exacerbate these losses.

Even though it does not appear in the PAFC and TFMSA power plants, a battery is required for warm-up operation. How these various components respond to power-demand sequences and controls are questions that have not been addressed and should be resolved as a part of understanding parasitic power losses.

It seems unlikely that any of the other systems will be acceptable for the advanced vehicle even if they perform as projected. The weight and volume requirements along with start-up, cool-down, and severe transient problems are almost insurmountable for a mass-produced private automobile. The integration of an electrolyzer unit and the storage tanks (H_2 and O_2) in the SPE system (and possibly the others) is a notable attempt to solve the start-up problem. However, the projected costs of the systems are extremely high relative to conventional heat engines.

Regardless of the fuel-cell system chosen, there remain some important questions (at the cell and system levels) to be answered before the system can be seriously considered:

(1) Actual fuel required for initial and subsequent start-ups.

(2) Time required for initial and subsequent start-ups.

(3) Capability of system to follow rapid power transients.

(4) Allowable ambient conditions with long-term shutdown.

(5) Possible undesirable exhaust emissions (aldehydes, carbon monoxide).

(6) Realistic consumer cost for mass-produced units.

(7) Effect of accelerations and vibrations on component life.

(8) Determination of realistic parasitic power losses.

However, the fuel-cell system has the potential for the most efficient utilization of fuel of any system considered. Because the scenario for the advanced vehicle includes the unavailability of petroleum fuel, the fuel cell has to be a candidate for further study.

B. HEAT ENGINES/NONPETROLEUM FUELS

1. Introduction

Internal-combustion engines will continue to be the most widespread automotive power source in the 1990s. This is not only the result of product momentum, but also focused research efforts in response to the perceived decreases in fuel availability as well as market demand and government pressures for improved fuel economy.

Spark-ignition (SI) engines have dominated the vehicle market to date and will continue to be the baseline for comparison. The efficiency of this engine type will continue to improve while retaining satisfactory emission levels. The main technical areas where improvements are being sought are summarized in Table 3-5 (Reference 3-4).

The Sloan Automotive Laboratory of the Massachusetts Institute of Technology judges that total vehicle fuel economy gains of about 35% should be realizable over a 10-year period, based on reasonable success of the developments listed.

Another means for using methanol in a spark-ignition engine is by decomposing methanol into hydrogen and carbon monoxide prior to ignition. Discussions with the JPL team involved in the California Methanol Assessment (Heft, R., JPL, personal communication, August 1982) indicate that significant improvements in efficiency can be achieved through using engine exhaust heat to facilitate the endothermic reaction of decomposition, increasing the compression ratio (possible because of the anti-knock properties of the dissociated gases), and leaning the fuel mixture (which is possible because of the lower lean limit misfire point). The research work to date implies that a 30 to 40% increase in decomposed methanol engine efficiency relative to current gasoline engines is practically realizable, of which about half of the improvement could be realized without dissociation of the fuel.

The use of prechamber-type diesel compression-ignition (CI) engines is growing rapidly in passenger cars. Further improvements in the efficiency of these engines are expected if developers solve the problems of the direct-injection (open chamber) diesel engines. Fuel economy improvements of about 15% are expected by General Motors (Reference 3-5), based on this change alone. The Sloan Laboratory cites the primary prechamber diesel developments as those shown in Table 3-6.

Table 3-5. Spark-Ignition Engine Development Prospects

(1)	Improved control and optimization of engine operating conditions (air/fuel ratio, fraction of exhaust gas recycled, spark advance). Use of programmed fuel injection, on-board computers, and sensors for major engine variables
(2)	Better emissions control technology, combustion chamber design, emission control system components. [This combined with item 1 above will ease the constraints that emission control places on fuel economy optimization]
(3)	Operation with higher compression ratios to increase engine efficiency. Use of knock sensors to control operating conditions prone to knocking. Lean operation to reduce partial load throttling losses
(4)	Reduced weight of engine components
(5)	Reduced engine displacement for given maximum power realized through improved engine design, improved engine-transmission matching, use of turbocharger. (Reduced displacement gives increased efficiency at partial load)

Table 3-6. Prechamber Diesel Development Prospects

(1)	Improved control of NO_x and particulate emissions levels inside the engine cylinder, which reduces the impact of emissions standards on engine efficiency
(2)	Control and optimization of engine operating conditions (injection timing and duration and exhaust gas recycle) for maximum fuel economy for given emissions constraints
(3)	Improvements in maximum engine torque by engine design modifications and use of turbocharger to permit use of smaller and lighter-weight engines
(4)	Combustion chamber design and materials improvements to reduce heat losses, reduce pumping losses between the main and prechambers, and improve efficiency

In summary, current baseline engines will continue to improve and provide formidable competition to the alternatives proposed in the Advanced Vehicle Assessment. This engine assessment characterizes improved versions of these baseline engines with nonpetroleum fuels for the purpose of simulating advanced hybrid vehicles as well as advanced baselines for comparison.

The scope of this task was limited to assessing major fuel effects only and assumed that the necessary changes and adjustments would be made to the engines to allow operation on nonpetroleum fuels. Hence, the effort did not include a detailed modeling of engines (which would account for fuel-rated displacements of the specific fuel consumption island pattern relative to absolute speed and power), but rather took the approach of developing conversion factors to adapt current engine maps to the nonpetroleum fuel of choice. Emissions are only accounted for by the choice of air/fuel ratios that avoid the peaking of objectionable steady-state emissions (NO_x in particular).

Fuels considered possible for use in vehicles in a petroleum-constrained market are methanol, ethanol, ammonia, and natural gas. Discussions with representatives of the automotive industry over the course of this study have indicated that methanol would be the fuel of choice for widespread use in the U.S. However, this opinion is influenced greatly by the possibility of production from coal, of which very little methanol-from-coal capacity is available at the present time. Ethanol is already being used outside the United States to power passenger vehicles (e.g., in Brazil). Methane (natural gas) is readily available and is the primary source of methanol. Presently, more ammonia is in production in this country than methanol, and this fuel is attractive as a storage medium for hydrogen, which can be used in fuel cells or heat engines. The advantages and disadvantages of the fuels and their effects on engine characteristics (rather than supply scenarios) are presented in this report.

The major fuel properties influencing engine power are the heat of combustion, the amount of air needed for chemically correct combustion, and the latent heat of vaporization. These and other characteristics are shown in Table 3-7.

2. Spark-Ignition Engines

The naturally aspirated, three-way catalyst-controlled, electronically fuel-injected, four-cycle spark-ignition (SI) engine is the dominant concept among all new passenger cars currently marketed. Efforts to improve this engine include, among the others presented in the introduction, increasing the compression ratio and breathing capability as well as decreasing engine weight.

Examples of the development of high-compression concepts are underway at Porsche in Germany (Reference 3-11) and Ricardo in England (Reference 3-12). High-compression ratios of 12.5:1 to 15:1 have been investigated, with highly turbulent combustion chambers in conjunction with electronic anti-knock systems that detect incipient knocking. In fact, the Ricardo May-Fireball engine with a 12.5:1 compression ratio is currently offered as an option in the Jaguar Sports Coupe (Reference 3-13). Volkswagen (VW) of Germany has also experimented with high-compression engines and has found that high-temperature "squish" flow (so-called because of the flow resulting from the high-compression piston and head designs) can cause flame erosion surface damage on pistons of conventional materials (Lee, W., VW, personal communication, March/April 1982). The chambers are not completely free of knock, and ignition has

Table 3-7. Major Nonpetroleum Fuel Properties[a]

Criteria	Regular gasoline	Diesel	Methanol	Ethanol	Methane	Ammonia
Research octane number (RON)	92	NA	106	106	115	130
Cetane number	17	40 (minimum)	Negligible	8	NA[b]	NA[b]
Lower heating value, MJ/kg	38.9	38.6	18.0	24.1	44.9	16.7
Stoichiometric air/fuel ratio	14.8	14.5	6.4	9.0	17.2	6.0
Latent heat of vaporization, kJ/kg	377 to 502	544 to 795	1110	904	457	1234
Boiling point, °C	25 to 210	150 to 360	65	78	-162	-33
Freezing point, °C	-40	-15	-97	-117	-182	-78

[a]References 3-6 through 3-10.

[b]NA = not applicable.

to be retarded in the low-speed range with torque penalties. Volkswagen feels that high-compression engines will dominate in the 1990s, but with transmissions that allow for operation in the upper-end speed range where knocking is weak. Bavarian Motor Works (BMW) is also experimenting with high-compression engines and expect a 15% fuel savings for the average user if designed for maximum low-end torque at the expense of peak-power output (Reister, D., BMW, personal communication, March/April 1982). It seems that a 12:1 ratio may be a reasonable limit to avoid unacceptable wear with gasoline operation.

Other efforts to increase the breathing capability of SI engines include turbocharging and supercharging. Several manufacturers currently offer knock-controlled SI engines as options (i.e., Saab and Buick). Based on sales, the high-speed power boost potential of the turbocharged engines is apparently attractive to a relatively small group of consumers. This is probably the result of the cost differential associated with the turbocharger option and the 4 to 24% lower EPA fuel economy ratings (Reference 3-14). However, VW and Audi claim that advantages in fuel economy can result from the use of low-speed sized, wastegated turbochargers and lower axle ratios (Reference 3-15).

Experiments by Bendix and Fiat have shown that there are economic advantages with superchargers as well, with engine undersizing and optimum axle ratios (Reference 3-16). In the past, cost and noise development have been the primary deterrents to this type of system's entering the market.

Notable efforts have been made to increase fuel economy through efforts to control the engine operation so that fuel is not wasted during idling or periods of low power demand. These include the General Motors 4/6/8 cylinder cut-off engine in Cadillacs (References 3-17 and 3-18), the 3/6 cylinder cut-off efforts at BMW (Reference 3-19), and the engine stop/start concept at VW (Heitland, H.H., Volkswagen AG, personal communication to H. Schneider, March/April 1982). The GM 4/6/8 was discontinued because it was unreliable, and the cylinder cut-off and on-off engine operation schemes of the European manufacturers are viewed as concepts that should be used only if all other means to improve efficiency are exhausted (primarily due to complexity and reduced reliability).

Other SI engine types of interest include Wankel-type rotary engines and two-cycle engines. Rotary engines are attractive because of their power-to-weight and volume characteristics. Disadvantages include fuel economy and service life of the early models, though NSU claims now that their engines are as good or better than piston engines of comparable power output (Reference 3-20). It is difficult to raise the compression ratio to keep abreast of competing piston engine development. In fact, Curtis Wright has made a major development effort just to raise the compression ratio from 8 to 9 (References 3-21 and 3-22).

Two-cycle engines were phased out of the passenger car market in Europe and the United States years ago because of noise, smoke, and difficulties in meeting mission control requirements. Because of their mechanical simplicity and compatibility with extremely low-octane fuels, engines of this type are still marketed in some countries where high-octane fuels are not readily available. If the emission problems can be resolved (e.g., through timed injection), their advantages (i.e., simplicity, low cost, low weight, and fuel insensitivity) would be attractive features for hybrid vehicles.

In summary, it is expected that the four-cylinder, four-cycle, liquid-fueled and electronically fuel-injected piston engine of transverse front-wheel drive design will be the dominant power-plant concept for small passenger cars through the end of the century. With this in mind, six SI engine types were chosen as representative of possible production engines during this period. These include two low-compression (naturally aspirated and turbocharged) engines, which were selected because engines of this type with improved characteristics will dominate the market through the current decade. Two high-compression engines were chosen to represent the dominant production engines during the 1990s. Two rotary engines (current and advanced design for aviation use) were selected for study, because of their compactness, for possible use in a hybrid vehicle.

The selected engine types, which will be used as generic examples, are shown in Table 3-8. It is not implied that these engines developed by the indicated manufacturers will dominate the market in the 1990s.

Table 3-8. Representative Spark-Ignition Engines

Engine	Compression ratio	Specific power, W/kg	Power density,[a] W/l	Development status
1.7 l Audi 1700, NA[b]	8.4	448	497	Production
1.6 l VW Caspan RSV, TC[b]	8.1	567	732	R&D
2.0 l Porsche TOP, NA	12.5	539	798	R&D
2.0 l Ricardo May-Fireball, NA	15.0	575	693	R&D[c]
3.0 l NSU Wankel, NA	7.5	547	642	Production
1.0 l Curtiss Wright, NA	8.5	547	412	R&D

[a]Box volume estimates.

[b]NA = naturally aspirated; TC = turbocharged.

[c]12.5 compression ratio version on 12-cylinder Jaguar (1982).

3. Spark-Ignition Engines/Nonpetroleum Fuels

With the exception of methane, the heat of combustion of the alternate fuels is nearly one-half that of the gasoline reference, and more fuel is needed for chemically correct combustion for the same amount of air. Starting at low ambient temperatures is a problem with alcohols and ammonia. In contrast to gasoline, the alcohols have a fixed boiling point at temperatures higher than those usually existing under the hood on starting, and the heats of evaporation are more than twice as high as those of gasoline. If more volatile fuel additives cannot solve this problem, a heater system will be necessary for low-temperature starting.

Gasoline-fueled engines were assumed to be throttled, three-way catalyst controlled and to operate at a fixed stoichiometric mixture ratio. Engines operating on the alcohols were assumed to be leaner by 12% to avoid high flame temperature and NO_x while simultaneously minimizing the emission of aldehydes, which increases with further leaning (Reference 3-23).

Tests with methane-fueled cars (see Reference 3-9) show that the best thermal efficiencies are obtained at fuel-to-air equivalence ratios on the order of 0.8. Methane should also be used in a lean mixture to reduce combustion temperatures and to minimize NO_x.

For ammonia, an equivalence ratio of approximately 0.8 is recommended for vehicular operation. Such an equivalence ratio yields thermal efficiencies near the optimum without losing too much power (approximately 3%) and minimizes the emission of unburned ammonia (which is considered more objectionable than NO_x). In contrast to all other fuels, the NO_x

emissions from ammonia peak at extremely lean equivalence ratios (on the order of 0.65).

Because of temperature drop resulting from vaporization, the breathing capability of the engine is greater with alcohols than with gasoline. The temperature drop for full vaporization is on the order of 132°C for methanol, 82°C for ethanol, and 19°C with gasoline (see References 3-8, 3-24, and 3-25). An average of 60% of the induced fuel vaporizes in the intake manifold depending upon system design and the turbulence of the inlet flow. It was, therefore, assumed that in a turbocharged engine all fuel can be vaporized, i.e., the gain in breathing capability is slightly higher in a turbocharged engine. This does not apply if external heat is introduced to evaporate the fuel.

In the alcohol cases, the power output relative to gasoline at a given speed for 60% vaporization should be used for all naturally aspirated engines, including rotaries. A 100% vaporization value for relative power can be applied to turbocharged engines. The relative power value for 100% evaporation could also be applied to supercharged engines because the flow behind the compressors is highly turbulent, and the temperature of the induced air is higher.

The power output producible at a given engine speed is strongly reduced by the use of either natural gas (methane) or ammonia. The maximum producible power output obtainable from ammonia is severely limited because engine speed is limited to 73% of that obtainable with gasoline. This is due to the slower flame propagation speed of the ammonia-air mixture in the combustion chamber.

The assessment of major contributing factors for equivalence ratios and the summary of conversion factors are shown in Table 3-9. These factors do not represent the ultimate potential (or JPL projections) but indicate the expected effects of changing fuels in an SI engine with only minor adjustments.

4. Compression-Ignition Engines

Diesel-powered passenger cars are capturing a larger share of the U.S. market primarily because of perceived reliability, increased fuel economy, and associated decreased fuel costs. Current efforts to improve passenger car diesels are in the direction of open-chamber combustion and engine noise insulation.

Two engines were chosen to represent generic production compression-ignition (CI) engines (with improvements) during the period of interest. These include the naturally aspirated (NA) and turbocharged (TC) VW engines, as shown in Table 3-10. It should not be assumed these engines nor their manufacturers would dominate the market at that time.

5. Compression-Ignition Engines/Nonpetroleum Fuels

There are several concerns in using nonpetroleum fuels in CI engines. The characteristics of the fuel are such that, without corrective

Table 3-9. Summary of Major Contributing Factors for Equivalence Ratios and Engine Map-Conversion Factors (SI Engines)

Criteria	Vaporized fuel fraction	Methanol	Ethanol	Methane	Ammonia
Equivalence ratio		0.88[a]	0.88[a]	0.80	0.80[a]
Thermal efficiency relative to gasoline		1.08	1.03	0.75	1.08
Breathing capability relative to gasoline	0.6 (NA)[b]	1.026	1.008		1.0
	0.7 (TC)[c]	1.044	1.013	1.0	
Combustion energy relative to gasoline		0.921	0.890	1.302	0.657
Power output relative to gasoline at given speed fraction	0.6 (NA)	1.02	0.92		1.0
	0.7 (TC)	1.04	0.94	0.77	
Specific fuel consumption relative to gasoline at given operating point		2.044	1.576	1.180	2.220
Maximum engine speed relative to operation with gasoline		1.0	1.0	1.0	0.73

[a]Compromise of NO_x emissions and thermal efficiency.

[b]NA = naturally aspirated.

[c]TC = turbocharged.

Table 3-10. Representative Compression-Ignition Engines

Engine	Compression ratio	Specific power, W/kg	Power density,[a] W/l	Development status
1.5-l VW Diesel, NA	23.0	312	346	Production
1.5-l VW Diesel, TC	23.0	437	441	Preproduction

[a]Box volume estimates.

measures, detonation and abnormal burn rates will occur. Efforts to combat this behavior include the investigation of additives to increase the cetane rating (to control the ignition quality) and experimentation with small amounts of pilot fuels (injected to initiate the combustion) in concert with fumigation of nonpetroleum fuels. The possibility of the dual-fuel requirement is not likely to be a popular approach for passenger cars in comparison to the single-fuel capability of SI engines with nonpetroleum fuels.

The SI engine maps (Reference 3-26) are for throttled engines with a constant fuel/air ratio; therefore, constant equivalence ratios based on parameters such as the breathing capability are appropriate. In contrast, CI engines use leaning for control (i.e., variable fuel/air ratio), and the fuel is injected after compression (i.e., the breathing capability is not affected by the fuel). Therefore, the primary considerations for the conversion factors are the caloric value differences. The thermal efficiency differences are expected to be negligible if CI engines can be successfully operated on the fuels. A summary of major fuel effects is shown in Table 3-11.

6. Vehicle System Consideration

Advanced vehicle systems will be affected by several factors not apparent in the engine map conversions discussed in Reference 3-26. These include the effects on drivability, fuel storage requirements, compatible material selection, and cost.

a. Drivability. The low vapor pressure of the alcohols at ambient temperature is the source of cold starting problems. Several methods have been considered in the efforts to solve this problem. The first is the addition of highly volatile materials to increase the vapor pressure. A second method employs electric heating of the intake manifold to vaporize the fuel. Dual-fuel systems have also been considered. These systems use a more volatile pilot fuel to start and warm up the engine prior to the introduction of alcohol.

b. Fuel Storage. The volume of the fuel tank in the nonpetroleum-fueled cars will be larger for a given range than petroleum-

Table 3-11. Summary of Engine Map-Conversion Factors (CI Engines)

Criteria	Diesel	Methanol	Ethanol	Methane	Ammonia
Specific fuel consumption relative to diesel at given operating point	1.0	2.14	1.60	0.86	2.31
Thermal efficiency	1.0	1.0	1.0	1.0	1.0

fueled vehicles. Methanol storage tanks require about 70% more volume than gasoline based on the lower energy content but higher thermal efficiency in a system optimized for methanol. Similarly, ethanol storage tanks will require about 40% more volume.

Storage tanks for the gaseous fuels are expected to be larger and heavier than comparable-range gasoline tanks. These fuels will require high-pressure or cryogenic storage. High-strength (and high-cost) materials could alleviate this problem somewhat; however, highly stressed pressure vessels could also present a safety hazard in an accident. It is interesting to note that Ford has developed a compressed natural gas system for small passenger cars.

c. Compatible Material Selection. Material changes will be required due to corrosion problems. Alcohol tanks will require a corrosion-resistant material or internal coating. Ammonia is generally compatible with conventional vehicle materials with the exception of copper and brass.

d. Cost. It has been assumed that compatible materials will be selected with minimal effects on the eventual manufacturing costs of the SI and CI engines discussed in this report. Detailed cost analyses were not within the scope of this task; hence, the redesigns discussed in this report are considered part of the expected research of the engine developers, and the increased manufacturing costs (due to specific redesign) are minimal. Otto (three-way catalyst) costs were based on the JPL EHV Cost Handbook (adjusted to 1982 dollars), and the CI engine cost per kW is based on the manufacturing cost ratio, relative to the SI engine, derived from previous JPL engine studies (References 3-27 and 3-28). The cost relationships are as follows (1982 dollars):

(1) Manufacturing cost (Otto, three-way catalyst) = $240\ (kW)^{.33}$.

(2) Manufacturing cost (compression-ignition) = $260\ (kW)^{.33}$.

7. Summary

With appropriate modifications, the thermal efficiency expected from heat engines burning nonpetroleum fuels is greater than or equal to the same engines burning petroleum fuels. Further modifications to increase the compression ratio (to take advantage of the anti-knock properties) up to 12 to 15:1, improved fuel distribution and engine control should boost efficiency by another 15% relative to low-compression SI engines. The projections are summarized in Table 3-12.

Table 3-12. Projected Heat Engine/Non-petroleum Fuel Characteristics

Characteristics	Methanol	Ethanol	Methane	Ammonia
Thermal efficiency relative to gasoline	1.22	1.18	1.15	1.22
Specific fuel consumption relative to gasoline	1.81	1.38	0.77	1.92
Thermal efficiency relative to diesel	1.0	1.0	1.0	1.0
Specific fuel consumption relative to diesel	2.14	1.60	0.86	2.31

SECTION III REFERENCES

3-1. McElroy, J., Assessment of Solid Polymer Electrolyte Fuel Cells for Vehicular Power Systems, Final Report, General Electric, Los Alamos National Laboratory Contract No. 4-L61-3863V-1, November 1981.

3-2. King, J. M., Assessment of Phosphoric Acid Fuel Cells for Vehicular Power Systems, Final Report, United Technologies Power System, Los Alamos National Laboratory Contract No. 4-L61-3862V-1, March 1982.

3-3. Patel, D. N., Assessment of Trifluoromethane Sulfonic Acid and Phosphoric Acid Fuel Cells for Vehicular Powerplants, Final Report, Energy Research Corporation, Los Alamos Scientific Laboratory Contract 4-L61-3861V-1, December 1981.

3-4. Heywood, J. B., "Automotive Engines and Fuels: A Review of Future Options," Prog. Energy Combust. Sci., Vol. 7, pp. 155-184, Pergamon Press Ltd., 1981.

3-5. Route, W. D., Amawn, C. A., and Gallopoulos, N. E., Developments in Automotive Technology, Fuels, and Lubricants, General Motors Research Laboratories, GMR-3863R, F&L-736, November 5, 1981.

3-6. Taylor, C. F., The Internal Combustion Engine, The Massachusetts Institute of Technology Press, 1978.

3-7. "Nonpetroleum-based Fuels," Current Status of Alternative Automotive Power Systems and Fuels, Vol. III., EPA-460/3-74-013-C, July 1974.

3-8. Bosch Automotive Handbook, 1st English Edition, translated 1978.

3-9. Afflech, W. S., et al., "Converting a Small Car to LNG: What are the Problems and What Can it do for Economy and Emissions?," SAE Report No. 760376, Society of Automotive Engineers.

3-10. Graves, R. L., et al., "Ammonia as a Hydrogen Carrier and Its Application in a Vehicle," paper presented at the Hydrogen Economy Energy Conference, Miami Beach, Florida, March 18, 1974.

3-11. Gruden, D. O., and Hahn, R., "TOP - The Thermodynamically Optimized Porsche Engine," presented at the 5th International Automotive Propulsion Systems Symposium, April 14-18, 1980.

3-12. May, A., and Spinner, F., "Betriebserfahrungen mit hochverdichteten Ottomotorennach dem May Fireball - Verfahren."

3-13. "High Swell Chamber Hikes Jaguar 12 Power in XJ-S," Wards Engine Update, August 1, 1981.

3-14. 1982 Gas Mileage Guide, U.S. Department of Energy, DOE/CE-0019.

3-15. Emmenthal, K. D., Hagemann, A., and Walzer, P., "Fuel Economy Improvements by Turbocharging," Volkswagen presentation handout.

3-16. McElroy, T., Turbochargers vs. Supercharger, Automotive Industries, November 1981.

3-17. "Unique V-8-6-4 Engines for Cadillacs," Automotive News, September 15, 1980.

3-18. "82 Cadillacs Lose V-8-6-4," Ward's Engine Update, February 1, 1981.

3-19. "BMW's Route to More Power From Less Fuel," The Engineer, November 16, 1978.

3-20. Van Basshuysen, R., and Wilmers, G., "An Update of the Development on the New Audi NSU Rotary Engine Generation," SAE Report No. 780418, Society of Automotive Engineers, February 27 - March 3, 1978.

3-21. "The Rotary Combustion Engine - A Candidate for General Aviation," NASA Conference Publication No. 2067, February 28, 1978.

3-22. Johnes, C., "A Review of Curtis Wright Rotary Engine Development with Respect to General Aviation Potential," SAE Report No. 790621, Society of Automotive Engineers, April 3-6, 1979.

3-23. Menrad, H., et al., "Development of a Pure Methanol Fuel Car," SAE Report No. 770790, Society of Automotive Engineers, September 1977.

3-24. Bardow, M. F., "Comparison of the Cold Temperature Performance of Gasoline and Alcohols in Spark-Ignition Engines," ASME Report No. 80-Pet-17.

3-25. Ebersole, G. T., "Engine Performance and Exhaust Emission: Methanol vs. Iso-octane," SAE/PT-80/19, Society of Automotive Engineers.

3-26. Hardy, K. S., Klose, G. J., Rippel, W. E., Roan, V. P., Rowlette, J. J., Schneider, H. W., Uchiyama, A. A., Advanced Vehicle Subsystem Technology Assessment, JPL Internal Report D-230, Rev. A, Jet Propulsion Laboratory, Pasadena, California, January 1983.

3-27. Heft, R. C., and Heller, S. C., Hybrid Vehicle Potential Assessment, Vol. X: Electric and Hybrid Vehicle Cost Handbook, JPL Internal Report 5030-345, Jet Propulsion Laboratory, Pasadena, California, September 30, 1979.

3-28. Should We Have A New Engine?, Vol. II. Technical Reports, JPL SP 43-17, August 1975.

SECTION IV

POWERTRAIN COMPONENTS

A. MOTORS/CONTROLLERS

1. Introduction

This section covers electric motors and the corresponding processors that are required. Specifically, theory, cost, and performance information is presented for ac and dc components.

a. Background on Motors. The principle common to all machines[6] is that current-carrying conductors experience forces when in the presence of externally produced magnetic fields. Thus, all electric motors (dc, ac, electronic, etc.,) produce shaft torques resulting from magnetic fields being produced by one part while currents flow in another part. In this respect, all motors share the same principles of physics. The only differences are at the engineering level.

Typically, motors currently used with electric vehicles are of the dc brush-commutator variety. In the past, ac and dc brushless motors that require inverted power have not been practical because of cost, efficiency, and weight limitations associated with the inverter. It should be noted, however, that both the ac and brushless machines are less expensive, more efficient, lighter, and more rugged than dc brush-type machines. Were it not for the inverter limitations, ac and brushless dc drive systems would have both performance and economic superiority over their dc brush-type counterparts. Fortunately, the electronic technologies are rapidly advancing, and inverter drive systems seem to have future promise.

b. Brush-Type DC Motors. With commutator-type dc machines, electrical energy is applied to rotor windings via a brush-commutator system. In a sense, the brush-commutator combination serves as a mechanical inverter (and transferring energy from a stationary to a moving frame). It should be noted that the brush-commutator system limits performance because:

(1) Forty to 60%[7] of the machine losses are due to brush-commutator losses (electrical and mechanical).

---

[6] "Machine" and "motors" are used interchangeably.

[7] For a typical traction machine such as GE's 2366 motor, the brush drag is about 0.034 Nm (0.5 ft-lb) or about 2.5% of the output torque at continuous load; the brush voltage drop is about 2.3 V, which is 2.1% of the input power. The electrical commutation losses are estimated at 1.5% of the input power under nominal load. Under rated load, the efficiency is 89%. (11% of the input power is lost, 5.9% at the brush-commutator.) It follows that the brush-commutator accounts for 53% of the total losses.

(2) For most designs, mechanical integrity of the commutator limits maximum rev/min and, hence, limits the power density.

The required magnetic field is produced by the stator. For small machines, permanent magnets may serve; for traction-type machines, where weight and cost are critical, stator windings are typically used. These windings may be connected in series with the armature (series machine), in parallel with the armature (shunt machine), or excited independently of the armature circuit (separately excited). Prior to the era of electronic power processing, the series machine was used due to a torque-speed characteristic that was closer to constant power than the alternatives. With the advent of power electronics, the separately excited machine has become the favorite because regenerative braking and improved high end torque are more easily achieved than with the series machines. The separately excited machine tends to cost about 20% more than the series machine due to the requirement of interpole compensation i.e., small magnetic field coils are added to compensate for distortions in the field flux caused by currents in the armature (General Electric, El Monte, California, personal communication, 1981). Both the South Coast Technology and the GE vehicles use separately excited machines that are electronically controlled.

c. Brushless DC Motors. The role of the brushes and the commutator can be replaced by electronic switches, for example, transistors or silicon controlled rectifiers (SCRs). The most effective mechanical design is the "inside out" machine where the rotating member produces the magnetic field and power is applied to the stator (in this case the stator is the armature).

The rotor may use either permanent magnets or windings that derive external power. Most current designs feature permanent magnets to achieve simplicity while eliminating the need for slip rings. Unfortunately, the only magnetic material capable of producing flux levels comparable with energized windings is extremely expensive (e.g., Samarium-Cobalt). Using lower-priced materials, such as Alnico or ferrites, on the other hand, leads to reduced specific torque and power.

An alternative dc brushless design uses a wound rotor and eliminates the use of permanent magnets. With this approach, high flux levels are possible, thus enabling high specific torques and powers. Operation emulating conventional brush-type, separately excited machines is possible where field control may be used to either provide limited speed control or to optimize efficiency as torque and speed vary. Power transfer (dc) to the rotor field may be achieved by either slip rings or by inductive coupling where on-rotor diode rectification is included.

Wound rotor dc brushless machines will probably have costs and performance levels superior to dc commutator motors but inferior to induction ac motors. In the near term, the wound rotor systems could be the best choice economically because simple motor commutated SCR inverters suffice. This type of system, however, requires that the motor idle; hence, a transmission is required. By using a pre-regulator (buck-type chopper connected in front of the inverter) the idle speed can be reduced to a low value. With simultaneous control of the wound field and the pre-regulator, efficiency optimization is

possible. Motor starting may be accomplished by pulsing of the pre-regulator (only light torque loads can be handled during starting; this strategy, therefore, requires the use of a transmission). This system is nonideal in terms of complexity and also because energy is processed twice: once at the pre-regulator and once at the inverter. For the present, however, it could be the most economical approach to electric vehicle propulsion, with economic superiority over both conventional dc and ac induction and with performance superiority (power-to-weight and efficiency) over conventional dc. With the expected emergence of low-cost modulating inverter technology, induction-machine-based systems should, however, gain dominance.

d. AC Induction Motors. With induction machines, ac electrical energy is applied to stator windings tha produce a rotating magnetic field in the gap between the stator and rotor surfaces. This causes electrical currents to flow in the shorted rotor windings; thus, a rotor torque is produced by the interaction of stator fields and rotor currents.

Where balanced, sinusoidal, three-phase power is available, a nearly ideal motor is achieved by employing three separate stator windings symmetrically spaced. Under these conditions, a magnetic vector of constant magnitude and uniform rotation rate is produced. This results in a rotor torque that is proportional to the so-called slip speed (the difference between electrical and mechanical rotation frequencies).

For stationary, integral horsepower applications, the three-phase induction machine is nearly ubiquitous. Its advantages include very low cost per horsepower, high reliability, and excellent full-load efficiency. Its main disadvantage is lack of speed control (except by variable frequency excitation); idle losses and part-load efficiencies are also less than ideal.

With the advent of power processing, where frequency and voltage transformations are possible, the control and part-load deficiencies of the induction motor are eliminated. Furthermore, with excitation frequencies above 60 Hz and with minor design changes, inverter-motor systems are possible for achieving extremely high conversion efficiencies over large four-quadrant regions of the torque-speed plane while affording high continuous and peak-power densities.

Until recently, these potentials remained untapped due to the high cost of suitable inverters. With the emergence of low-cost switching transistors and practical Gate Turn-Off Thyristors (GTOs), inverter drives are now gaining industrial markets at a rapid pace (Reference 4-1).

This technology has direct application to electric vehicle (EV) propulsion. The engineering characteristics of ac drives are ideal for electric vehicles as demonstrated by high efficiency over wide torque and speed ranges, inherent regenerative braking, high power density, and relatively maintenance-free operation. As with the dc brushless systems, the primary impediment is the inverter cost. However, unlike the dc brushless, the ac drive technology is currently being developed for a mass non-EV market. Thus, as inverter costs fall in response to industrial sales, the ac drive technology should become available for EVs on a spin-off basis.

2. Comparisons Between Brush-Type DC and AC Propulsion Components

Comparing dc and ac systems is made difficult by the lack of production ac components specifically for vehicle systems. Therefore, the latest system developments of each type were chosen to represent the present status. The GE ETV-1 system was chosen to represent brush-type dc systems, and the Eaton system was chosen as representative of possible production ac-induction systems. There are some notable inequities in trying to compare production costs of these systems. Neither system is composed of production components although production cost estimates have been made by the Eaton Corporation. GE did not publish detailed component cost estimates, and currently available dc propulsion component prices were quoted as representative original equipment manufacturer (OEM) costs. Production quantities for these components varied as well. The Eaton system estimates were made as a function of quantity (10,000 or 100,000 per year) and main power transistor cost ($40 to $100 each). Quotes for the dc components were made for quantities of 1000-unit lots although costs for the wound motors are not expected to drop substantially in higher quantities. For comparison, the 1000-unit lot dc components were compared to the 10,000 per year production Eaton systems (with $100 transistors, currently $180 to $210 each). The comparison is shown in Table 4-1.

Table 4-1. Comparison of Present Brush-Type DC and AC Induction Drives[a]

	DC OEM cost quotes,[b]	AC OEM cost estimate,[b]	Specific power[b] W/kg		Power density,[b] W/l		Efficiency, %	
Components	$/kW	$/kW	DC	AC	DC	AC	DC[c]	AC[d]
Motor	70	25	150	280	395[e]	1100	84	95-90
Controls	50	50-165	350	445	290[e]	500	99	85-95
Combination	125	75-190	105	170	170	345	83	72-86

[a]DC performance data, GE ETV-1 (Reference 4-2).
DC cost data, 1000-unit lots, 15 kW series-wound GE BT2366 motor and matched GE M1 controller (Reference 4-1).
AC performance data and lower cost estimate for 10,000 units per year, Eaton (Reference 4-3).

[b]Continuous power rating.

[c]Efficiencies in motoring mode (not including regenerator) over J227aD cycle.

[d]Motor efficiency at speeds and torques above 25% rated value; inverter efficiency at 92 Hz stator frequency; transaxle efficiency in both gears; 14 to 41 Nm input torque.

[e]Volumetric data from Aerospace Corporation (Reference 4-4).

It could be inferred from this comparison (with the caveats noted) that ac systems are currently on a par with their dc counterparts. However, a brief survey of available ac components in 1000-unit lots (to compare with dc) indicate present OEM costs at $165/kW for ac controls based on the lowest cost industrial drives (about $200/kW) with allowance made for rectification and other circuitry that may be deleted (price quotes on Lovejoy Electronic's MPR IV line of motor controls, 1981).

This comparison does not include the components necessary in the vehicle propulsion system. The transmissions must also be considered. In this case, the transmissions differed substantially, i.e., the ETV-1 used a HY-VO chain fixed reduction and the Eaton system used a two-speed transaxle. Cost estimates for the fixed reduction gears are as low as $5/kW compared to $45/kW (continuous) for the transaxle (Eaton estimate for 10,000 units per year).

It should also be noted that most of the system costs and performance limitations reside with the inverter. Thus, as the "electronic revolution" continues, ac inverter drives may be expected to gain simultaneous economic and performance superiority. This can be seen in the next subsection, which compares dc brushless and ac induction systems.

3. Comparisons Between DC Brushless and AC Propulsion Components

Comparisons of cost and performance of dc brushless and ac drives, projected for the 1990 time frame, are summarized in Table 4-2. Estimates were obtained as follows: Induction motor costs are assumed to range from the present value of $10/kW to a value 50% higher. The 50% increase is attributed to the expected use of improved magnetic materials and other improvements (such as reduced lamination thickness). Based on the assumption that wound rotor types (which are estimated at $15/kW in large production) are the least expensive, dc brushless motor costs are estimated to exceed $15/kW.

The projected cost of controls (power processors) is based on an estimated five-fold reduction in cost relative to the present. The controls for the dc brushless systems are estimated to cost twice that of ac controls due to the required additions of a bidirectional pre-regulator, shaft position sensors, and sensor electronics in present systems. In the event that the pre-regulator is not necessary and the development effort is comparable to ac systems, then the cost differential would be negligible.

The full range of present dc brushless specific power is included because it is not clear whether permanent magnet or wound rotor versions would be more acceptable. The specific power and estimated efficiencies for the controls were derived from studies of advanced inverters conducted at JPL. A variety of advanced transmissions can be used with these systems. They are described in a later subsection (B), and the effects on the propulsion system costs and characteristics are detailed in the summary (subsection C).

Table 4-2. Comparison of Projected DC Brushless and AC Induction Drives

	OEM cost estimates,[a] $/kW		Specific power,[b] W/kg		Power density,[b] W/l		Efficiency, %	
Components	DC	AC	DC	AC	DC	AC	DC	AC
Motor	15-15	10-15	330-1000	455-525	1040-3150	1430-1655	93-95	93-95
Controls	40-80	20-40	500-1250	2000-3000	400-1005	1610-2680	94-96	94-96
Combination	55-100	30-55	200-555	370-455	290-760	760-1025	87-91	87-91

[a]Production of 100,000 units or more per year.

[b]Continuous power rating.

4. Induction Machine Capabilities

Quantitative findings regarding performance, efficiency, and economics of traction-type ac induction motors are reported herein.

a. Machine Design. The stator winding is characterized by the number of pole pairs and the number of phases. The simplest, practical polyphase machine is a two-pole, three-phase configuration consisting of three stator windings, each displaced by 120 deg to the next. Each of these windings is designed so that the "density of turns" varies sinusoidally with respect to angular location. When such a winding arrangement is excited by a three-phase source, a rotating magnetic field results that has an angular rotation rate matching the electrical frequency.

With four and higher pole numbers, the winding pattern repeats two (or more) times over the stator circumference. As the number of poles is increased, the field rotational speed proportionately decreases for constant-frequency excitation. In normal operation, the rotor speed will approximate the field rotational speed. Under load, the rotor speed will be slightly less than the field rotational speed; during regeneration, the rotor speed will increase slightly above the flux rotational speed. The speed difference, called "slip speed," follows from the requirement that flux lines must cut the rotor conductors to generate rotor currents (rotor currents are required for rotor torques).

Configurations other than three-phase may be used. For single-phase systems, degraded performance results because the magnetic field produced by the stator is not constant in magnitude; harmonic currents are induced into the rotor which cause increased losses but do not increase the output torque. Furthermore, copper and iron utilizations are less than for polyphase machines. For two or more phases, it is possible to achieve an ideal, constant-magnitude, uniformly rotating flux vector. Two-phase windings, however, are ruled out because of their high sensitivity to "multiple-three" inverter-produced harmonics. While three-phase windings are sensitive to all even harmonics, inverter-type waveforms (while non-sinusoidal) are symmetric and, therefore, lack even harmonics. For phase numbers greater than three, improved flux uniformity is possible where inverter drives are used. While this leads to reduced rotor losses, overall motor efficiency does not necessarily improve because stator crest factors degrade with increasing phase multiplicity. Literature reviews indicate that the trade-offs are yet to be fully understood.

There are currently two rotor designs: wound rotors and squirrel-cage shorted rotors. With the former, a non-shorted rotor winding is connected through slip rings and brushes to an external circuit. With this design, the rotor resistance may be varied (by external means) to modify the torque-speed characteristics. This design also permits "double excitation" wherein energy is either supplied to or received from the rotor via the slip ring system. This design, which is more expensive and requires brush maintenance, has little or no relevance to EV-type traction application; the shorted squirrel-cage rotor will undoubtedly be the rule for ac traction applications.

Variations in squirrel-cage rotor designs affect such machine parameters as efficiency, breakdown torque (maximum torque capability before stall), and starting torque (torque at zero rev/min with nominal voltage and frequency excitation). Specifically, rotor designs in which resistance is minimized achieved maximum efficiency and maximum breakdown torque but with diminished starting torque. For this reason, conventional machines designed to operate from 60-Hz lines use compromised rotor designs so that acceptable starting torques are achieved. In contrast, machines designed for use with variable frequency inverters need not be compromised in this way; in these situations, minimizing rotor resistance actually maximizes "starting torque" as well as breakdown torque and efficiency. Hence, with traction applications, minimum resistance rotor designs are ideal.

b. Torque Below Base Speed. Base speed, ω_o, in an inverter drive system is defined as the machine synchronous speed that corresponds to maximum flux and maximum excitation voltage. Under the above excitation conditions, there exists a continuous torque rating (based on thermal considerations), and there is also a corresponding breakdown torque. From data gathered from GE's Small AC (SAC) Motor Division, the continuous torque capability (at base speed) is on the order of 0.65 Nm/kg of machine weight (0.22 ft-lb/lb), and the breakdown torque is on the order of 3.0 Nm/kg of machine weight (1.0 ft-lb/lb). These numbers are based on state-of-the-art, 30-kW continuous traction designs (H. Harmes, GE's Small AC Motor Division, personal communication, 1981). In practice, a safety margin must be provided between peak torque demand and the breakdown value. Hence, peak torque capabilities at base speed will be somewhat less than 3.0 Nm/kg for these designs.

For operation below base speed, the excitation voltage must be decreased as the frequency is decreased, i.e., excitation "voltage per Hertz" must not exceed a certain critical value or magnetic saturation results with fault-type currents following. With the voltage-to-frequency ratio held constant, the above values of continuous and breakdown torque will be nearly independent of speed. Where cooling is provided by a rotor fan, the continuous torque, however, must be derated at low speeds because of the reduced air circulation. With external forced cooling, no such derating is necessary.

Because of stator and rotor resistance and reactance combinations, modifications to the constant volts per Hertz regime are needed. First, at very low frequencies and speeds, the stator IR^8 drop becomes appreciable compared with machine electro-motive force (EMF). Thus, at low speeds, a "voltage boost" is required to compensate for this drop. Ideally, a voltage boost equal to the current times the effective machine resistance should be applied for all points of operation below base speed. At higher frequencies, a second component of voltage drop proportional to leakage inductance, current, and frequency becomes significant. Compensation for this component is complicated because it is in quatrature to the EMF. With adequate compensation (i.e., additional voltage boosting), peak torque levels well above 3 Nm/kg can be produced for speeds below base (see Figure 4-1).

It should be noted that rotor currents and rotor torque are the result of a difference between mechanical and electrical rotational speeds. This difference, which may be expressed either in terms of shaft rev/min (relative to synchronous) or electrical frequency (relative to shaft speed) is called the slip frequency. For small values of torque, slip frequency and torque are linearly proportional. For larger values of torque and slip, the two are no longer proportional due to rotor reactance effects. For state-of-the-art (SOA) four-pole traction-type designs using low rotor resistance, breakdown torque corresponds to approximately 3 Hz (Figure 4-2). The breakdown torque is proportional to the square of the excitation voltage while the breakdown slip frequency (i.e., slip frequency at breakdown) is nearly independent of both the excitation voltage and excitation frequency.

c. Torque Above Base Speed. For operation above base speed, the maximum excitation voltage is bounded by the battery voltage, and, hence, the volts/Hertz and flux levels must fall with increasing frequency and speed. Torque is proportional to the product of flux and rotor current. Because rotor current is proportional to rotor voltage, which is in turn proportional to the flux (and the slip frequency), it follows that the breakdown torque decreases as $1/f^2$ for speeds above base speed. In contrast, the continuously rated torque drops off as 1/f because efficiency is roughly constant with speed. The result of these dependencies is that the ratio between the peak and continuous torque capabilities diminishes as rev/min is increased above base speed (Figure 4-3.)

---

[8] Current times resistance (i.e., resistive voltage).

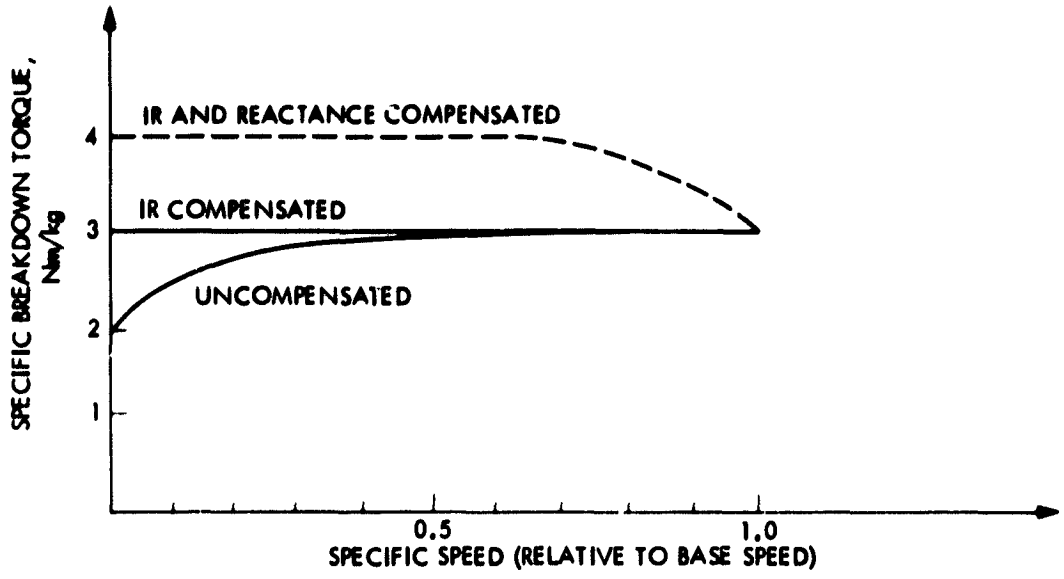

Figure 4-1. Specific Breakdown Torque vs. Specific Speed (SOA Traction-Type Induction Machines)

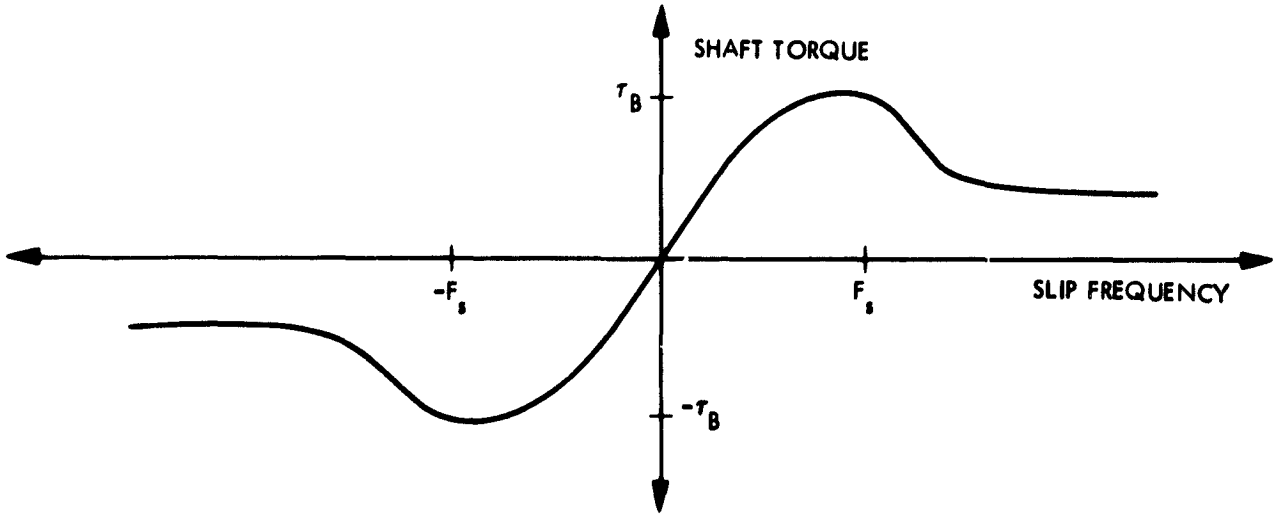

Figure 4-2. Shaft Torque vs. Slip Frequency for Fixed Voltage Excitation (τ = Breakdown Torque, f_s = Breakdown Slip Frequency)

By designing ω_o to be moderately high, high power-to-weight ratios are possible. For example, with ω_o = 4500 rev/min, a peak-power/weight ratio (at ω_o) of about 1.9 hp/kg is possible. (For rev/min below ω_o, peak power is approximately proportional to f, and above ω_o, peak power falls off as 1/f.)

The corresponding continuous power density is 0.36 kW/kg for speeds between ω_o and ω_1. ω_o is limited by inverter considerations; as ω_o is increased, the inverter output to input voltage ratio is lowered for each torque-speed point, and the resulting increased currents lead to higher inverter losses and costs. ω_1 is the maximum allowable rev/min (red line speed) as limited by rotor centrifugal considerations. For traction machines in the 30-kW class, ω_1 is about 15,000 rev/min. As ω_1/ω_o is increased, inverter cost and efficiency improves while the motor power density degrades. Present considerations indicate that ω_1/ω_o optimizes at about 2.5 (i.e., ω_o = 6000 rev/min and ω_1 = 15,000 rev/min).

d. Motor Losses and Efficiency. Minimizing machine loss is extremely important because EV electrical energy is "at a premium." To compensate for incremental losses, both the battery and vehicle structure must be enhanced. The charger and each element of the propulsion system must be sized accordingly. Hence, both vehicle and energy costs are directly affected by motor losses.

Data on a motor developed by Eaton indicates average efficiencies of 85 to 90% over the J227aD cycle (see Reference 4-3). JPL test data (ETV-1) indicate an average J227aD cycle efficiency of 84%; at steady state, efficiencies of over 90% may be expected.

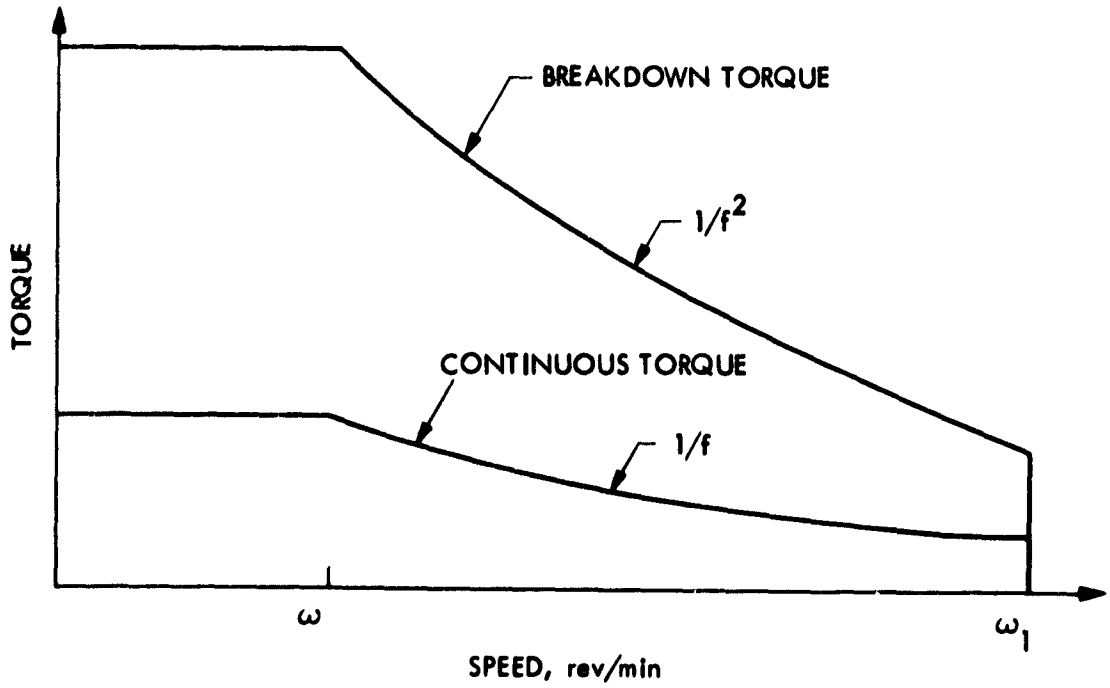

Figure 4-3. Continuous and Breakdown Torque vs. rev/min for Induction Machine (ω_o = Base Speed, ω_1 = Centrifugal Limit)

For most points on the torque-speed plane, losses in order of importance are stator copper, stray, iron, and rotor (see Table 4-2). Little can be done to reduce the stator copper losses below the conventional values. Increasing pole multiplicity helps somewhat because inactive span copper is reduced. As the number of poles is increased, however, the required excitation frequency must be proportionally increased (to maintain rev/min speed); this leads to increased inverter and iron losses. Analyses and experience indicate four poles are optimal without inverter constraints. However, GE implies that two poles are optimal with the present inverter limitations (Advanced Electric Vehicle Powertrain Program, Preliminary Design Review, Ford Motor Company, September 1, 1982).

Iron losses are definitely subject to control. With silicon steel, which is now universally used for high efficiency applications, magnetic losses are half that of soft iron (conventionally used). Machines using silicon steel, however, cost and weigh about 20% more than their soft iron counterparts. Eddy and stray magnetic losses decrease as lamination thickness is decreased. Hence, these losses may be further reduced by using laminations that are thinner than the present 19 mil standard. As thickness is reduced, material and stamping costs increase rapidly. Nonetheless, a trend to thinner laminations may be expected as energy costs continue to rise.

Rotor losses are directly proportional to rotor bar resistivity. Using copper bars in place of the conventional aluminum alloy, for example, cuts these losses by about 60%. On the other hand, little is gained by doing this substitution because rotor conductor losses are relatively small. Furthermore, technical problems associated with copper casting seem to be significant.

Windage losses, not previously mentioned, may be significant at high rev/min and low-power points of operation. By using external blowers, as opposed to integral rotor fans, these losses may be reduced. As a point of reference, a fanless rotor capable of handling 30 kW continuously and 60 kW peak has a length and diameter of about 15 cm and a windage loss at 15,000 rev/min of about 300 W (windage increases as the speed squared).

Table 4-3 lists component losses for a four-pole, three-phase machine designed by GE capable of handling 30 kW continuously and 60 kW peak (base speed is 5000 rev/min and total weight is 85 kg (187 lb). With most inverter drives, voltage is maintained proportionate to frequency for below base speed (constant volts per Hertz) and maintained constant for above base speed. This "algorithm" (while optimal in terms of inverter efficiency and inverter simplicity) is non-optimal in terms of motor and system efficiency. An algorithm developed by GE (and others) that seems close to optimum provides constant slip frequency, independent of torque and speed. This requires that volts per Hertz be maintained proportionate to P/f, where P is the shaft power and f is the excitation frequency. With this algorithm, the percentage loss associated with each component (e.g., magnetic, copper, etc.) remains approximately constant.

Table 4-3. Component Losses for the General Electric 30-kW High-Efficiency Traction Machine[a,b]

Rev/ min	Torque, Nm	Input power, W	Stator copper, W	Stray loss, W	Iron loss, W	Rotor loss, W	Output power, W	Efficiency, %
1000	13.6	1605	93	17	10	55	1420	88.4
1000	40.7	4796	279	52	30	165	4259	88.9
1000	81.4	9583	558	105	60	331	8518	88.8
1000	135.7	16056	1015	175	105	551	14197	88.4
3000	13.6	4583	95	89	43	56	4259	92.9
3000	40.7	13666	283	266	126	167	12777	93.5
3000	81.4	27290	565	532	251	334	25554	93.6
3000	135.7	45569	1030	888	443	550	42591	93.5
6000	13.6	9207	97	256	125	57	8518	92.5
6000	27.1	18295	193	512	247	113	17036	93.1
6000	54.3	36470	385	1024	491	226	34073	93.4
6000	95.0	64468	898	2418	687	536	59627	92.5
10000	6.8	7994	51	303	154	29	7098	88.8
10000	13.6	15703	100	606	301	58	14197	90.4
10000	27.1	31118	199	1212	594	115	28394	91.3
10000	40.7	48476	575	3508	591	346	42591	87.9

[a]Voltage adjusted to give constant slip frequency = 1.28 Hz.

[b]Design based on 19-mil silicon steel laminations; 10-mil laminations should increase efficiencies by about 2%. Rotor shorting bars use aluminum alloy having a conductivity rating equal to 54% that of copper. Data received from GE's Small AC Motor Division (H. Harmes, personal communication with W. Rippel, 1981).

5. Chopper Technology

a. General Considerations. Voltage control for dc traction machines may be smoothly, efficiently, and bidirectionally controlled by chopper-type systems. The technology of such systems has much in common with inverter-type systems. As with inverters, the trend is away from inductance/capacitance (L-C) commutated SCR approaches and toward transistors and GTOs for reasons of cost, weight, and efficiency. With present SOA designs based on transistors, single-quadrant systems are now in production that sell for about $25/kW, weigh less than 0.5 kg/kW, and have typical efficiencies in excess of 97% (personal communication with EVC, Inc., Inglewood, California, 1981).

b. Power Loss Considerations. Two types of losses exist: (1) direct losses that occur within the chopper itself and (2) induced losses in the battery and the motor that are a result of chopper-produced current harmonics. The direct losses, in turn, resolve principally into semiconductor forward drop losses, switching losses, and parasitic losses. These will be discussed subsequently.

With a chopper operating in the buck mode, the primary mechanism of motor-induced losses is the flow of eddy currents within the frame. Because these currents are determined by the voltage waveform applied to the motor, the eddy losses are virtually load-independent and are a function of only the chopper voltage and duty cycle. For typical solid frame dc motors, the motor induced losses range between about 2 and 5% of the full-rated power under worst-case conditions (Reference 4-5). These losses can be greatly reduced with the use of laminated frame designs. Alternatively, filtering and multi-phase techniques may be used to reduce the chopper harmonics.

Battery-induced losses may even be higher than the motor-induced losses due to the discontinuous nature of the currents drawn by the chopper. Unlike the motor-induced losses, the battery-induced losses are dependent on current levels (squared dependence). Worst-case induced losses occur at maximum current when the chopping duty cycle is 50%. Under these conditions, the battery-induced losses may approach 25% of the maximum dc losses (which occur under maximum current and 100% duty-cycle conditions).

As mentioned above, the internal chopper losses resolve into three components. The semiconductor forward drop losses (associated with the switch and freewheel diode) are approximated by

$$P_f \simeq I_{av} \left[V_{fs}\, D + V_{fd}\, (1 - D)\right] \qquad (1)$$

where I_{av} is the average motor current, V_{fs} is the forward drop of the switching semiconductor, V_{fd} the diode drop, and D the duty cycle. Where $V_{fs} \simeq V_{fd}$, Equation (1) may be simplified to give

$$P_f \simeq I_{av}\, V_{fs} \qquad (2)$$

With transistor systems, V_{fs} and V_{fd} typically range between 1.0 and 1.5 V, thus accounting for a loss that is between 0.01/D and 0.015/D of the through power.

The switching losses are approximated by

$$P_{sw} = V_P \, I_{av} \, f t_{sw} \tag{3}$$

where f is the chopping frequency, and t_{sw} is the average of the turn-on and turn-off switching times.

With typical transistor choppers, the effective switching times, t_{sw}, range between about 2 μs and 5 μs. With series motors, f is typically 500 Hz; with shunt (or permanent field) motors, f is typically 3000 Hz. Accordingly, in a typical series motor application (V_B = 100V, f = 500 Hz, and t_{sw} = 5 μs), $P_{sw}/P_{mot} \simeq 0.003/D$. Likewise, in a typical shunt motor application (V_B = 100V, f = 3000 Hz, and t_{sw} = 3 μs), $P_{sw}/P_{mot} \simeq 0.01/D$. Where snubbers are required, additional, fixed losses are added.

The parasitic losses, which include base drive, "housekeeping" and snubbing losses, are typically equal to about 0.5% of the maximum through power. Under light load, these losses may equal a high percentage of the through power. With conventional L-C forced commutated SCR choppers, much larger parasitic losses (associated with "trapped" L-C energy) are experienced. Because these systems are approaching obsolescence for EVs, no further comments will be made.

6. Inverter Technology

To provide optimum performance and efficiency, the inverter must perform a number of functions:

(1) Convert dc to symmetric polyphase ac.

(2) Provide optimal frequency for each torque-speed point.

(3) Provide optimal voltage for each torque-speed point.

(4) Suppress harmonics so that the sum of the inverter and motor harmonic losses is minimal for each torque-speed point.

Inverter systems may be divided into three subsystems:

(1) The main power-handling components (power train).

(2) Signal processing and logic components.

(3) Support and interface components (drive circuits and power supplies).

At the present time, most of the cost, weight, and power loss is associated with the power train. Transformerless bridge-type topologies and their variations will undoubtedly remain universal for reasons of economics and weight. In the past, bidirectional buck-type pre-regulators have been used in conjunction with bridge inverters; with these schemes, the pre-regulator controls voltage while the inverter operates in a simple six-step, non-regulating mode. With the higher speed switching devices now available, pulse-width modulation (PWM) systems are currently gaining vogue; here the inverter switches are modulated so that they perform the dual roles of voltage regulation and inversion. This latter approach reduces cost, weight, and losses at the expense of higher technology switching devices.

a. Switching Devices. In the past, inverter-grade SCRs (thyristors) were the only devices capable of handling the power levels encountered in EV applications. The external commutation circuitry required for the SCRs, however, contributed to most of the system's costs, weight, and power loss. High-power Darlington transistors are now enabling reduced system costs, weight, and losses as compared with SCR systems. Darlington transistors are being aggressively developed and marketed for industrial applications. While transistor-based systems seem to be superior to their SCR counterparts, the Darlington transistor is still not the ideal device; safe operating area limitations and base drive requirements remain significant impediments.

The newly developed power field effect transistor (FET) is ideal in virtually all performance respects. The only drawback is an extremely high cost factor (more than 20 times that of the Darlington transistor). The question remains as to whether production costs could fall sufficiently, given the large potential volume for EV and industrial applications.

A third recent development is the high-power Gate Turn-Off Device (GTO). New device geometries and fabrication technologies have enabled scale up to the 1000-kVA class. Despite the requirement for high current turn-off pulses, it seems that the drive circuits may actually be less expensive than counterpart transistor drive circuits. Other advantages over transistors include improved voltage and safe operating area characteristics. For devices below 10 kVA, GTOs are less expensive than the low-cost Darlingtons ($0.35/kVA for the GTOs and $0.65 for the Darlingtons). Unfortunately, the high-power devices are still expensive (devices rated above 200 kVA run in excess of $2/kVA). At present, GTOs are being successfully used in small inverter systems rated up to 20 kVA. If large GTO prices are substantially reduced, it is possible that the GTO will be the dominant device for inverters.

So-called hybrid topologies, wherein two or more switching device technologies are synergistically combined, may have economic potential. One example of this concept is an inverter scheme wherein a single FET is used to commutate all of the SCRs in a bridge. This approach offers high efficiency combined with good economy. Various other synergistic device combinations exist that warrant investigation.

b. Current vs. Voltage-Fed Inverters. The dc input to a polyphase bridge may be either current- or voltage-fed. In the case of

current-fed systems (Figure 4-4), the bridge input is connected in series with an inductor, and voltage control is achieved by a pre-regulator. The inverter switching algorithm is such that each switch conducts for one-third cycle, with one positive switch and one negative switch always conducting. This algorithm automatically constrains the motor currents to six-step waves where the current harmonics are fixed fractions of the fundamental current (fifth harmonic = 20%, etc.).

With voltage-fed systems, the bridge input is shunted by a capacitor. Voltage control may be achieved either by a switching pre-regulator (Figure 4-5) or by pulse-width modulation of the inverter switches. In the case where a pre-regulator is used, the inverter switches are operated in the classic six-step mode where each has a 50% duty cycle. This algorithm defines the motor voltage to a six-step waveform. Harmonic currents are, in turn, determined by the machine impedance. For low-reactance machines, harmonic currents are large, and the fifth harmonic may greatly exceed 20% of the fundamental.

With pulse-width modulation systems, a switching frequency of usually a few kHz is applied to each switch, and switching duty cycles are modulated so that a Fourier Fundamental Component of desired amplitude and frequency is produced while the other Fourier components caused by the switching process are optimally suppressed. With this technique, current harmonics may be reduced to arbitrarily low values, depending on the magnitude of the switching frequency.

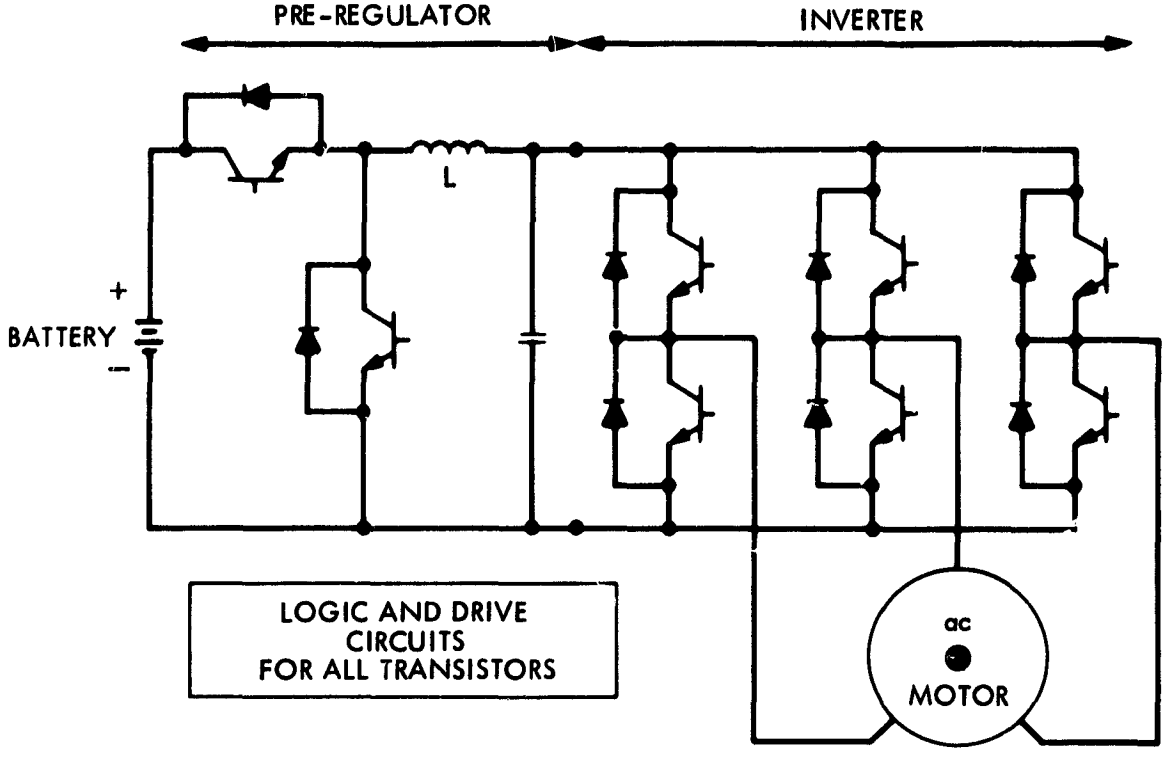

Figure 4-4. Current-Fed Inverter (pre-regulator must be bidirectional if regenerative capability is desired)

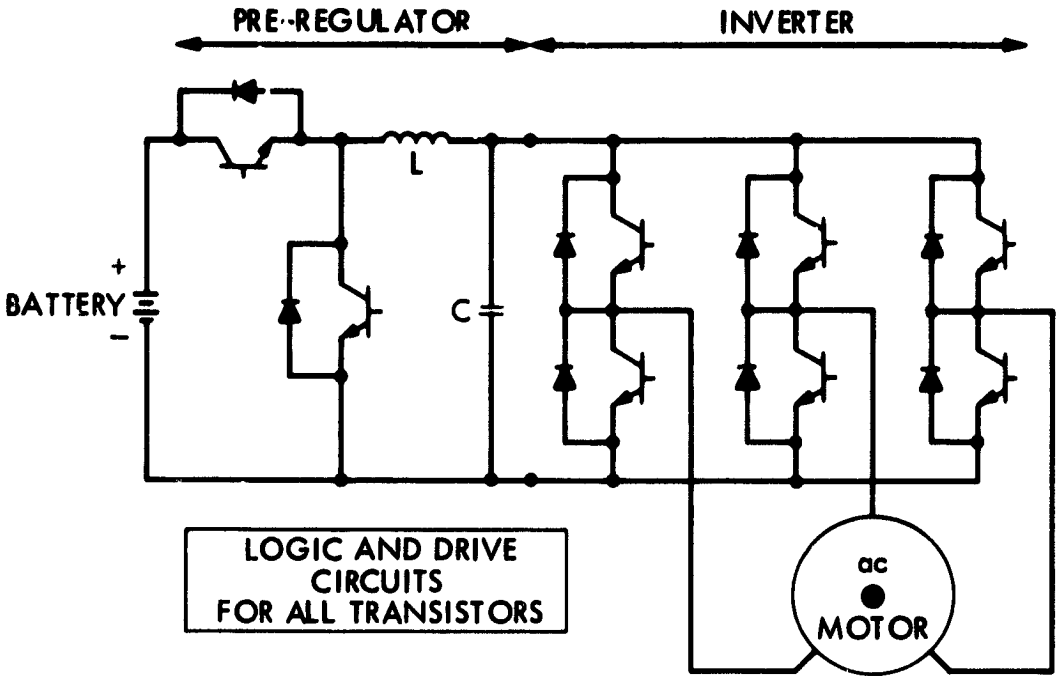

Figure 4-5. Voltage-Fed Pre-Regulator Inverter (note addition of capacitor C)

Although complex in terms of algorithms, the PWM approach is ideal because losses, switch multiplicity, and reactive component weights are all minimized. For these and other reasons, the PWM approach will probably become universal for traction applications.

c. Switching Algorithms. A considerable effort yet remains for determining the algorithm that will provide optimum efficiency for all torque-speed points. As mentioned, the function of the switching algorithm is to achieve the commanded torque for each speed with minimal system losses. The switching algorithm that will achieve this must generate the correct frequency and voltage while optimally suppressing harmonics. Numerous algorithms have been implemented and are under investigation. Thus far, however, there is no evidence of a fully comprehensive approach. With today's integrated circuit technology, algorithm implementation promises to be inexpensive.

d. Inverter Losses and Efficiency. As with chopper drives, inverter drives produce two types of losses: direct losses within the inverter itself and induced losses within the battery and motor resulting from inverter generated harmonics. With pre-regulated inverters, ac currents drawn from the battery are caused by the pre-regulator. Accordingly, these losses are comparable to those of a dc chopper system (operating at the same frequency and containing the same input filtering).

With PWM inverters, the type generally used for EV applications, ripple currents drawn from the battery are typically small compared with pre-regulator systems for the following reasons:

(1) With each switching event, the change of input current is equal to the current associated with one phase and not the sum of the phases.

(2) Switching times for the different phases are typically time-staggered, thus leading to harmonic suppression.

(3) Input ripple frequencies are fairly high (typically 3 to 10 kHz), thus enabling effective filtering of the ac currents. Because the battery-induced losses are proportionate to the square of the ac components, these losses fall rapidly with filtering.

With six-step inverters, the motor harmonic losses are typically 2% of the full-load power (i.e., the motor heating is increased about 20% relative to the full power). The actual heating depends on the specific motor parameters. With PWM inverters using sinusoidal modulation, harmonic losses are typically nil.

As with choppers, the direct inverter losses mainly consist of semiconductor forward drop, switching, and parasitic losses. For PWM sinusoidally modulated, three-phase, full-bridge systems where the switch and anti-parallel diode drops are each equal to V_f, the sum of the switch and the diode forward drop loss is

$$P_f = \frac{1.56 V_f P}{V_{mot}} \tag{4}$$

where P is the apparent power supplied to the motor, and V_{mot} is the root mean square (phase-to-phase) output of the inverter. Because P_R (the real power supplied the motor) is P times the power factor (PF),

$$P_f = \frac{1.56\ V_f\ P_R}{V_{mot}\ (PF)} \tag{5}$$

Equation (5), it should be noted, applies equally well to regenerative power flow because both P_R and PF reverse signs.

In a typical application where V_{mot} = 200 V, V_f = 1.4 V and PF = 0.85. The associated loss fraction, P_f/P_R, is 2.6%.

Switching losses are extremely sensitive to the actual topologies used. With a pre-regulator system, it could appear that total switching losses exceed those of a PWM system because two conversions are involved. Closer

observation reveals the opposite. First, because the inverter switches in a pre-regulated system operate at the fundamental frequency and not at a higher carrier frequency, the inverter switching losses are much lower than with PWM. As a matter of fact, because six-step circuits are amenable to lossless snubbers, the switching losses of the inverter portion can be reduced to nil. While the major portion of switching losses occur within the pre-regulator, these losses may also be reduced to values that are small when compared with PWM switching losses. The use of large inductance and low pre-regulator frequencies is one approach. Another is to design the system so that the motor usually operates above base speed, which allows the pre-regulator to remain fully on with no switching. However, while pre-regulator topologies may be superior in terms of internal switching losses, the advent of moderately fast Darlington transistors and GTOs enables PWM systems to compete -- especially when cost and weight advantages of PWM are considered. Assuming pre-regulator switching losses dominate over inverter switching losses, Equation (1) may be applied where I_{av} is the current supplied to the inverter.

For PWM systems, switching losses may be found by using Equations (3) and (5). From Equation (5), it follows that the sum of the average currents through the six switches (in a three-phase system) is $1.56\ P_R/V_{mot}(PF)$. Using this value for I_{av} in Equation (3) gives

$$P_{sw} = \frac{1.56\ V_B\ P_R\ f\ t_{sw}}{V_{mot}\ (PF)} \qquad (6)$$

where f is the "carrier frequency" and V_{mot} is the phase-to-phase rms voltage.

For a typical application, where $V_B/V_{mot} = 2$, $f = 2$ kHz, $t_{sw} = 2$ s, and $PF = 0.85$, P_{sw}/P_R (the loss fraction due to switching) is 1.5%. It should be noted that where snubbers are used, t_{sw} will lengthen reciprocally with load, thus causing the partial-load efficiency to degrade.

With PWM inverters, parasitic losses are typically higher than with choppers due to the increased numbers of switches and switching frequency. With the present state of the art, parasitic losses (excluding snubber losses) are about 1% of full load. In Figure 4-6, measured efficiency data on the Eaton drive system is displayed (Reference 4-3). While the peak-point efficiency (95.5%) is extremely good, part-load efficiencies are not so good. The main reason for poor part-load efficiency is high snubbing losses. With recent transistor developments, snubbing requirements are reduced or eliminated; future inverter generations using such transistors should display greatly improved part-load efficiencies.

Performance and Economics. At the present time, cost, weight, and loss factors imply that inverter drives are closing the gap with dc systems for both industrial and traction applications. With the successful implementation of inverter technology now predictable, power densities and system economics should each improve two-fold, and the system efficiency should increase to the "low nineties."

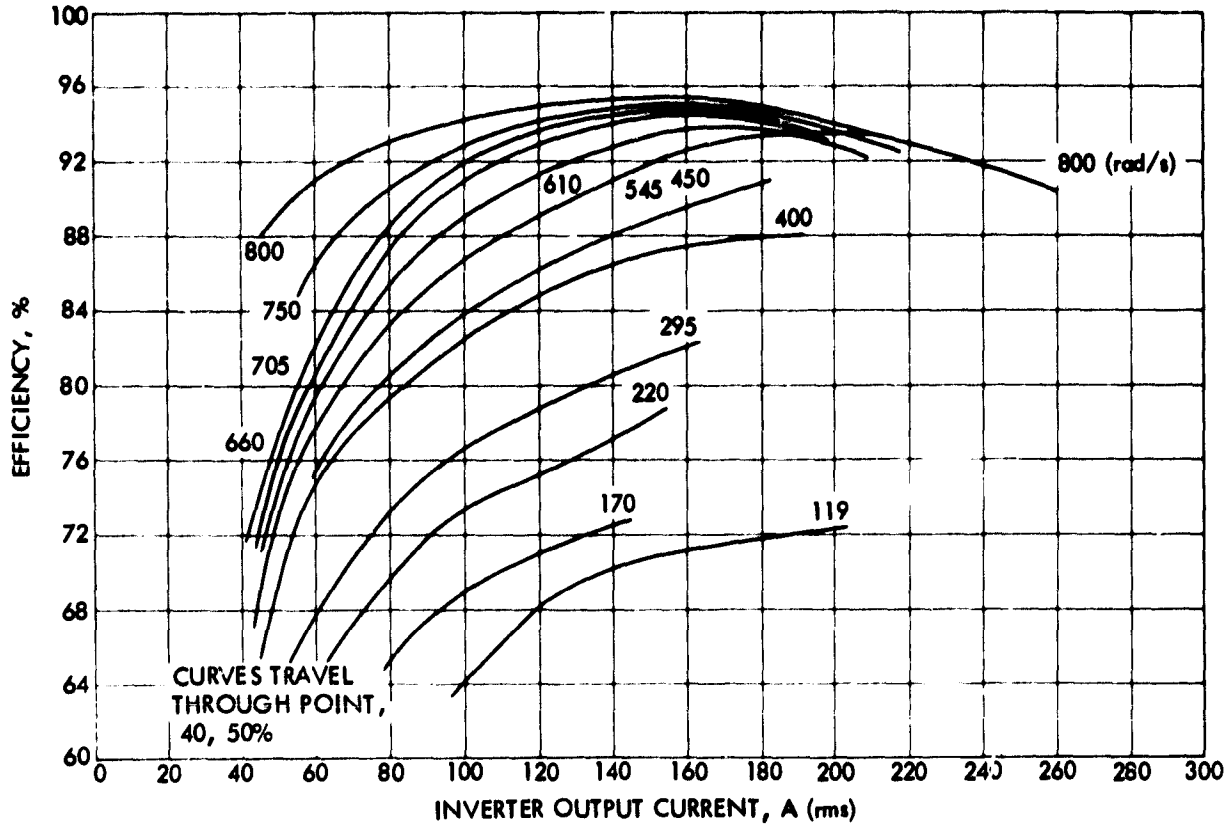

Figure 4-6. Eaton ac System Efficiency (Source: Eaton Corporation)

7. Performance Characteristics

a. Motor Efficiency. Generalized efficiency modeling equations were produced using the data supplied from NASA Lewis Research Center (LeRC) which graphically provides efficiency in terms of power and speed for several propulsion systems (personal communication to J. Graf from P.A. Thollot, LeRC, January 9, 1980). These equations were motivated by the following observations from the data:

(1) Over the torque-speed plane, there is only one peak efficiency point.

(2) For different speeds (rev/min), peak efficiency occurs at approximately the same torque. Likewise, for different torques peak efficiency occurs at approximately the same rev/min.

(3) The efficiency function is not symmetric with respect to either the torque or speed axes.

From observation (1) above, an equation of the following form was sought

$$E = k_o\, f(T, \omega) \tag{7}$$

where E is efficiency, k_o is the peak point efficiency, and $f(T, \omega)$ is a function of torque (T) and rev/min (ω), which reaches unity for the T and corresponding to the peak efficiency.

From observation (2) above, it follows that $f(T, \omega) = g(T)h(\omega)$ where $g(T)$ reaches unity for the "peak torque" and $h(\omega)$ reaches unity at "peak rev/min." Finally, specific forms for g and h were found that satisfy observation (3); there are many other forms that also would work. The selected forms are

$$g(T) = 2\, G^a - G^{2a} \tag{8}$$

$$h(\omega) = 2\, H^b - H^{2b} \tag{9}$$

where $G = T/T_o$, $H = \omega/\omega_o$, T_o and ω_o are the torque and rev/min that correspond to peak efficiency, and a and b are curve-fit constants.

Combining Equations (7) through (9) gives

$$E = k_o(2\, G^a - G^{2a})(2\, H^b - H^{2b}) \tag{10}$$

An equivalent equation was derived that expresses efficiency in terms of power and rev/min

$$E = k_o\ \ 2(Y/H)^a - (Y/H)^{2a}\ \ (2\, H^b - H^{2b}) \tag{11}$$

where $Y = P/P_o$, P is power, and P_o is the power level corresponding to peak efficiency. Equation (11) follows from the fact that $Y = GH$. Equations (10) and (11) are extremely easy to use because k_o, T_o, and ω_o are found by inspection. Because a and b are virtually uncoupled, each may easily be found on a trial-and-error basis. Using Equations (10) and (11), curve fits for three LeRC-described propulsion systems were obtained. The systems are described in Table 4-4, and the curve-fit constants are listed in Table 4-5.

Data were sought for dc machines, which include efficiency under regeneration as well as motoring and provide peak power and peak torque versus speed. Only one source of suitable data was found: Siemens graphical data for their 1GV1 separately excited 144-V, 16-kW traction motor (Reference 4-6). Using these data, the constants for motoring and regeneration were found using the equations and methods of the previous subsection. The results are listed in Table 4-6.

Table 4-4. Propulsion System Descriptions

Characteristics	AC induction	DC shunt	Electronically commutated
Motor type	3-phase induction	dc shunt wound	Samarium-Cobalt
Motor weight, kg	40	100	16
Motor size, cm	28 D x 38 L	31 D x 34 L	16 D x 27 L
Controller type	SCR inverter chopper	Transistor field plus SCR inverter	Transistor chopper
Controller weight, kg	30	8	30
Controller size, cm	61 x 30 x 51	25 x 20 x 15	61 x 30 x 51
Battery voltage, kg	120	180	180
Comments	Combined system 15 kW continuous at 7200 rev/min	30 kW continuous	13 kW continuous

Table 4-5. Selected Curve-Fit Constants

Characteristics	AC induction	DC shunt	Electronically commutated
Peak-point efficiency, %	0.880	0.915	0.900
Torque, Nm	23.9	53.7	6.62
Rev/min (ω_o)	6000	2667	22,500
Power, kW	15	15	15.6
Constant, (a)	0.25	0.25	0.15
Constant, (b)	0.30	0.20	0.55

It is interesting to note that the Table 4-6 constants closely agree with the dc shunt system. Using the Table 4-6 constants with Equation (4) and comparing calculated efficiencies with the original data shows that the worst discrepancies (under extreme values of torque and speed) are between -6 and +6% for motoring data and between -4 and +4% for the regenerating data.

Table 4-6. Curve-Fit Constants for Siemens 1GV1 Data

Characteristics	Motoring	Regenerating
Peak-point efficiency, %	0.87	0.88
Torque, Nm	50	50
Rev/min (ω_o)	2400	3800
Constant, (a)	0.25	0.25
Constant, (b)	0.30	0.40

Noting that the 1GV1 peak-point motoring efficiency is within 1% of the GE 2366 peak-point efficiency, it is probable that the 1GV1 data (and the model) are representative of SOA dc traction motor performance.

b. Torque-Speed Envelope (DC Machines). Again, the only detailed available information was for the Siemens 1GV1 traction motor. For below base speed (2000 rev/min) the continuous torque capability (with external blower) is 80 Nm, and the peak-torque capability for 3 min is 160 Nm. Because the machine weight is 90 kg, the continuous and peak-specific torque capabilities are 0.88 Nm/kg and 1.78 Nm/kg, respectively. These values seem to be typical of most traction-type dc and ac motors and, as such, may be used for generic modeling. Relating these specific torque values to power gives a continuous output kW rating that is equal to 0.00837 times rev/min and a peak power rating that is equal to 0.0167 times rev/min.

For above base-speed operation, one of two limits prevails: either power or commutation. For speeds between base speed (2000 rev/min) and approximately 4100 rev/min, a power limit prevails: 16.7 kW continuous output (0.185 kW/kg) and 33.4 kW peak output (0.371 kW/kg).

For speeds between 4100 and 6700 rev/min (centrifugal limit), the continuous power rating remains 16.7 kW while the peak power is commutation-limited in accordance with the following equation derived from Siemens graphical data:

$$P = 33.4\ (\text{rev/min}/4100)^{-0.83} \qquad (12)$$

8. Conclusions

The information gathered indicates that present state-of-the-art ac and dc propulsion systems will soon be competitive in terms of cost, weight, and efficiency. With continued power semiconductor advances coupled with the ongoing development of inverter systems for industrial applications, ac propulsion should gain superiority.

An alternative technology, the dc brushless drive, like the ac drive, is "electronics intensive" and has the potential for achieving large weight and cost reductions relative to conventional brush-type dc systems.. Compared with the ac drive, the dc brushless seems to have no clear-cut advantages or disadvantages. The fact that inverter/induction motor combinations are now being developed for mass industrial markets probably will give the ac drive an economic edge.

Realizing that EV developmental resources will be small compared with the resources in place for industrial drives, it is recommended that traction-type ac drives be developed as a spin-off to existing industrial technology. Even with such a "head start," design optimization poses a significant challenge.

A few comments are due concerning specific parameters for ac drive. The PWM (pulse-width modulation) scheme will undoubtedly remain standard for traction applications; the high switching stresses are more than offset by reduced cost and weight. Conventional L-C commutated SCR approaches are not cost and weight competitive with transistor and GTO schemes. Actual device technology and power topology details are presently open issues.

The option of phase numbers greater than three is open. Analyses and measurements, however, indicate no clear-cut advantages with higher than three-phase systems. Modulation algorithms are still in flux. It is known that the "constant volts per Hertz" approach is non-optimal and that constant slip is "close to optimal," but an ideal and standardized approach has yet to emerge (and may not emerge).

Design algorithms and standards for the traction motor are still not available. Two poles seems to be optimal with the present inverter limitations; four- and six-pole designs could conceivably demonstrate an advantage. Optimized traction-type machines will use rotors with minimized resistance. Copper rotor bars would be desirable if the casting techniques were perfected. Lamination grades higher than those used with high-efficiency 60 Hz machines likely will be standard due to the importance of high efficiency.

Reduction gear technology is discussed in the subsection below. Although today's technology is easily capable of handling the expected input speeds of 10,000 to 20,000 rev/min, gear-train design algorithms have yet to be established. Specifically, reduction gear technology is required to provide adequate life (>5000 h) under high input shaft speeds (>15,000 rev/min). Low spin losses are extremely important to preserve high efficiency.

This study is continuing with an investigation of propulsion system sensitivity to voltage, which is made difficult because of the lack of information concerning advanced batteries and the variables that are affected by the voltage choice.

B. TRANSMISSIONS: PERFORMANCE AND COST CHARACTERISTICS

The simulation tool of the Advanced Vehicle \ssessment, ELVEC, has the capability of simulating various conventional transmission types; therefore,

the investigation of transmissions for advanced vehicles deals primarily with assessing the methods of reducing the high-speed output shaft of advanced dc brushless or ac motors to a usable speed (e.g., shaft speed as high as 30,000 rev/min). Speed control could be accomplished with electronic control and fixed gear reduction. Another interesting approach is the continuously variable transmission (CVT), which would relieve some of the stress from the electronics.

The NASA Lewis Research Center has been involved in the development of CVTs for several years and described the history and recent developments of CVTs at an EHV Advanced Technology Seminar (Reference 4-7). Of specific interest were the results of preliminary design studies conducted under a NASA contract for DOE on four CVT concepts. The CVT concepts and associated contractors are shown in Table 4-7.

A primary consideration with transmissions is the energy efficiency in speed reduction. The design studies were summarized in a NASA report (Reference 4-12), and the resulting comparison is shown in Figure 4-7.

At this power level (16 kW), the belt-type CVTs seem to have about a four-point efficiency advantage over the traction types. However, all predicted efficiencies are significantly higher than the nominal 75 to 85% values measured for current automatic transmissions (References 4-13, 4-14, and 4-15). Predicted CVT efficiencies at low power (5 kW) are 89 to 92%; hence, drive-train energy economy should improve with a CVT because the typical duty cycle of a car is modest.

Table 4-7. LeRC Preliminary Transmission Design Studies

CVT concept	Contractor
Variable pulley, steel V-belt	Battelle Columbus Labs[a]
Variable pulley, flat rubber belt	Kumm Industries, Inc.[b]
Toroidal traction	Garrett Corp., AiResearch Mfg. of California[c]
Cone-roller traction	Bales-McCoin Tractionmatic[d]

[a]Reference 4-8.

[b]Reference 4-9.

[c]Reference 4-10.

[d]Reference 4-11.

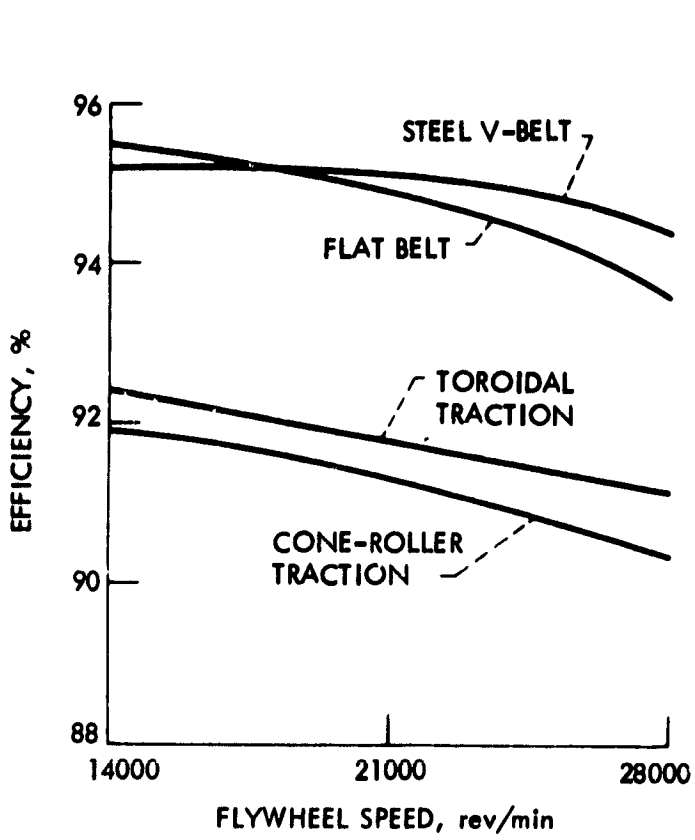

Figure 4-7. Comparison of Predicted CVT Efficiencies at Weighted Average Operating Conditions

A recent study by the Aerospace Corporation (Reference 4-16) summarized the development status and research needs of advanced automotive transmissions. This comprehensive survey indicates a large number of developments presently underway. Table 4-8, reproduced from that report, illustrates the current level of activity. Aerospace concluded that CVTs show significant potential for improvement of vehicle fuel economy. According to the Aerospace report, most domestic automobile manufacturers apparently view advanced conventional transmissions as the most cost-effective technology for the near term. However, CVTs are under investigation by most automobile companies, and several designs are in an advanced state of development. Some are being used in commercial applications, and it seems that one may be used in a production auto within the next 2 years (e.g., Van Doorne).

The advantages of a CVT can be seen in Figure 4-8, which compares the efficiency of the Volvo 343 CVT with manual and automatic transmissions for the same vehicle (Reference 4-17). The transmission, which is a derivative of the original DAF version (Volvo took over the DAF passenger-car operation), approaches the efficiency of the manual transmission and is superior to the automatic over the operating speed range.

Evaluating the projections of the transmission developers leads to the conclusion that CVTs are expected to outperform present transmissions; however, a great deal of information is still required to confidently compare the potential of the various types of transmissions for system integration. This includes consistent performance data or projections, volumetric

Table 4-8. Advanced Automotive Transmissions Presently Under Development

TYPE	DEVELOPER	DESCRIPTION	DEVELOPMENT STATE
HYDROKINETIC	FORD	VARIABLE PITCH TORQUE CONVERTER	FINAL DEVELOPMENT (GAS TURBINE)
	EATON, GM	ELECTRONIC SHIFT CONTROL	FINAL DEVELOPMENT
GEAR	AUTOMOTIVE PRODUCTS	CONSTANT MESH, COUNTER-SHAFT, HYDRAULIC SHIFT	FINAL DEVELOPMENT
	MAXWELL ENGINEERING	QUAD COUNTERSHAFT	PRODUCTION (LIMITED)
BELT	VOLVO/DAF	RUBBER V-BELT	PRODUCTION
	DAYCO	RUBBER V-BELT	SYSTEM ENGINEERING
	GATES	RUBBER V-BELT	SYSTEM ENGINEERING
	VAN DOORNE	METAL V-BELT	PREPRODUCTION
	PIV	METAL CHAIN	SYSTEM ENGINEERING
	BATTELLE	METAL V-BELT	INITIAL DEVELOPMENT
	KUMM	FLAT RUBBER BELT	INITIAL DEVELOPMENT
	U. OF WISCONSIN	RUBBER V-BELT	CONCEPT
HYDROSTATIC	ORSHANSKY	THREE-RANGE POWER-SPLIT	FINAL DEVELOPMENT
	LFIELD	HYDROSTATIC	INITIAL DEVELOPMENT
	NATIONAL RESEARCH COUNCIL OF CANADA	FOUR-RANGE POWER-SPLIT	CONCEPT
TRACTION	VADETEC	NUTATING CONE/RING	TBD (AUTOMOBILE) PREPRODUCTION (OFF-ROAD)
	TRACTION PROPULSION	TOROIDAL	SYSTEM ENGINEERING/ FINAL DEVELOPMENT
	BRITISH LEYLAND/ PERBURY	TOROIDAL	SYSTEM ENGINEERING
	GARRETT	TOROIDAL	PAPER DESIGN
	BALES-McCOIN	CONE/ROLLER	INITIAL DEVELOPMENT
	TRACTION RESEARCH	RING/CONE	INITIAL DEVELOPMENT
	YOUNG	OFFSET SPHERE	CONCEPT
	FAFNIR	RING/CONE	FINAL DEVELOPMENT (AGRICULTURAL IMPLEMENTS)
RATCHET	POWER-MATIC	VARIABLE ECCENTRIC / HYDRAULIC RATCHET	PAPER DESIGN (AUTOMOBILE) PREPRODUCTION (MOPED)
	KERR	NONCIRCULAR GEAR	PAPER DESIGN
	MANCHESTER	INERTIA	SYSTEM ENGINEERING

STAGE	END-OF-STAGE MILESTONE
CONCEPT	BASIC DESIGN CONCEPT DEFINED.
PAPER DESIGN	DETAILED DESIGN LAYOUT AND RELATED ENGINEERING CIRCULATION COMPLETE.
INITIAL DEVELOPMENT	PROTOTYPES BUILT AND BENCH TESTED.
SYSTEM ENGINEERING	PROTOTYPES PACKAGED AND VEHICLE TESTED.
FINAL DEVELOPMENT	REFINED DESIGN COMPLETE AND PRACTICAL PROTOTYPES AVAILABLE.
PREPRODUCTION	FINAL TESTING OF PROTOTYPE FLEET DONE OR IN PROGRESS. FINALIZED DESIGN COMPLETE AND READY FOR PRODUCTION.
PRODUCTION	IN PRODUCTION.

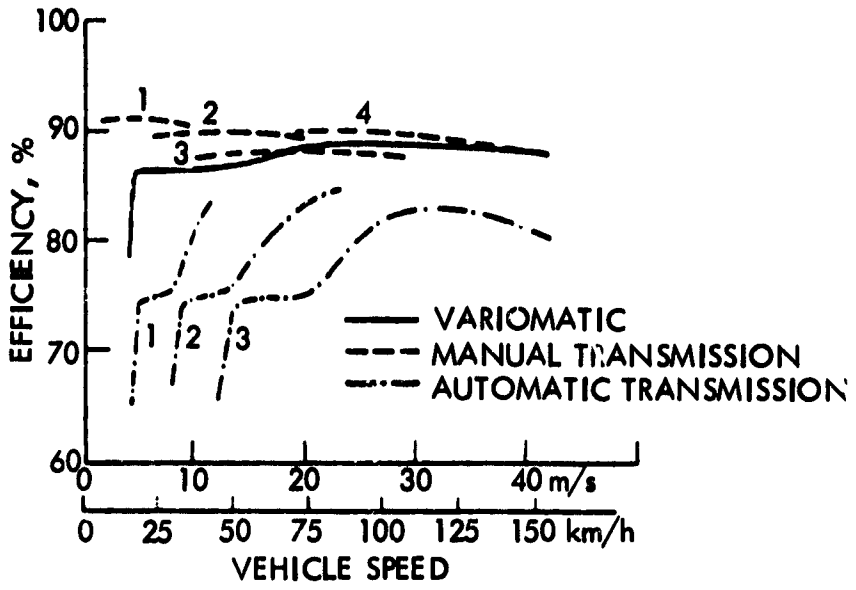

Figure 4-8. Full-Load Efficiency of the Volvo 343 CVT (Source: Aerospace Corporation)

characteristics, and production cost estimates. Further development also is required to resolve issues of durability, noise, and controls.

An effort was made to characterize the transmissions by the type of variable speed assembly (VSA), i.e., belt, hydrostatic, etc. The information was not consistent (i.e., power ratings), and all the types could not be assessed in terms of all the specific characteristics desired. Table 4-9 was formulated to show characteristics of the VSA and represents the assumptions that will be used in the AV systems evaluation (see References 4-3, 4-16, and 4-17).

C. SUMMARY: PROPULSION SYSTEM COMPARISON

The propulsion system is composed of the motor, controller, and transmission and must be compared as such. There are several choices for each of these subsystems, as described in the previous subsections, and this comparison will focus on the differences between the candidates for ac, dc brush-type, and dc brushless systems. The performance estimates have been sufficiently described previously, and the ultimate decision will be one of economics; hence, the comparison deals specifically with cost per unit power. As in the previous cost estimates, the cost estimates in this comparison could not be acquired under totally consistent scenarios. That is, the quotes were not available for the same annual unit production rates. The subsystem production costs vary with production rate, and this relationship is not constant for the various subsystems due to material and production cost differences. However, the comparison in Table 4-10 represents the estimates that were used in the system studies of the Advanced Vehicle Assessment.

Table 4-9. Transmission Plus Differential Characteristics

Characteristics	Specific power,[a] W/kg	Power density,[a] W/l	Mass density, kg/l	Speed ratio	Average efficiency, %	OEM costs,[b] $/kW
Gear reduction	2200	2800	1.3	5:1	95	2.00
Chain reduction[c]	1200	1080	0.9	8:1 or 20:1	93	2.20
Two-Speed Automatic[d]	860	780	0.9	8:1 to 20:1	88	3.60
Four-Speed Manual[e]	1640	1450	0.9	4:1 to 13:1	90	2.40
Belt CVT[f]	1700	850	0.5	Infinite	91	4.80
Hydrostatic CVT[g]	570	900	1.6	Infinite	83	5.50
Ratchet CVT[h]	2420	5330	2.2	Infinite	90	5.00
Traction CVT[i]	2190	2400	1:1	3:1 to 33:1	85	5.50

[a]Peak power, box volumes estimated.

[b]1982 dollars, peak-power rating, greater than 300,000 units produced per year. Adjusted costs from JPL EHV Cost Handbook (Reference 4-18). Fixed reduction costs scaled from manual transmission costs. CVT cost estimates based on perceived relative complexity.

[c]Based on theoretical modifications to Eaton 33.6 kW-peak, two-speed automatic.

[d]Eaton 33.6 kW-peak, two-speed automatic transmission and differential.

[e]GM X-Car 67 kW, four-speed manual transmission.

[f]Kumm Industries, 75 kW-peak (5 s).

[g]Sundstrand DMT-25, 186.5 kW-peak.

[h]Power-Matic PM-1, 186.5 kW-peak, without differential.

[i]Bales-McCoin, 75 kW-peak (5 s), without differential.

Table 4-10. Comparison of Projected Propulsion System Sales Prices[a]

Component	DC brush,[b] $/kW	DC brushless,[b] $/kW	AC induction,[b] $/kW
Motor	53 to 105[c]	23 to 30	15 to 23
Controller	42 to 83[c]	60 to 120	30 to 60
Transmission	2 to 6	2 to 6	2 to 6
System	97 to 194	85 to 156	47 to 89

[a]Sales price = 1.5 times OEM price.

[b]Continuous power rating, maximum power overload of 100% assumed.

[c]Allows for production cost to reduce up to one-half in large quantities.

This study indicates that the ac induction systems are expected to improve to the point that they will become the system of choice in advanced vehicle systems. This expectation is based on the foreseen improvements in electronics cost and performance as well as the ongoing commercial pressure to develop ac systems independent of the vehicle development programs. If the commercial development pressure for ac systems diminishes or the development effort for dc systems is comparable to ac, the cost differential would be negligible.

SECTION IV REFERENCES

4-1. Ben Daniel, D. J., "Semiconductor Alternating-Current Motor Drives and Energy Conservation," Science, November 1979.

4-2. Kurtz, D. W., ETV-1 Phase III Final Report Performance Testing and System Evaluation, JPL Publication 81-93, Jet Propulsion Laboratory, Pasadena, California, December 1981.

4-3. AC Propulsion System for an Electric Vehicle, Phase I Final Report, Eaton Corporation, DOE/NASA/0 125-81/1, August 1981.

4-4. Forrest, L., Lee, W. B., and Smalley, W. M., Assessment of Candidate Vehicles for Advanced Battery Demonstration, Interim Draft, Report No. ATR-81(7850)-1, Aerospace Corporation, June 1981.

4-5. Rippel, W., Three State-of-the-Art Individual Electric and Hybrid Vehicle Test Reports, Vol. II, DOE Publication HCP/M1011-03/2, November 1978.

4-6. "DC Traction Motor 1GV1," Technical Bulletin, Siemens Corporate Office, Iselin, New Jersey.

4-7. Loewenthal, S. H., "Advanced Continuously Variable Transmissions for Electric and Hybrid Vehicles," paper presented at the Electric and Hybrid Vehicle Advanced Technology Seminar, California Institute of Technology, Pasadena, California, December 8-9, 1980.

4-8. Swain, J. C., Klausing, T. A., and Wilcox, J. P., Design Study of Steel V-Belt CVT for Electric Vehicles, DOE/NAA/0116-80/1, NASA CR-159845, 1980.

4-9. Kumm, E. L., Design Study of Flat Belt CVT for Electric Vehicles, (P-1006, Emerson L. Kumm; DEN3-114) DOE/NASA/0114-80/1, NASA CR-159822, 1980.

4-10. Raynard, A. E., Kraus, J. H., and Bell, D. D., Design Study of Toroidal Traction CVT for Electric Vehicles, Report 80-16762, AiResearch Manufacturing Co., DEN3-117; also DOE/NASA/0117-80/1, NASA CR-159803, 1980.

4-11. Walker, R. D., and McCoin, D. K., Design Study of a Continuously Variable Cone/Roller Traction Transmission for Electric Vehicles, DOE/NASA/0115-80/1, NASA CR-1598a41, September 1980.

4-12. Parker, R. J., Loewenthal, S. H., and Fischer, G. K., Design Studies of Continuously Variable Transmission for Electric Vehicles, DOE/NASA/1044-12, NAA TM-81642, 1981.

4-13. Bujold, M. P., Small Passenger Car Transmission Test - Chevrolet 200 Transmission, ERC-LIB-79168, Eaton Engineering and Research Center, DEN3-124; also DOE/NAA/0124-1, NASA CR-159835, 1980.

4-14. Bujold, M. P., Small Passenger Car Transmission Test - Ford C4 Transmission, ERC-LIB-8060, Eaton Corporation, DEN3-124; also DOE/NASA/0124-2, NAA CR-159881, 1980.

4-15. Bujold, M. P., Small Passenger Car Transmission Test - Chevrolet Citation 1.25 Transmission, DOE/NASA/0124-4, NASA CR-159883, 1980.

4-16. Advanced Automotive Transmission Development Status and Research Needs, The Aerospace Corporation, DOE/CS/50286-1, April 1982.

4-17. Heft, R. C. and Heller, S. C., Hybrid Vehicle Potential Assessment, Vol. X: Electric and Hybrid Vehicle Cost Handbook, JPL Internal Report 5030-345, Jet Propulsion Laboratory, Pasadena, California, September 30, 1979.

SECTION V

VEHICLE SUBSYSTEM

Several characteristics of the vehicle subsystem are examined in this section, including vehicle mass reduction, aerodynamic drag, rolling resistance, and heating/cooling loads. These topics are not attributes of the propulsion and energy-storage subsystems; however, they have a definite impact on the road-power requirement and thus on the overall performance of the vehicle system. Changes in the power dissipation that are due to these non-propulsion factors will affect the necessary capabilities of the propulsion and energy-storage subsystems for the vehicle to perform a specified mission; therefore, establishing baseline values for these parameters is essential to the system evaluation tasks.

Four basic vehicle sizes were established for the study: two-, four-, and five-passenger cars as well as small vans. The general assessment method was to determine parameters for the baseline ICE (Internal-Combustion Engine) vehicles, and from these develop appropriate AV configurations providing equivalent passenger space, performance and cargo. This included the weight changes due to the various components, plus weight propagation and the changes in vehicle volume that are required to accommodate the subsystems.

A. VEHICLE-MASS REDUCTION

The objective of considering the vehicle-mass reduction potential is to define the 1992 baseline ICE car weights and thus the AV baseline weights, by projection from the weights of cars presently produced. Three potential levels of technology for the vehicle are considered: 1992 baseline, high-strength steel (HSS) plus composites, and all-aluminum or advanced composites. As a starting point, specifications for current production cars show curb weights for the lightest four-passenger cars (VW Rabbit, Honda Civic, Renault LeCar) to be in the 820 to 890-kg range, so it seems reasonable to select 820 kg (1800 lb) as the current minimum weight for four-passenger cars. Above this level, cars are available with continuously increasing size and weight, and at which point a true five-passenger capacity is attained can be a subjective judgment. Looking at rear-seat width, the GM X-cars (Chevrolet Citation) at 1135 kg and Chrysler K-cars at 1070 kg certainly qualify, while other cars in the 1000-kg range (Plymouth Horizon, Audi 4000) are somewhat marginal on rear-seat capacity. Because the main reason for considering a separate five-passenger category in the AV study is to consider a car distinctly larger than a four-passenger vehicle, we selected 1088 kg (2400 lb) as the current baseline curb weight for five-passenger cars.

The two-passenger subcompact category presents a problem because no such low-weight, high-fuel economy cars are presently available that differ from small, four-passenger cars. An idea of their likely characteristics may be obtained by looking at the Japanese micro-cars, made only for Japan's domestic market. To take advantage of special licensing laws, these cars have a 550-cc maximum engine displacement and curb weights of about 545 kg. While there are seats for four occupants, the space would be quite inadequate for typical U.S.

passengers. Eliminating the two rear seats and adapting such a car to U.S. safety requirements would probably have cancelling weight effects, so 540 kg (1200 lb) was established as the baseline curb weight for this (hypothetical), current two-passenger car.

The potential for mass reduction in the next decade (1990s) is difficult to assess. With the best of the current cars, as included in the preceding baseline descriptions, many approaches to lower vehicle weight are already incorporated, such as thorough attention to design details and better vehicle packaging, partially through front-wheel drive. The major remaining area is material substitution, primarily by replacing conventional steel-body components by HSS plastic composites or aluminum. So far, this has not been adopted to any large extent by the industry for either cost or production capacity reasons although "soft" front ends with integrated bumpers and fiberglass-reinforced plastic (FRP) grille-surround/headlight panels are becoming widely used. These applications allow one single complicated part to replace numerous separate metal parts and are thus justified on the basis of cost reductions in piece parts and assembly labor.

The weight-saving benefits of composites and FRP have certainly been demonstrated. As part of JPL's EHV Project, the Budd Company fabricated an outer door panel for a 1977 Chevrolet Impala sedan, complete with integral side-intrusion beam weighing 6.6 kg, which replaces a multi-part steel assembly of 11.6 kg, for a 43% weight saving (Reference 5-1). On a larger scale, PPG Industries undertook a project to reconstruct the body and numerous chassis components of a 1976 Cadillac Seville almost entirely of FRP (Reference 5-2). The curb weight was reduced from 1900 to 1590 kg, which reflected a 37% decrease in the affected portion of the car (although it did not meet the crash standard). Yet there is some question about how relevant such examples are to small cars at the lower end of the weight scale. Both of the above examples used large, heavy American cars of the older design generation when weight was still an end in itself. The Seville was originally derived from the 1400-kg Chevy II, so its steel components may not have been designed to the minimum possible weight.

An indication that weight reductions in small cars may be more difficult to achieve can be found in reports from the Frankfurt Auto Show (Reference 5-3), where several futuristic prototypes were shown with emphasis on high fuel economy through good aerodynamics and low weight. Volkswagen's Auto 2000 used items such as plastic wheels and seats, a plastic front body, FRP rear axle, and an all-aluminum engine. Basically a Rabbit-sized package, it weighs 780 kg (without US-spec bumpers), within 45 kg of a German Rabbit. Audi's project car was more closely based on their 5000 model, using a plastic sandwich floor/subframe structure, plastic roof, aluminum fenders, and an aluminum sandwich hood, it weighs 1200 kg, compared to the current 5000's 1226 kg. There is substantial evidence, therefore, that the scope for weight reductions of the steel structural parts of current weight-efficient small cars may be more limited than old, heavy car designs would indicate.

In summary, estimating the baseline car-weight reductions that can be reasonably expected in the next decade is rather judgmental. The evidence seems to favor moderate magnitudes, limited by the factors of feasibility, production cost, and safety requirements. Although safety is only an

externally imposed constraint, the inherently higher injury exposure as car sizes continue to decrease makes it unlikely that present attention to crash safety will be eased substantially. Based on available data and projections at the time of this report, the weight reductions in the baseline cars are projected at 45 kg, 70 kg, and 90 kg, respectively, for the next decade.

Recent interest in electric vans has prompted the addition of advanced vans to this assessment. At the time of preparation of this report, the Chrysler T-Van, the first "minivan" of the three largest automotive manufacturers, is available; and the other manufacturers are preparing to release their competition. The Chrysler product has the advantage of front-wheel drive, allowing placement of the batteries below the floor of the cargo area. It also has attractive aerodynamics and represents a reasonable effort at reducing weight. However, in the interest of being reasonably consistent with the other vehicles, an additional 10% reduction was assumed possible with another decade's development. Hence, the weight of the ICE-powered baseline vehicle was projected to be 1080 kg. The other characteristics remain the same as the current van and are compared to the passenger vehicles in a later section.

Another way to reduce automobile weight is to decrease the engine power. This has the cumulative results of, first, lower engine and drivetrain weight and then decreased weight in the rest of the vehicle due to weight propagation effects. This is an appropriate topic for the discussion of baseline vehicle weights because the performance level specified for the 1992 AV is substantially below that in current production cars. Typical 1981 gasoline-engined four-passenger cars have a power-to-weight ratio[9] of 0.049 kW/kg (0.030 hp/lb) or higher, which gives them 0 to 97 km/h (60 mi/h) acceleration times of 14 s or less. The AV acceleration specification of 090 km/h (56 mi/h) in 20 s, which is intended to be equivalent to current typical naturally aspirated (non-turbocharged) diesel cars, requires about 0.030 kW/kg (0.018 hp/lb) of venicle weight. Using the specific engine and transmission data developed in this study, the weight reduction due to performance decrease can be significant. The low weight of the micro-cars, from which the two-passenger baseline car is derived, is partly due to their small engines. In fact, their power-to-weight ratio closely equals the AV value, so their true weight difference from the four-passenger baseline is smaller than it would seem at first glance. This effect can be seen from Table 5-1.

Depending on the powertrain and energy storage system of a specific AV concept, the base vehicle weight may have a much stronger effect on overall performance (including range) than for an ICE car. This would justify a greater effort toward additional weight savings, despite the probable higher cost. This was the primary reason for investigating the HSS plus composites and aluminum vehicle options. The sources for this investigation were a report by Alcoa (Reference 5-4) that contrasts HSS, plastics, and aluminum-intensive cars; discussions with GM (personal communication between R. Nelson and G. Klose at the General Motors Electric Vehicle Project Center, July 1982.) concerning their aluminum prototype EVs; and previous JPL studies

[9] Based on EPA test weight, curb weight + 136 kg (300 lb).

Table 5-1. Effect of Vehicle Weight Reduction and Performance on the Baseline Passenger Vehicles

Vehicle	Power-to-weight ratio	Two-passenger, kg	Four-passenger, kg	Five-passenger, kg
1982 ICE	0.05 kW/kg	NA	820	1100
1992 ICE	0.05 kW/kg	560	750	1000
Baseline	0.03 kW/kg	500	670	895

(References 5-5, 5-6). The results, shown in Table 5-2, imply substantial weight savings can be achieved. However, it remains to be seen if the increased cost is justified.

The methodology of deriving the AV parameter set from the (ICE) baseline vehicle is to remove the ICE-associated components, add the AV powertrain and energy-storage components, and apply weight propagation to the component weight differences to arrive at the total AV weight. A weight propagation factor of 0.30 is used, as generally adopted in automotive studies. Whether the process starts with the baseline car at the current ICE power level or at the AV power level will make no difference, as long as the procedure is carried out consistently. Current diesel-powered cars could even be used; their substantially higher engine and driveline weight per horsepower would subtract out to result in the same AV characteristics.

B. AERODYNAMIC DRAG

Both the drag coefficient (C_D) and the vehicle frontal area affect the aerodynamic drag. The frontal area depends primarily on the assumed seating package but may have to be increased for some AV configurations with large subsystem volume requirements. For the baseline cars, area values near the lower range of current cars can be established. A two-passenger package may include a more reclining seating position and thus have slightly lower area than the four-passenger car; the five-passenger vehicle will require somewhat more width. Thus, frontal area values of 1.70, 1.85, and 2.00 m^2, respectively, are used.

Claimed drag coefficients of current domestic production cars range down to 0.37. The ETV-1 prototype achieved a measured C_D value of 0.31, but that required some design features that might not be adopted in series production, such as compound-curved side windows that do not roll down. Several of the automobiles of 2000 prototypes exhibited at the Frankfurt Auto Show were projected to have C_D values as low as 0.24. Some of these were rather radical body shapes whose marketplace acceptability was a concern even to their creators. Also, past experience indicates that in the process of becoming production cars, such prototypes experience inevitable increases in

Table 5-2. Projected ICE Passenger-Vehicle Curb Weights as a Function of Material Substitution

Primary vehicle materials	Two-passenger, kg	Four-passenger, kg	Five-passenger, kg
Mild steel (1992 baseline)	650	750	1000
HSS plus plastics	475	640	850
Aluminum or advanced composites	390	525	700

C_D, partly through the elimination of features, like the full belly underpan, which are not feasible in everyday auto use. The most optimistic value that can be justified for the actual C_D of an operating production car is probably 0.30. A pure-electric vehicle like the ETV-1 benefits from the absence of cooling-air flow through a radiator, which is required for a powertrain that includes a heat engine and typically causes a C_D increment of at least 0.02.

Finally, for realistic simulation of actual vehicle operation, the effect of typical ambient winds must be included. Such winds, combined with the headwind due to the car's forward motion, impinge on the car at an angle to the centerline, or, technically, with a non-zero angle of yaw; this causes a drag increase of 6 to 10%, depending upon the car's aerodynamic characteristics and the speed-time relationship of the driving cycle (Reference 5-7). The resulting value is called the effective (wind- weighted) drag coefficient, C_D(eff.). Summarizing all these points, C_D(eff.) = 0.32 for baseline vehicles with radiator cooling airflow and 0.30 for those without. For specific vehicle/powertrain configurations, individual adjustments to these values may be appropriate.

C. ROLLING RESISTANCE

Tire-rolling friction is the most significant single source of power dissipation in urban driving. It can be reduced by increasing inflation pressure and using harder rubber compounds, and much work has been done in recent years to minimize the resultant adverse effects on handling and safety. The ETV-1 coast-down tests showed a C_{RR} (tire-rolling resistance coefficient) of 0.0095 on specially made, high-pressure radial tires at 29/41 (front/rear) psi, with brakes and drive line disconnected, but including wheel bearing and seal friction. Tire-only tests at high pressures (60 psi) have given C_{RR} = 0.008, but it is not established that in-use road behavior of such tires would be acceptable. Bearing and seal losses would add at least 0.001 to any measured tire-only value. Allowing for continued development over the next 10 years, C_{RR} = 0.008 can be used for simulations, with bearing and seal losses included.

Cold tires have substantially higher rolling resistance than the steady-state value until they warm up, because of the heat generated by the tire's flexing as it rolls. The ELVEC simulation program incorporates a tire warm-up factor that adds 30% to C_{RR} at the beginning of a trip, decreasing exponentially to 14% at 5 km of travel, 4% at 14.5 km, and under 1% at 24 km. Although the effect is dependent upon initial temperature and trip-speed profile, the warm-up factor has been formulated to represent typical operating conditions. This also applies to freely rolling tires. When transmitting large torque loads, such as during acceleration, C_{RR} can increase up to 30%. If sufficiently quantified data is available, the importance of this effect over typical driving missions will be assessed and will be incorporated in the simulation program, if feasible.

D. ACCESSORY POWER

Significant auxiliary power requirements are primarily the passenger compartment ventilation fan and the headlights for some fraction of the daily driving; these total a few hundred watts. A specified level of accessory power can be input to the simulation program. Air conditioning, if desired, completely overshadows the other auxiliary demands. According to a recent study performed for JPL's EHV Project (Reference 5-8), even with special design features to minimize losses to the outside, a four- or five-passenger car will require 5 kW of air-conditioning (A/C) capacity at design conditions. A typical automotive A/C system operates with a coefficient of performance (COP) of 2.0 and thus needs 2.5 kW of input power. To put this into perspective, at the 31.2 km/h average speed of the EPA Urban cycle, this is about 81 Wh/km, which equals half the entire average propulsion power; in other words, turning on the air conditioner would increase the energy consumption of an Advanced Vehicle to one-and-a-half times its normal value. This clearly has strong design trade-off implications, especially for powertrain configurations with sharply constrained energy-storage capacity.

Fortunately, the full capacity of the A/C system is only required at maximum temperature conditions. Most of the time, after an initial 5- to 10-minute cool-down effort, the system will switch to a lower output level required to maintain the passenger compartment temperature with the existing outside conditions. Specific statistical data on the A/C output demands may be difficult to obtain. Also, the trip-length distribution has an obvious effect because every time the car is parked (even a few minutes), the heat build-up will require a new cool-down cycle.

An ideal AV environmental control system would be completely without on-board power requirements, relying entirely on stored energy. A variety of such systems have been proposed, and the only disadvantage is that the storage capacity chosen for a specific system is a definite limit, with no adaptation possible for a trip length beyond the design point. The most promising system identified in the recent study is an ammonia-water split heat pump system that could provide both heating and cooling, with a capacity of 2.5 h of full-power cooling operation; this choice was based on trip-length profiles. Such a system has no moving parts and no power demands on-board the vehicle, with the regeneration carried out with home-based, off-vehicle equipment. Although the individual components are all feasible with today's technology at acceptable

cost, several years of system development would be needed, still allowing the system to be available within the decade time frame of the AV. The on-board weight is projected to be 143 kg, compared to 45 to 55 kg for current A/C systems. The effect of this extra weight on the AV's overall road energy consumption will also have to be determined but will undoubtedly be less severe than the energy requirement of a conventional A/C system incorporated in an electric vehicle.

E. SUMMARY

The following table summarizes the previous sections and the assumptions that will be used in the AV systems evaluations.

Table 5-3. Advanced Vehicle Baseline (ICE) Characteristics

Characteristics	Two-Passenger[a]	Four-Passenger	Five-Passenger	Van
Curb weight, kg	500	670	895	1080
Frontal area, m^2	1.70	1.85	2.00	2.50
C_D(eff.)				
With radiator	0.32	0.32	0.32	0.47
Without radiator	0.30	0.30	0.30	0.45
Tire-rolling resistance (C_{RR})	0.01	0.01	0.01	0.011
A/C power, kW	2	2.5	2.5	3.0

[a]Theoretical two-passenger commuter vehicle.

SECTION V REFERENCES

5-1. Budd Co., A Mass Reduction Effort of the EHV, TCR-0513, DOE/JPL Report No. 955283-1, March 1980.

5-2. "Operation Seville Evokes FRP Designs," Design News, April 6, 1981.

5-3. Feast, R., "Cars of Tomorrow at Frankfurt Show," Automotive News, September 28, 1981.

5-4. Cochran, C. N., and McClure, R. H. G., "Automotive Materials Decision: Energy, Economics, and Other Issues," Society of Automotive Engineers Congress and Exposition, SAE 820149, 1982.

5-5. Should We Have a New Engine? An Automobile Power Systems Evaluation, Vol. II, Technical Report, JPL SP43-17, August 1975.

5-6. Klose, G. J., and Kurtz, D. W., "Weight Propagation and Equivalent Horsepower for Alternate-Engined Cars," SAE Report No. 780348, Society of Automotive Engineers; February 1978.

5-7. Kurtz, D. W., Aerodynamic Design of Electric and Hybrid Vehicles: A Guidebook, JPL Internal Report No. 5030-471, Jet Propulsion Laboratory, Pasadena, California, September 1980.

5-8. Electric and Hybrid Vehicle Environmental Control Subsystem Study, Report No. MTI 81TR56, Mechanical Technology, Inc., May 1981.